Titre: Title:	Modelling Neighborhood-Scale Energy Scenarios
Auteur: Author:	Louis Leroy
Date:	2020
Type:	Mémoire ou thèse / Dissertation or Thesis
Référence: Citation:	Leroy, L. (2020). Modelling Neighborhood-Scale Energy Scenarios [Master's thesis, Polytechnique Montréal]. PolyPublie. https://publications.polymtl.ca/5206/

POLYTECHNIQUE MONTRÉAL

affiliée à l'Université de Montréal

Modelling Neighborhood-Scale Energy Scenarios

LOUIS LEROY

Département de génie mécanique

Mémoire présenté en vue de l'obtention du diplôme de *Maîtrise ès sciences appliquées*

Génie mécanique

Avril 2020

POLYTECHNIQUE MONTRÉAL

affiliée à l'Université de Montréal

Ce mémoire intitulé :

Modelling Neighborhood-Scale Energy Scenarios

présenté par

Louis LEROY

en vue de l'obtention du diplôme de *Maîtrise ès sciences appliquées*

a été dûment accepté par le jury d'examen constitué de :

Michel BERNIER, président
Michaël KUMMERT, membre et directeur de recherche
Étienne SALOUX, membre

ACKNOWLEDGEMENTS

First of all, this research was mainly supported by the Institut de l'énergie Trottier. I also wish to thank the resident and workers of the diverse studied areas who generously provided energy datasets.

Thanks to the team I work with for the *PPU des Faubourgs* that taught me a lot about HVAC systems in buildings in general and energy sharing network equipment and conception.

I would like to thank Barbara Rojas-Jardin that always supported me in my choices and work.

A thought to my family that live abroad and who helped me realize this project.

Thanks to the BEE-Lab's teachers and students with whom it was nice to work and spend time together.

Finally, I am grateful to Michaël Kummert who helped me in my work and with who it was pleasant to work with.

RESUME

Ce mémoire porte sur les approches de modélisation pour évaluer le potentiel des réseaux de partage de chaleur de 4ème et 5ème génération. Pour cela, plusieurs outils et techniques de modélisation sont utilisés. La modélisation de bâtiments typiques (i.e. archétypes) est d'abord étudiée, pour ensuite être capable de réaliser des modèles énergétiques de quartier (*UBEM*, pour *Urban Building Energy Model*, en anglais), et finalement pouvoir modéliser un réseau de partage d'énergie pour définir l'impact énergétique et environnemental de l'utilisation d'une telle technologie.

Différents archétypes (entre 4 et 5 par bâtiment) ont été utilisés (ou créés) pour 4 bâtiments montréalais (3 résidentiels et 1 commercial) dans différents logiciels de simulation énergétique (UMI, EnergyPlus, TRNSYS et SIMEB) avec différents niveaux de détail (jusqu'à un modèle calibré) et différents niveaux d'effort pour sélectionner les paramètres de ces archétypes. Les résultats de simulation ont ensuite été comparés avec des données mesurées, permettant d'effectuer des « coups de sonde » au sein du quartier étudié. Les résultats de cette étude montrent que le niveau d'effort pour définir les paramètres des archétypes n'est pas toujours garant d'une meilleure précision. De plus, il s'est avéré que transférer des paramètres de modèles calibrés (effectués dans TRNSYS ou SIMEB) dans un autre logiciel (ici UMI) se traduit par des résultats de simulation montrant jusqu'à 70 % de différence pour la consommation totale d'énergie, indiquant que les simplifications et approximations conduisent probablement à des erreurs de simulation qui s'annulent entre elles. Après comparaison des résultats des différents archétypes pour un même bâtiment, les archétypes développés par NRCan basés sur les *Prototype Buildings* développés aux USA et adaptés au code national énergétique canadien des bâtiment 2011 ont été sélectionnés pour la suite du travail.

Deux modèles énergétiques urbains ont été développés pour un quartier de l'arrondissement de Ville-Marie à Montréal, suivant 2 approches : une dépendante du contexte (*context-dependent*), dans UMI et une indépendante de celui-ci (*context-free*) avec EnergyPlus. La comparaison des résultats de ces *UBEMs* montrent que les consommations énergétiques et pointes annuelles entre les 2 modèles sont du même ordre de grandeur. Cependant, la dynamique des modèles est très

différente. Des doutes sur certains aspects des résultats d'UMI ont conduit à choisir les résultats du *context-free UBEM* pour la suite de l'étude sur les réseaux de chaleur urbains.

D'après les résultats de simulation du *UBEM* sélectionné, des modèles quasi-statique et dynamique de réseau de chaleur ont été réalisés. Le modèle quasi-statique consiste en des bilans énergétiques régis par des pertes et COP constants, et ses paramètres ont été sélectionnés par l'équipe de projet de l'étude de cas réelle sans connaissance des résultats du modèle détaillé. Le modèle dynamique est un modèle de réseau de chaleur réalisé dans TRNSYS et fait appel à des composants existants ainsi qu'à un nouveau composant développé pour modéliser les pompes à chaleurs centralisées et leurs différents modes d'opération. Au premier abord, les 2 méthodes confirment que l'implémentation d'un réseau de chaleur dans un quartier est bénéfique d'un point de vue énergétique, avec au minimum une diminution de 20 % de la consommation énergétique, et de l'environnement grâce à l'élimination des rejets thermiques dans l'atmosphère et la réduction des émissions de GES d'au moins 90 %. Les deux modèles montrent un excellent accord, ce qui témoigne de la grande expérience de l'équipe de projet qui avait sélectionné les hypothèses du modèle simplifié. La comparaison entre les réseaux de 4ème et 5ème génération montre des différences assez faibles entre les deux, avec un léger avantage pour le réseau de 4ème génération lié en partie aux hypothèses faites sur la disponibilité d'une source / puits de chaleur (les égouts dans notre cas). Les différents modèles développés permettraient de raffiner la conception des réseaux et d'analyser différentes stratégies de contrôle.

ABSTRACT

This thesis focuses on modelling approaches to assess the potential of 4th and 5th generation energy sharing networks. For this purpose, several modelling tools and techniques are used. First, the modelling of typical buildings (i.e. archetypes) is studied, then UBEM (Urban Building Energy Model) approaches, and finally modelling an energy sharing network to define the energy and environmental impact of such a technology.

Different archetypes (between 4 and 5 per building) were used (or created) for 4 Montreal buildings (3 residential and 1 commercial) in different energy simulation software (UMI, EnergyPlus, TRNSYS and SIMEB) with different levels of detail (up to a calibrated model) and different levels of effort to select the parameters of these archetypes. The simulation results were then compared with measured data. The results of this study show that more refined archetype's parameters does not always guarantee better accuracy. Moreover, it turned out that transferring parameters from calibrated models (carried out in TRNSYS or SIMEB) to another software (here UMI) results in simulation results showing up to 70% difference in total energy consumption, hinting that simplifications and approximations probably lead to cancelling errors. After comparing the results of the different archetypes for the same building, the archetypes developed by NRCan based on the Prototype Buildings developed in the USA and adapted to the Canadian National Energy Building Code 2011 were selected for further work.

Two urban energy models were developed for a neighborhood in the borough of Ville-Marie in Montreal, following two approaches: one context-dependent, in UMI, and one context-free with EnergyPlus. Comparison of the results of these UBEMs shows that the energy consumption and annual peaks between the two models are of the same order of magnitude. However, the dynamics of the models are very different. Doubts on some aspects of the UMI results led to the choice of the UBEM context-free results for the continuation of the study on energy sharing networks.

Based on the simulation results of the selected UBEM, we created simple pseudo steady-state and detailed dynamic models of district energy sharing networks. The pseudo steady-state model consists of energy balances governed by constant losses and COP, and its parameters were selected by the project team of the real case study without knowledge of the results of the detailed model. The dynamic model is built in TRNSYS and uses existing components as well as a new component

developed to model centralized heat pumps and their different modes of operation. Both methods confirm that the implementation of a district heating network in a district is beneficial from an energy point of view, with at least a 20 % reduction in energy consumption, and from an environmental point of view, eliminating waste heat rejection to the ambient air and reducing GHG emissions by at least 90 %. The two models show excellent agreement, reflecting the extensive experience of the project team that selected the assumptions of the simplified model. The comparison between the 4th and 5th generation networks shows fairly small differences between the two, with a slight advantage for the 4th generation network linked in part to the assumptions made on the availability of a heat source/sink (sewers in our case). The different models developed would allow to refine the design of the networks and to analyse different control strategies.

TABLE OF CONTENTS

LIST OF TABLES

LIST OF FIGURES

LIST OF SYMBOLS AND ABBREVIATIONS

4G	4th generation
5G	5th generation
ACH	Air Change per Hour
ALE	Appliances, Lights, Equipment
ASHRAE	American Society of Heating, Refrigerating and Air-conditioning Engineers
BEM	Building Energy Model
CHP	Combined Heat and Power
COP	Coefficient Of Performance
CVRMSE	Coefficient of Variation of the Root Mean Square Error
DC	Data Centre
DHW	Domestic Hot Water
DOE	Department Of Energy
EIA	Energy Information Agency
EUI	Energy Use Intensity
GHG	GreenHouse Gases
GIS	Geographic Information System
HP	Heat Pump
HVAC	Heating, Ventilation and Air Conditioning

IECC	International Energy Conservation Code
LiDAR	Light Detection And Ranging
MIT	Massachusetts Institute of Technology
NECB	National Energy Code of Canada for Buildings
NMBE	Normalized Mean Bias Error
PLR	Part Load Ratio
SHGC	Solar Heat Gain Coefficient
TRNSYS	Transient System Simulation (simulation software)
Tvis	Visible Transmittance
UBEM	Urban Building Energy Model
UMI	Urban Modelling Interface
UNEP	United Nations Environment Programme
US	United States
WA	Weighted Average
WWR	Window-to-Wall Ratio

LIST OF APPENDICES

CHAPTER 1 INTRODUCTION

District energy systems represent one of the most economically and technically viable ways of reducing the carbon footprint of the built environment in urbanized areas (UNEP, 2015). These district energy systems have evolved over time, from high-temperature district heating systems using steam as the heat transfer medium to low-temperature district heating and cooling systems using water, and to so-called "ambient temperature" heat sharing networks using water or an antifreeze solution (Buffa, Cozzini, Antoni, Baratieri, & Fedrizzi, 2019).

Current research on district energy systems focuses on efficiently integrating fluctuating renewable energy sources (Buffa et al., 2019), offering energy flexibility to the electric grid (Lund et al., 2014), and using waste heat to improve the overall energy efficiency of urban areas and to reduce heat rejection in the environment and the heat island effect (Heiple & Sailor, 2008).

1.1 District energy sharing systems of the 4th and 5th generations

This thesis focuses on modelling approaches to assess the potential of heat-sharing networks of the 4th and the 5th generation, which are mainly differentiated by their operating temperatures and the requirements for buildings to be equipped with individual heat pumps (for more detail, see section 2.5).

Figure 1.1 presents how a 4th generation sharing network works. Two water loops – one hot (in red) and one cold (in blue) – satisfy the heating and cooling loads of the buildings (from left to right, residential/offices; healthcare; data centre; supermarket) thanks to heat transfer stations placed between the water loops and the buildings. The supply temperature is typically between 50 °C and 80 °C for the hot loop and around 6 °C for the cold loop (Buffa et al., 2019). Centralized heat pumps can supply heat to the hot loop and extract heat from the cold loop, using a renewable resource or long-term storage as a heat source/sink. Other forms of heat/cold supply can be used, such as gas boilers or conventional chillers rejecting heat to the ambient air. Heat recovery (i.e. heat transfer from the cold loop to the hot loop) can be achieved by the same centralized heat pumps. Note that the schematic shows one heat pump for each function, while in reality a bank of heat pumps would be used, with all the heat pumps capable of operating in heat recovery, cooling, or heating mode.

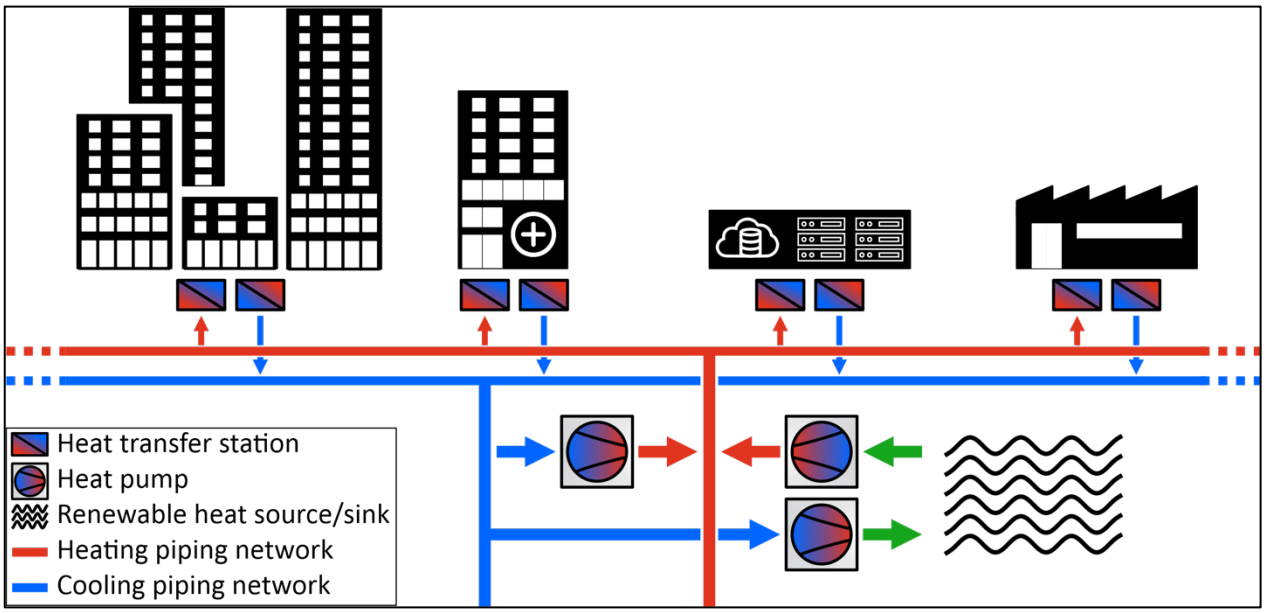

Figure 1.1 – Schematics of a 4th generation energy sharing network

Figure 1.2 schematizes the operation of a 5th generation network. There is one loop of low-temperature fluid (in green) where buildings can draw or reject heat thanks to decentralized heat pumps (little HPs next to the buildings in the figure) to satisfy their heating and cooling loads. Temperature of the loop is usually maintained between 0 °C and 30 °C (Buffa et al., 2019) thanks to centralized heat pumps (bigger HP in the figure) using a renewable resource or long-term storage as a heat source/sink (symbolized by a river in the figure). As for the 4th generation network, these heat pumps are not required, more common equipment, such as boilers or chillers, can also be used to balance the loop.

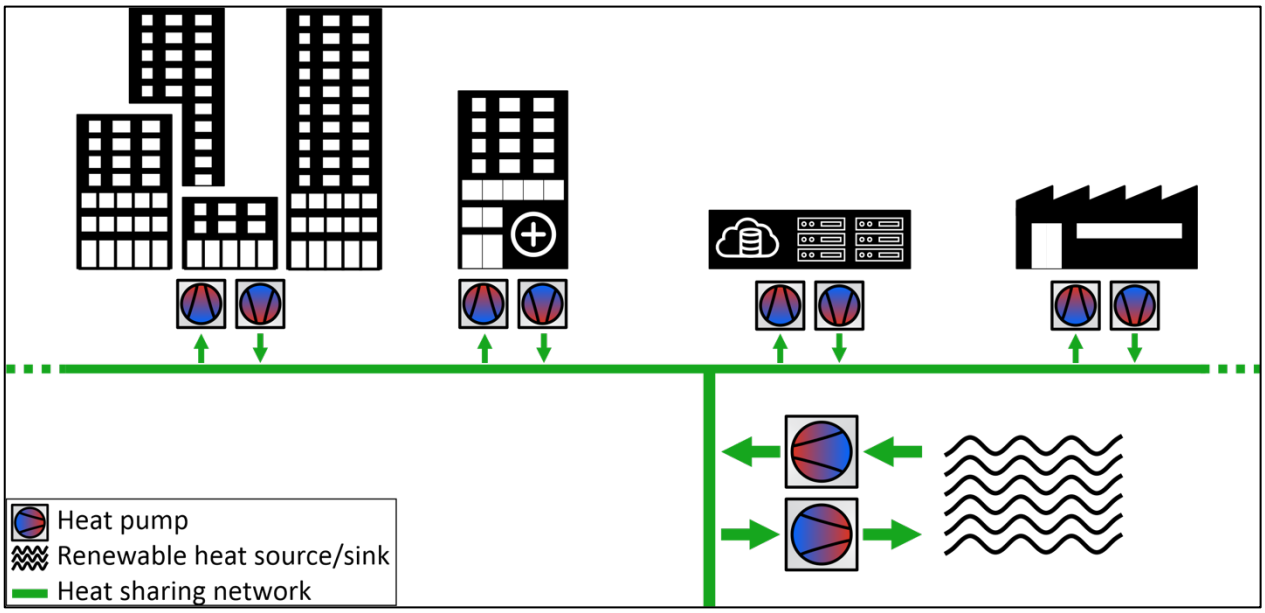

Figure 1.2 – Schematics of a 5th generation energy sharing network

1.2 Urban Building Energy Models (UBEM)

An important aspect of planning and assessing district energy systems is to correctly predict the heating and cooling demands of buildings within the studied area. The current building stock in the area must be accounted for, but also planned additions and energy efficiency measures. This makes it difficult or impossible to rely on measured energy data, which represent a snapshot of the current situation or historical values, and are often incomplete or unavailable to the general public (Seskus, 2019). The assessment must rely on a model of all existing and future buildings in a neighborhood or city, called an Urban Building Energy Model (UBEM) (Cerezo, Sokol, Reinhart, & Al-Mumin, 2015).

Various UBEM methods rely on "building archetypes" (see Figure 1.3, top-left) that are a representation of buildings with similar usage, thermal properties, age, etc. (Letellier-Duchesne, 2019). Those archetypes are used to represent the different building model in the UBEM. Geographical Information System (GIS), LiDAR or CAD data is used to find out the proportion, or the geographical location (see Figure 1.3, bottom-left) of each archetype to be able to assess an energy signature (from the archetypes) to each building represented in the UBEM.

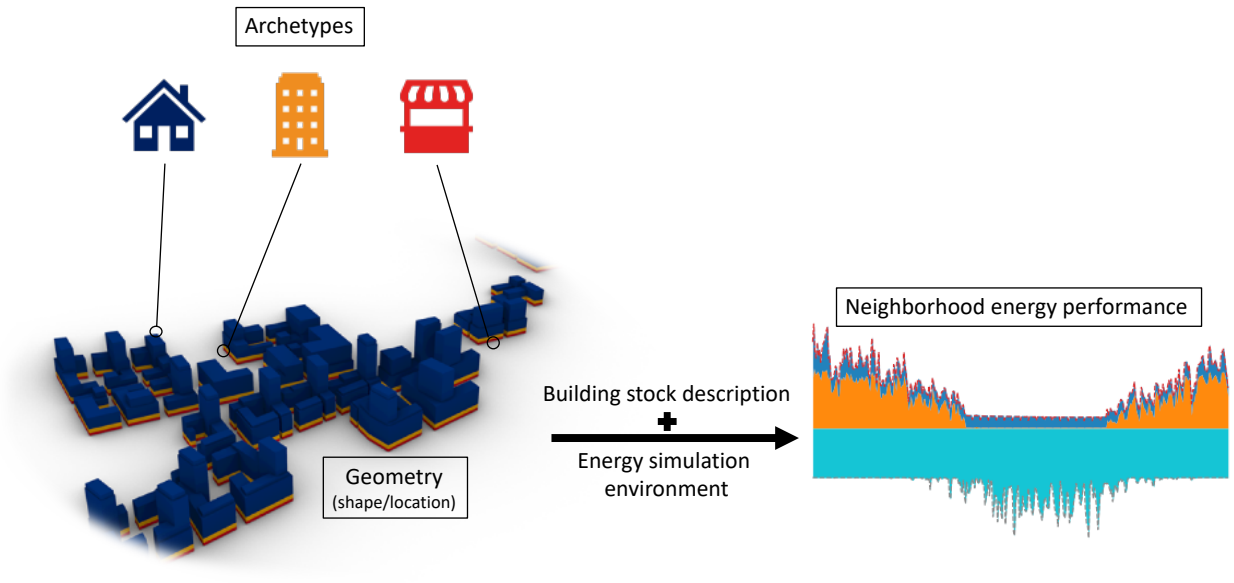

Figure 1.3 – Workflow for UBEM creation

1.3 Objectives

The goal of this thesis is to propose and apply a methodology to model urban energy scenarios relying on energy sharing networks. This goal is split into three specific objectives:

- Review and assess available archetypes and compare different levels of effort in selecting their parameters. The objective is to compare the results obtained with different archetype definitions for typical residential and commercial buildings to measured energy use data for selected buildings and make recommendations for archetype definitions and refinements.
- Define an Urban Building Energy Model for a selected case study and assess the dynamic energy flows of the neighborhood without a district energy system, defining a "business as usual" scenario. Two different UBEM approaches will be compared, a simple method based on predefined archetypes simulated independently of their context, and a context-aware model based in the UMI software platform (C. Reinhart, 2019).
- Define a simplified model of district energy networks for the selected case study and assess the dynamic energy performance and the greenhouse gas emissions of different options (4th

generation vs. 5th generation). Compare the results obtained with a detailed model of the 4th generation network to assess the impact of simplifying assumptions at planning stage.

1.4 Thesis overview

This thesis is divided into 7 chapters. Chapter 2 presents a review of the literature relating to urban building energy models, archetypes and district heating and cooling networks. Chapter 3 deals with the creation and comparison of archetypes with different level of details for commercial and residential buildings. Chapter 4 introduces a case study on the implementation of 4th and 5th generation district energy systems in a neighborhood, which is used in the following chapters. Chapter 5 presents the comparison of 2 UBEM methods applied to the case study, and Chapter 6 presents the results obtained with different modelling approaches for 4th and 5th generation networks. Finally, Chapter 7 highlights the conclusions and contributions made by this work, and the next steps to be explored.

CHAPTER 2 LITERATURE REVIEW

Urban building energy modelling (UBEM) is increasingly becoming the focus of discussion and research inside energy modelling circles. Generating UBEM requires defining archetypes, which include information from the building geometry (nowadays, by using footprints from Geographic Information System (GIS) databases that are extruded in 3D), building usage, thermal properties and climate zone (usually associated with a typical hourly weather file) (Cerezo et al., 2015). This archetypal method is employed because it would be impractical to list all the properties (mostly thermal) building-by-building to recreate an exact model of a building stock (C. F. Reinhart & Cerezo Davila, 2015). The simulation of detailed individual buildings and building stocks are starting to merge as we seek to better understand and analyse the energy performance of a targeted district (C. F. Reinhart & Cerezo Davila, 2015). The latest technical developments have enabled energy assessments of neighborhoods and even entire cities with an acceptable calculation time, hourly or even sub-hourly, thus allowing UBEM to become a relevant planning and decision-making tool in different fields.

UBEM helps urban development planning by studying neighborhood densification and diversification for the implementation of systems such as an energy sharing network. It is also a tool often used in the development of building retrofit policies to understand and analyse the energy impact of building modifications. It is increasingly used to optimize energy systems, such as new sources of renewable energy (solar collector fields, geothermal boreholes, etc.) in neighborhoods. Early UBEM studies often focused on analysing the impact of building retrofits or quantifying heat rejection by building blocks, *e.g.* evaluating their impact on the urban heat island effect (Heiple & Sailor, 2008) and then finding ways to reduce it. Recent studies continue to focus on building retrofitting scenarios such as improving the building's envelope, or the installation of more efficient HVAC systems, but are also increasingly aiming to assess the potential of district energy systems. For example, Sokol et al. (Sokol, Cerezo Davila, & Reinhart, 2017) created models to study building retrofits and district energy potential in Cambridge, MA.

2.1 Defining archetypes for building stocks

Analysing the energy consumption at the neighborhood level requires the creation/use of archetypes. Some studies have focused on the definition of these archetypes in an energy planning

context. It would be a tedious task to calibrate every building of the stock so they are often grouped by different typologies (i.e. *archetypes*). Theodoridou et al. (2011) studied the classification of residential buildings in Greece, in order to better understand the residential building stock heating energy consumption and the impact that retrofits would have on CO_2 emissions. In their study, they proposed to classify the archetypes in 6 different categories based on the age of the buildings. As Huang et al. (1991) showed, Theodoridou et al. confirmed that the year of construction is a good indicator to reveal the building's thermal properties and typology. Having all thermal properties based on the age of the building and the climate zone, the study used data from government and surveys to determine the different geometric parameters of the archetypes (number of floors, kind of roof, etc.). As mentioned by the authors, this last step can be difficult since surveys are often incomplete. The study showed differences between the modelled and actual energy consumption, mainly attributed to differences between survey-based construction data and actual building features.

The study by Theodoridou et al. showed that archetype definitions were mostly driven by the building's construction period. Filogamo et al. (2014) used the same approach in their study in the classification of large residential buildings stocks in a Sicilian context, but refined the definition of "typological buildings" (i.e. archetypes) with other criteria. Archetypes were classified by building age (7 categories) (since construction type is directly linked to the building's age), geometric properties (Window-to-Wall Ratio [WWR], floor area, volume, shape ratio, etc.), thermo-physical properties (loss coefficient, thermal capacity), HVAC systems, and climate zones (using the Degree-Day method). By refining the archetype definitions, Filogamo et al. obtained maximum differences in the order of 8 % between the simulated building stock and statistical data over a 1-year period, for thermal energy, electrical energy use, and total consumption. Their study showed that the refinement of the archetype classification can improve the accuracy of the building stock results.

A broader study was performed on thousands of residential and non-residential buildings from 4 different European countries (France, Germany, Spain and United Kingdom) to analyse energy conservation measures potential and cost implementation. In their work, Mata et al. (2014) developed a 4-step-method to aggregate the calculated energy consumption through building archetypes of a building stock. First, *segmentation* allowed the authors to determine the number of

archetypes needed to represent the building stock, based on building type (usage, geometry, etc.), construction year, type of heating system and climate zone. Then, each archetype was characterized by determining its thermal properties (U-values, occupancy, infiltration rate, etc.). Step 3 involved the quantification of each archetype within the building stock. Usually, this step requires statistical data to match the different archetype distributions existing in the building stock. Afterwards, the method is validated for each building stock by comparing the final energy use of the models with national statistical data for a particular reference year. Mata et al. created 593 archetypes and compared final annual energy demand by end-use ("heating", "hot water", "electricity" and "total energy") with statistical data from government surveys and individual building utility bills. The method resulted in a maximum difference of 6 % for the total energy consumption of the building stock. Their results showed the advantage of using building archetypes to compare end-use consumption with statistics from aggregated and area-normalized consumption values. However, as mentioned earlier by other authors (e.g. Kohler et al. (2002)), this method developed by Mata et al. may be difficult to implement due to the absence of reliable statistical data.

2.2 Generating UBEMs

Archetypes are used in estimating a building stock energy consumption by aggregating the consumption of each individual building model (usually aggregation based on the Energy Use Intensity (EUI, kWh/m^2)). They are also crucial in creating an urban building energy model. The major difference between building stock aggregation and UBEM simulation is that urban models make it possible to study the interaction of the buildings between themselves.

First study, done by Heiple and al. (2008), estimated within 10 % the yearly energy consumption of existing buildings in Houston, Texas. The purpose of their study was to determine on a yearly basis the sensible and latent heat waste rejection from anthropogenic energy consumption, focusing on residential and commercial buildings where heat rejection comes from the HVAC systems. They developed an urban model with multizone prototype buildings (i.e. archetypes) based on the year of construction (allowing to determine thermal properties (Huang et al., 1991)) and the main fuel type used by each building. The lighting and equipment loads were based on ASHRAE standards. They built their urban model according to the bottom-up approach (see section 2.3) allowing them to estimate the hourly energy consumption used by the buildings and the energy consumption that

did not lead to atmospheric waste heat. Non-electric load data was available for individual buildings. Finally, the urban model mapping was done with the help of GIS and tax lot databases, a method frequently used by modellers.

Later, Reinhart et al. (2015) broke down a general method to create a reliable Building Energy Model (BEM) that can be applied to the study of a building stock energy performance. The research divides a BEM in three different categories: the simulation input (data input), the thermal model generation and execution (thermal modelling) and the result validation. Simulation data is defined by climate data, which can stem from a weather file (from a weather station) or a normal climatic file, building geometry (envelop shape, WWR, etc.) from pre-defined datasets or work on site, and thermal properties (construction type, HVAC systems, schedules, etc.). As mentioned before, thermal properties are not listed building-by-building, but building archetypes are created instead in order to make UBEM possible. As in Mata et al.'s study, archetypes were created in 2 steps: *segmentation*, where building stock were divided according to the building's age, usage, shape, etc. and *characterization*, where thermal properties were based on samples of buildings or on statistics. After defining simulation input, Reinhart et al. presented different type of thermal modelling based on their complexity. The simplest case is to simulate each archetype with single zoning method and then aggregate the result of each simulation based on the number of different archetypes in the building stock (could be a floor area-based aggregation). This model resolution is easy to set up but does not take in consideration the interaction between the buildings (shading, heat transfer if attached, etc.). To improve on this point, Reinhart et al. suggested creating dynamic multizone models for each archetype and implementing wind speed variation, shading and long-wave radiation between buildings in the UBEM. Lastly, their study recommends that validation done with statistical (government or survey datasets) or measured data may be in a range between 0 and 20 % error for end-use consumption of the studied building stock. However, large uncertainty remains in archetype definition; increasing the error range when looking at individual buildings can be a problem when analyzing peak load (important in our line of work on energy-sharing networks) where the difference between simulated and measured data can be up to 40 % (Heiple & Sailor, 2008).

After several studies on UBEM and definition of archetypes done at the MIT by Prof. Reinhart and his research team, Cerezo et al. (2016) developed "a workflow for the efficient generation and maintenance of urban building energy models from existing geospatial datasets" in Boston. In their work, the authors confirmed that the early implementation of UBEMs in energy audits, retrofit studies or the introduction of a new technology (e.g. a sharing energy network) is always preferred, especially because it helps to better understand how neighborhood/city energy ecosystems work. Moreover, the researchers wanted to ensure that the workflow could at least be replicable for other US cities. Thanks to GIS mapping, they modelled over 80,000 buildings on Rhinoceros, a 3D modelling environment (Robert McNeel & Associates, 2019), and then used EnergyPlus (US DOE - BTO, 2019) to simulate the energy model by assigning around 50 archetypes to represent the different buildings of the building stock. Archetypal segmentation was based on building usage and construction year. Geometry (building height, shape ratio, etc.) was not used to define archetypes since it was assigned by GIS datasets. Considering that the definition of archetypes involves non-negligible errors, the authors realized that 3D mapping could minimise at least some errors. Still, the results of Cerezo et al. study are mixed with an average error between 5 and 20 % on the EUI of total energy use when comparing simulated data and the data from Energy Information Agency (EIA) surveys, and the error on fuel type consumption by zip code was as high as 71 %. To remedy this, the authors proposed to calibrate the UBEM with measured data. However, as discussed before, modellers usually do not have access to this kind of data. In this case, the lack of available measured data was identified as the principal barrier in the workflow to create efficient/accurate UBEMs. Furthermore, Cerezo et al. mentioned that modellers should prioritize the use of measured data on a short-time basis (e.g. monthly instead of yearly) to compare and/or calibrate their UBEMs.

All of the previous studies were focusing on yearly (or monthly) energy consumption, even if the researchers wanted to simulate on an hourly basis. However, to build an energy-sharing network, we need a good approximation of the energy consumption on a shorter time basis (e.g. hourly). Recent studies are already heading down this path. Sokol et al. (2017) studied UBEMs with a different purpose as their predecessors, who were mostly interested in buildings retrofit (for energy or cost savings). Sokol et al. developed a method to define residential archetypes in an UBEM, focusing on new energy efficiency solutions such as district heating/cooling networks. Their work

interests us knowing that our study is about energy-sharing networks and that we need to create an urban model as precise as possible on a short-time basis (hourly) to understand the energy dynamics of a district. The authors validated the utilisation of a Bayesian-based method to define residential archetypes. Their work is innovative because it attempted to find a way to build an accurate UBEM, while facing the lack of information for archetype definition mentioned before. The main idea of this method joins the work done by Cerezo et al. (2015) by applying probabilistic distributions from measured data to unknown or uncertain archetype parameters. Sokol et al. confirmed that UBEM calibration is needed for better results of the simulated data. Their approach was divided in 3 steps: meta-modelling, optimisation, and Bayesian calibration. Meta-modelling concerns the creation of a statistical model as a surrogate of a detailed one, allowing less computational resources for the calibration process. Then, optimisation and Bayesian calibration involves the minimisation of an objective's function by modifying the model's parameters. The authors were able to validate their method by respecting the ASHRAE-14 Guideline about calibration errors (see section 2.4) for the majority of their buildings (99.7 % in respect for the yearly NMBE <5 % and 83.5 % in respect with the monthly CVRMSE <15 %).

2.3 Comparison of UBEM workflow

As seen previously, there are different ways to define archetypes to assign to individual buildings in a neighborhood. To create a UBEM, there are 2 main schemes: the "bottom-up" and the "top-down" method. The bottom-up method is characterized by creating large-scale models (e.g., a neighborhood) from more specific models (e.g. a building). While the top-down method uses data (often statistical) on a large scale (e.g., country), then refines it to smaller scales (e.g. neighborhoods, or buildings). Building modellers typically favor bottom-up approaches over top-down approaches for building stock modelling as they enable detailed diagnostics and predictive studies at various scales, from country/region to specific neighborhoods, and are more versatile, making it possible to model different scenarios at high temporal and spatial resolutions (C. F. Reinhart & Cerezo Davila, 2015; Sokol et al., 2017). On the other hand, top-down models of specific neighborhoods show lack of accuracy for building energy consumptions (C. F. Reinhart & Cerezo Davila, 2015). Moreover, the bottom-up approach can estimate the hourly profiles of energy consumption by end-use and fuel type. It should be noted that the bottom-up approach is more time

consuming than the top-down method (Heiple & Sailor, 2008). With a bottom-up modelling approach, modellers rely on extensive datasets that characterize each and every building inside the study area. To reduce the data preparation task, several authors have proposed different approaches.

Cerezo et al. (2015) remarked that with the archetypal approach (assignment of an archetype to each building), the estimated energy required for the whole building stock is accurate within 5 to 20 %, whereas this error can go up to 99 % for individual buildings. The limitation in building data availability, as occupancy patterns, and the uncertainty in UBEMs inputs are the primary culprits. They studied the impact of using archetypes to represent building categories in an urban model, and how it can affect and misrepresent the energy demands. To do so, they developed 3 methods to characterize building archetypes for a unique building stock in Kuwait City. Two of these methods are (A) a common deterministic approach for defining archetypes and (B) a probabilistic base approach that defines the uncertain parameters, such as occupancy. Method A is based on available literature, and buildings sharing the same usage (residential, commercial, etc.) are modelled by the same archetype. Furthermore, the different parameters of the archetypes are defined from construction codes or published research while the method B is based on local expertise. The number of archetypes in method B is larger than in method A, considering that buildings are classified by usage, size and age. Window-to-Wall Ratio is assessed for each building of the model by photography analysis, and a survey of 50 residential buildings is used to estimate the occupancy's dependent variables (plug loads, equipment, etc.). A third method (C) is based on method B with high-uncertainty parameters assigned with probabilistic distribution. The accuracy of each method is evaluated by comparing the simulated data with measured data from 140 residential buildings. Results showed that refining the archetypes helped the precision for the average EUI (error on average EUI in Table 2.1), and mostly improved the distribution of different EUI within the building stock (error on standard deviation in Table 2.1).

Table 2.1 − Results from Cerezo et al. (2015) *study for different definitions of archetypes*

	Method A	**Method B**	**Method C**
Error on average EUI	18 %	3 %	4 %
Error on standard deviation	91 %	56 %	30 %

2.4 Model calibration (archetypes and UBEM)

These last studies demonstrate that the calibration of UBEMs is crucial in acquiring accurate results for individual buildings in a building stock and is mostly likely the key for studying energy sharing network's dynamics. Calibration reduces discrepancies between simulated and measured data. These differences usually come from a deviation between the way the model depicts the building design and occupation, and the way this building is really built and operated. Mostly, the occupancy adds several uncertain variables. However, calibration may be challenging due to the difficulty of finding enough accurate data to properly calibrate (discussed below) energy models. Samuelson et al. (2015) proposed to calibrate the archetypes to further improve the accuracy of UBEM results. Their method was applied on 18 commercial buildings from 416 m^2 to 51,000 m^2 and 1 to 16 stories. First, they developed a design-phase method with pre-calibrated models for each building, taking the geometry and thermal properties of each one as input parameters. For these first iteration models, they used default values for occupancy variables as the performance compliance protocol (National Research Council Canada, 1999) encourages. Afterwards, they calibrated the design-phase models by first performing a sensitivity analysis by isolating and changing every input parameter to determine which ones had the most impact on the total energy consumption of the model. Furthermore, with measured data, they calibrated each parameter by an iterative process. Results show that calibration helped rectify the discrepancy between the measured data and the design-phase models by reducing the total energy use errors over a year of the buildings from 36 % to 7 %. Their study was inspired by the methodology proposed in the ASHRAE's guideline 14 (2014). This guideline offers some help in the calibration process by defining the steps that should be taken to achieve the best results (compared to measured data) when calibrating a model. The

focus is on having accurate weather files representing the location of the model, having access to measured energy consumption data of buildings to be calibrated, and having information on its occupancy (operation schedule, etc.). The guideline mentions that the measured data must be consistent with a representative period of the building's use, and that if any parts of this period are missing, the data available should be interpolated.

A recent study conducted by Li et al. (2018) showed a stepwise calibration for residential buildings focusing on the heat consumption of these buildings. The authors characterize their calibration method in 2 steps: a sensitivity analysis and a stepwise calibration. The sensitivity analysis reduces the number of thermophysical parameters to calibrate from 14 to 6, reducing the length of the time-consuming iteration process. The calibration is semi-automatic and uses TRNSYS (Klein et al., 2018) and GenOpt (Wetter, 2016). The 6 sensitive parameters affecting up to 96 % the heat load simulation output of the buildings are (from more to less influent) the infiltration rates; external wall U-value; window U-value; wall specific heat; wall density; furniture heat capacity. Then, to proceed with the buildings' calibration, the researchers gathered as much accurate data as possible on the buildings. They collected weather data from local weather station, building construction and thermal properties, and monitored the heating energy consumption. The stepwise calibration was first done on the thermal parameters, then on the dependent occupancy variables. To calibrate the thermal parameters, they excluded the hour of the day where occupation behaviour is present, namely from 5 am to midnight. After this first step calibration, Li et al. focused on the occupancy related parameters (occupancy density, light power density (LPD), ventilation, etc.). They developed a novel method to create and assign schedules to those parameters. They noticed that these variables randomly fluctuate on a short time basis, while on a longer period their variations were showing similarities. Then, by using a clustering method they created schedules based on randomness and regularity, characterized by 2 different categories of schedules: indoor load schedules and ventilation schedules. The building calibration proved to be accurate and the results were in agreement with the ASHRAE-14 Guideline standards.

2.5 District energy networks

Since our work is in the field of energy sharing networks, it is important to look at the different existing network types and explain their particularities. Lund et al. (2014) have defined the first three generations of district heating/cooling network.

The first generation of district heating networks was developed in the 1880s and used steam, produced in a thermal power station as a heat carrier. This type of network was largely built to reduce the use of individual boilers in buildings and to decrease the number of fire incidents. Moreover, generating a large amount of energy with one system is generally more efficient than generating the same amount of energy with several smaller systems. These systems are now considered as obsolete since high steam temperatures generate large heat losses and severe accidents (*e.g.* steam explosions). The second generation of networks was introduced in the 1930s and was used until the 1970s. These systems used pressurised hot water (over 100 °C) as the heat carrier; the primary motivation to switch from first generation to the second was to increase the efficiency of network, thereby achieving fuel savings, by using a cooler heat carrier (less heat losses) and using cogeneration (also called combined heat and power (CHP), "the concurrent production of electricity or mechanical power and useful thermal energy […] from a single source of energy" (US DOE, 2019b)). The third generation emerged in the 1970s with pressurised water below 100 °C as the heat carrier. This network generation was developed to face the oil crisis and focus on increasing energy efficiency by using CHP and thermal solar plants. The principal enhancement throughout these three generations was to decrease the heat carrier temperature to increase efficiencies in the systems (less heat losses with a lower temperature difference with the outside) and to simplify the construction methods (leaner materials, etc.).

Likewise, Lund et al.'s study mentioned that generations also existed for district cooling networks with a first generation introduced at the end of the 1890s consisting of a centralized condenser and decentralized evaporators with a refrigerant as the heat carrier. The Second generation appeared in the 1960s and used water as a carrier fluid to avoid the use of polluting refrigerants. The water was cooled down by large chillers. Finally, a third generation, always using water as the heat carrier, was established in the 1990s, and uses different cooling systems such as absorption chillers, mechanical chillers, natural cooling from bodies of water (sea, lake, etc.), and cold storage.

With these different definitions, Lund et al. defined a district energy (heating and/or cooling) network as a system of pipes connecting buildings so they can be served from decentralized or centralized thermal plants in heat or cold.

For 4th and 5th generations (4G and 5G respectively), the goal is always to reduce the fluid temperature and reduce the size of the pipes (Averfalk & Werner, 2018) to minimise heat losses. Averfalk et al. (2018) explain that a key to improve the network's efficiency is to retrofit the buildings connected to the network as new high-performance buildings, requiring lower temperature supply to heat the building (and vice versa for cooling). New opportunities for these systems include integrating different renewable systems as energy sources, such as geothermal boreholes, thermal solar plants, and heat storage, which could be a solution to use surplus heat, generated at a specific time, later (e.g. usually energy consumption peaks are during mornings and evenings in residential buildings, but the maximal energy production with a solar system is in between these periods). Similarly, we agree with Lund et al. that new district energy should not be designed for our present energy systems, but for future ones answering by the name of "smart energy systems". The challenge lies in combining and coordinating the electricity, thermal and gas grids to find the synergies between each sector of a neighborhood/city/country.

The main difference between the 4th and 5th district energy network generations is the heat carrier temperature. The 5th generation operates at temperatures between 0 °C and 30 °C (Buffa et al., 2019), allowing this technology to provide simultaneously heating and cooling to different buildings. The 4th generation is usually designed for either heating demands (temperature around 60 °C) or cooling demands. The 5th generation will be more used in neighborhoods with a high diversity of buildings (to balance heating and cooling demands), while the 4th generation networks is chosen if there is a preponderant heating (or cooling) demand. However, both systems accept renewable energy systems and heat waste as thermal sources, helping in reducing the use of primary energy, the main goal of district energy networks. Figure 2.1 developed by Letellier-Duchesne (2019) presents the different generations of district energy network and their particularities.

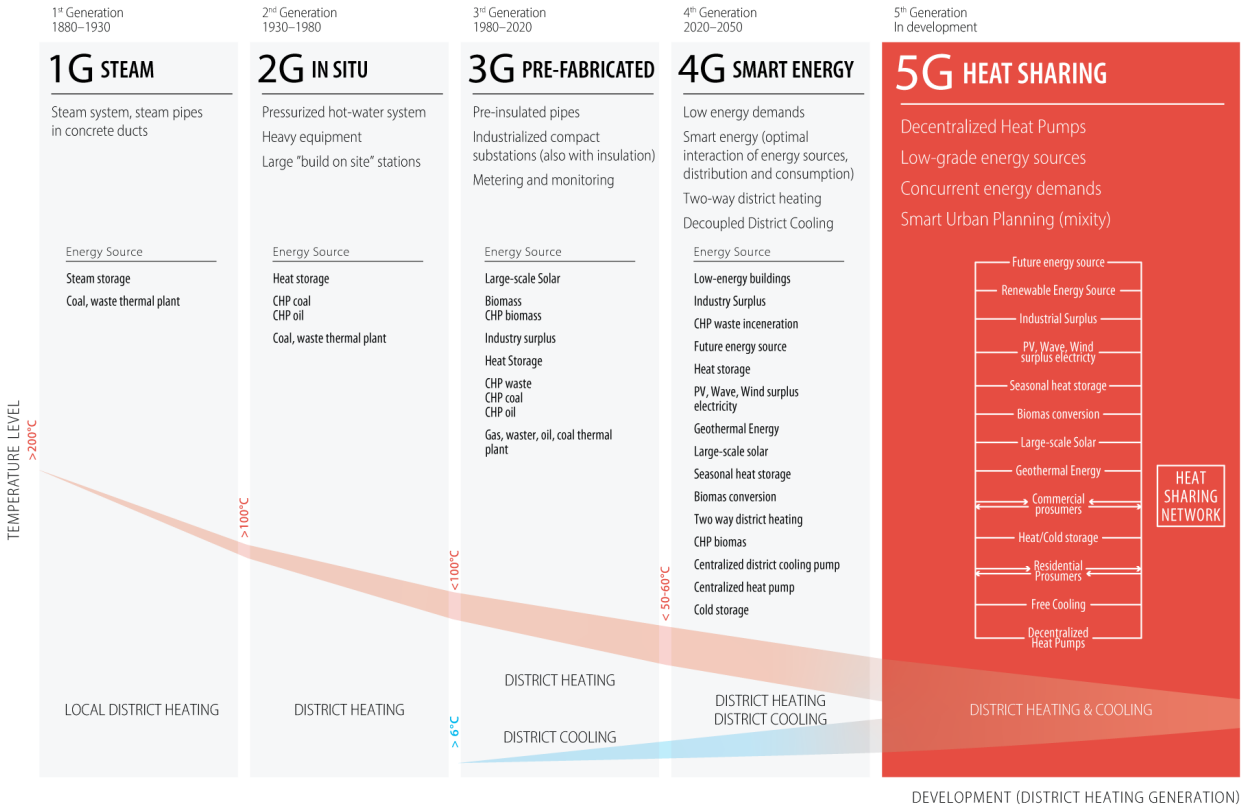

Figure 2.1 - District energy networks from 1st to 5th generation

Finally, part of our work will be to model energy sharing networks. Only a few studies have been conducted using pseudo steady-state or detailed models.

Allegrini et al. (2015) reviewed dynamic modelling methods and used software addressing energy networks system at a building stock scale. Their work gives an overview of models already in use and modelling approaches for district energy networks with the tools (software, plugin, etc.) used to create these models. The authors insisted that to realize a dynamic model of a thermal network, the focus should be on the interaction between the buildings themselves and the network. For low-temperature networks (4G and 5G), TRNSYS is usually used, as well as IDA ICE (EQUA, 2014). Other software exists such as Polysun (Vela Solaris, 2020) and energyPRO (Energy Soft, 2020). In their study, the authors mentioned that the identified modelling methods mainly focussed on a steady-state approach and there is room for improvement by modelling in detail the components of the energy networks (heat pumps, pipes, pumps, etc.), such as using Types 951 or 952 (models of buried pipes) in TRNSYS (TESS library). Filonenko et al. (2019) compared 2 “simulation tools for

district heating applications". Their work is part of the IBPSA Project 1 (2019), which has the goal of creating open-source tools to support design and operation of buildings and district energy network. The paper addresses 2 simulation tools, Termis (7-Technologies A/S, 2012) and Dymola Modelica (Dassault Systemes, 2020; LBNL, 2020), that are used to create pseudo steady-state or dynamic model respectively of a 4th generation heating network. Termis is usually used as a hydronic simulation tool to optimize a thermal network based on historical and real time data. However, Termis shows some limitations in running dynamic simulations or coupling different energy domains. Modelica is a tool specialized for dynamic simulation of multiple physics systems. The study shows that the dynamic tool allows modellers to analyze dynamic results of the thermal network and assess novel technologies for district heating networks. Termis, on the other hand, is used for simplified, pseudo steady-state models that do not model the temporal evolution of the network.

2.6 Summary

In conclusion, several studies have focused on the definition and the different ways of creating archetypes. But there is a lack of expertise in comparing archetypes with different level of detail and using Building Energy Model (BEM) in specialized environments (e.g. TRNSYS) versus urban-level ones (e.g. UMI).

The literature contains studies that focus on improving UBEM methods by coupling CAD software with simulation engine (e.g. UMI) instead of using predefined archetypes simulated independently of their context. However, no detailed investigation on comparing both approaches to create a UBEM has been done.

Finally, published literature has listed the different simulation environments that are able to either statically or dynamically model energy sharing networks and has compared very simplistic models (pseudo steady-state vs detailed) for heating networks but there is little information on comparing pseudo steady-state and dynamic models for more realistic energy sharing networks, which can satisfy heating and cooling loads of a building stock. This confirms the interest of achieving the goals outlined in Chapter 1.

CHAPTER 3 DEFINING ARCHETYPES

3.1 Introduction

Modelling individually each building in a city, or even in a neighborhood, would be an extremely time-consuming task and would require to obtain detailed information on each of these buildings, from geometry and construction data to operating schedules. This is generally not feasible, so UBEM approaches rely on archetypes that represent “typical” buildings in the studied neighborhood or city. The main objective of this chapter is to compare different urban-level models of selected buildings (residential and commercial) with measured data. This chapter is based on a paper published at the IPBSA – Building Simulation 2019 conference (Leroy, Letellier-Duchesne, & Kummert, 2019).

Successive refinements of the archetypal characterizations are implemented in UMI (see description next paragraph) and the energy consumption at the building level is compared with the measured data. For residential buildings, the measured data was provided by the inhabitants of the individual houses. While the measured data for the commercial building was obtained from Hydro-Québec as part of example files provided with SIMEB (Hydro-Québec, 2019b). The results are compared with archetypes developed by the US-DOE (known as *Prototype Building* (US DOE, 2019a)), ran in EnergyPlus (US DOE - BTO, 2019). Results are also compared with detailed and calibrated models developed in TRNSYS (Klein et al., 2018) for residential buildings and SIMEB for commercial building that represent the "best possible model". The increasing accessibility of measured data (for example, smart meters) offers new opportunities to calibrate models at different time scales, from annual Energy Use Intensity (EUI) to hourly electricity consumption. However, important challenges persist, especially with high-uncertainty parameters, such as occupancy based variables (schedules, etc.) (Heiple & Sailor, 2008).

UMI (Urban Modelling Interface (C. Reinhart, 2019)) is one of the few available state-of-the-art UBEM environments. The program is implemented as a Rhinoceros-based plugin, relying on the well-known 3D modelling environment (Robert McNeel & Associates, 2019) for geometrical aspects and implementing “templates” which contains non-geometric properties of the archetypes. Energy modellers are used to seeing archetypes as full 3D models with specific zoning schemes,

orientations and façade elements (e.g. windows), and even a full description of the HVAC system (see for example (US DOE - BTO, 2018)). UMI defines archetypes in a slightly different way. Archetypes defined in the template contain only non-geometric properties. Building shapes are created inside Rhino (for example using "2.5D" extrusions from building footprints) and WWRs are specified by the user. This geometrical information is then combined with the "template" information into an EnergyPlus model to solve the energy simulation (US DOE - BTO, 2019). The developers of this tool have proposed an original approach to handle thermal zoning: UMI creates distinct smaller finite volumes, called "shoeboxes"—at least 1 per orientation—depending on the chosen template, WWR and solar incidence. The shoeboxes are then simulated independently, and the building-level energy performance data is obtained by a weighted sum of the shoeboxes comprising that building. Systems are not explicitly modeled, and constant COPs are used instead. For more information on UMI, extensive documentation on the operation and use of UMI has been produced by the MIT Sustainable Design Lab (2017) and is available at the following link: https://umidocs.readthedocs.io/en/latest/index.html .

Furthermore, UMI is designed as an Application Programing Interface (API) to help the development of complementary modules. For example, the investigation of district-level energy supply scenarios is developed in the work done by Letellier-Duchesne et al. (2018).

3.2 Methodology

3.2.1 Selected buildings

Four all-electric buildings for which metered hourly energy use was available, have been selected: one medium-sized commercial building (offices), and three single-family residential buildings (row townhouses or condominium units). The 3 residential buildings have the following characteristics:

- House 1: row house, 188 m² floor area, 2 floors above ground, typical recent construction (relatively recent retrofit), occupied by a family of 4.
- House 2: housing unit within a row house, ground floor with an unoccupied (and unheated) basement, 94 m², occupied by a family of 4, typical older construction (no energy retrofit). Another housing unit is located above.

- House 3: row house with 2 floors above ground and an occupied basement, 150 m², occupied by 3 persons, typical older construction.

Those characteristics were retrieved from the design of the houses provided by the inhabitants and Google Maps views.
These 3 houses are all-electric, and hourly metered electrical use was obtained for one full year.

The commercial building is an all-electric 8-story building with 5600 m² floor area, mainly used for offices, with a relatively good building envelope. Meter data was obtained from a Hydro-Québec case study (Hydro-Québec, 2019b).

3.2.2 Predefined archetypes with floor area scaling

A simple method to obtain an estimate of the dynamic energy use of a large number of buildings is to associate each building with a reduced set of predefined archetype, normalize the simulated energy use of the archetype per floor area, and multiply that value by the floor area of the original building. The Prototype Buildings proposed by the US DOE (2019a) can be used for that purpose. In this case, the all-electric "single family without basement", "single family with unheated basement", "single family with heated basement", and "medium office" archetypes were selected to model the House 1, House 2, House 3 and the commercial building respectively. The archetypes performance levels correspond to the energy codes discussed in section 3.2.3.2.

3.2.3 Urban-level building models implemented in UMI

As mentioned in the chapter's introduction, UMI isolates the geometric characteristics of the building from its thermal parameters such as envelope thermal properties, internal gains, etc. The building's geometry is defined in Rhino and the WWR of each selected buildings is specified from collected information.

This section will present refinements in UMI models, consisting of modifying the "template" description. Only 2 templates are used, a residential building and an office building. The successive levels of refinement for UMI models are using:

- default parameters, which were obtained for a different local context;
- local building energy code parameters;

- statistical data on the thermal characteristics of buildings at the regional level;
- the calibrated parameters from the detailed models;
- selected adjusted parameters (see below).

3.2.3.1 UMI Default Model

UMI is developed at the MIT in Cambridge, MA (USA). The actual climate zone and the urban morphology are therefore different from those of Montreal, but both are North-American cities in a relatively cold climate (ASHRAE zones 5 for Cambridge and 6 for Montreal (2013)). Then, the predefined archetypes are an acceptable first step for a user trying to model a neighborhood in Montreal. The templates "B_Off_0" (office building) and "B_Res_0_WoodFrame" (residential building) were selected and used without adjustment. It should be emphasized that UMI developers do not recommend the use of default templates in a different context and that is certainly not good practice. But, from the perspective of the authors this is a good approximation of how beginners and non-experts users would use UMI.

3.2.3.2 UMI templates with data from building energy codes

Building energy codes are often used as a proxy in building stock modelling efforts. In Canada, the national CanmetEnergy research laboratory has adapted prototype buildings for various building energy codes (CanmetENERGY, 2019). Energy models for 16 different commercial buildings—the same as their American counterpart (Deru et al., 2011)—offer the modelling parameters for this set of commercial building UMI templates. More precisely, the modelling assumptions for these models are taken from the 2011 Canadian “National Energy Code for Buildings (NECB)” (NRC-IRC, 2011).

On the residential side, modelling assumptions from the IECC prototype buildings (US DOE, 2012) are used. For their similarity in construction types and equipment performance, the Vermont single-family residence (SFR) were selected as the base for this set of residential templates. Some assumptions were adapted to fit the imposed format of UMI templates: the different internal gains specified in IECC archetypes were summed and their respective schedules averaged by nominal weight.

3.2.3.3 UMI templates with statistical performance data

The third modelling assumption do not rely on building energy codes, but on statistical data (collected survey data). For the single-family residential buildings, the Energuide database (Natural Resources Canada, 2018) was used. This survey gathered pre- and post-retrofit detailed parameters (e.g. constructions U-value, etc.) for around 460 000 houses across Canada. The data is sorted by dwelling type in 11 different categories (apartment, row house, semi-detached/detached, etc.) Thermal parameters such as U-values, infiltration rate, HVAC system types, occupancy, etc. for the selected houses are available in the database, allowing us to create a set of UMI templates with those statistics. To compare different archetypes of residential buildings, we use this database to create a "weighted average" archetype based in Montreal, QC. The term “average” is used here, because for each characteristic needed (wall insulation, roof insulation, infiltration rate, window’s loss coefficient, window’s Solar Heat Gain Coefficient (SHGC) and visible transmittance, and number of occupants) we calculated a mean value weighted by the number of different types of housing (see Eq. 1).

$$WA = \frac{\sum_{i=0}^{n}(x * n_{house})}{\sum_{i=0}^{n}(n_{house})} \quad (1)$$

Where x is the value of a characteristic and n_{house} is the count of houses having the same value for this characteristic. “WA” stands for “Weighted Average”. A total of 7624 single-family residences were used to calculate average values for each archetype’s properties.

The Energuide database define windows with 6-digits codes (Hawk-Eye, n.d.), referring to the Hot2000 software program developed by Natural Resources Canada (2019). The first digit indicates the type of glazing (single, double, etc.), the second indicates the coating/tint type (Low-e, reflective, etc.), the third defines the fill type (13 mm air, 9 mm argon, etc.), the fourth digit describes the spacer type (metal, insulating, etc.), the fifth indicates the window type (picture, hinged, etc.), and finally, the last digit defines the frame material (aluminum, wood, vinyl, etc.). The 40 most frequently used windows (which represent 80 % of the database) were selected and modelled in WINDOW (LBNL, 2013) to get the equivalent SHGC, U-values and visible

transmittance. Those characteristic were then used as building parameters to calculate a weighted average.

3.2.3.4 UMI with calibrated parameters from detailed models

As indicated in the chapter's introduction, calibrated detailed models were developed to provide the "best achievable modelling accuracy". It seemed logical to transfer the calibrated parameters from the detailed models to the UMI template, in order to improve their accuracy. Typical daily, weekly and yearly schedules were created from the calibrated models to define the scheduled parameters such as domestic hot water (DHW) consumption, and lighting and equipment energy use. Equipment and lighting consumptions were gathered into one category (ALE) in UMI to facilitate data input. For the commercial building, a simple cubic geometry was inferred from the non-geometrical DOE-2 description of the building.

3.2.3.5 UMI model with adjusted parameters

The chapter's results section will show that some results from UMI model using calibrated parameters were worse than other UMI models using less refined parameters. We suggest that canceling errors might be at play both in the detailed calibrated and UMI models, so that "fitted" parameters for specific aspects cannot be transferred between models. An example of canceling errors would be to underestimate the infiltration rate and compensate the thermal gain by reducing the window U-value. Then, providing those calibrated parameters from a model to another one having a more correct infiltration rate would deteriorate the model performance. In order to still obtain an ***adjusted*** (if not fully calibrated) version of the UMI models, a last variant of the archetype templates was developed in which the infiltration rate (a usual target for rough "calibration") was adjusted to match the yearly energy use of the measured data.

3.2.4 Detailed models

The detailed reference models represent the best practices in modelling individual buildings, with a level of detail that would not be in line with urban modelling. They were added to the comparison in order to obtain an educated guess of the energy end-use breakdown, and to offer an upper target for the accuracy of urban-level models.

A detailed SIMEB model from an Hydro-Québec case study was used for the commercial building. 3 functional zones were defined : office, corridors and server/computer rooms. SIMEB can use different computational engines, and the DOE-2 engine was selected in this work. Basic assumptions representing typical constructions were used to define the thermal properties with a thermal resistance of 3 m²-K/W for exterior walls and of 4.75 m²-K/W for the roof, and windows with heat loss coefficient of 3.2 W/m²-K.

For the residential buildings, TRNSYS was used to develop individual detailed models of each house. The 3D geometry of the buildings was entered in SketchUp. Basic assumptions representing typical constructions were used to define the thermal properties in a multizone building model (TRNSYS Type 56). The lighting and equipment consumptions (Appliances, Lighting and Equipment, ALE in the following) were determined through calibration as one of the 23 electric measured profiles published by Johnson and Beausoleil-Morrison (2017). Likewise, DHW energy consumption was selected from one of the 12 measured profiles published by Edwards et al. (2015).

3.2.5 Model calibration

3.2.5.1 Methodology

Calibration was performed through an iterative trial-and-error process where simulation results were compared with hourly electric (all buildings are all-electric) measured data at the building level. The adjusted parameters were the infiltration rate, the wall insulation layer width, and the ALE and DHW energy consumption selected from Johnson et al. and Edwards et al. measured profiles (see Figure 3.1).

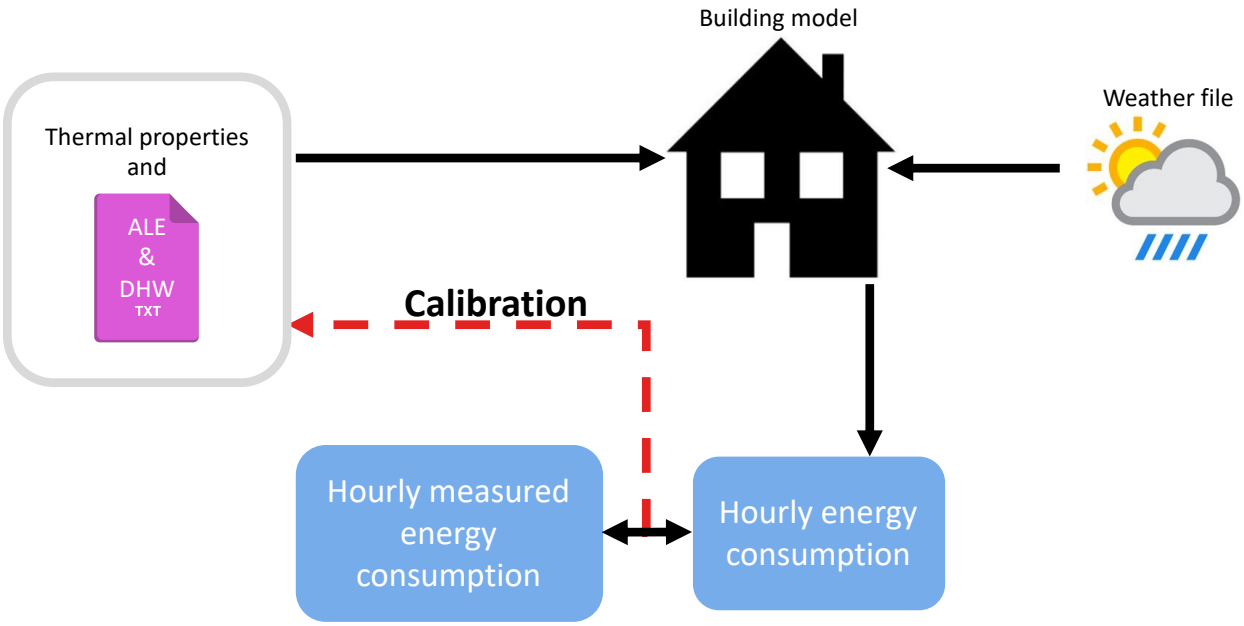

Figure 3.1 – Schematics of building calibration

Weather files were matching the year of the measured data and were gathered from Hydro-Québec's SIMEB website (2019b) for the nearest weather station.

Envelop structure and thermal properties were obtained (indirectly) from the inhabitants and show some similarity with typical local construction.

For occupancy, schedules depending on the hour of the day and the day of the week from the U.S. Department of Energy (2018) were used.

Space heating represents a major share of energy use in Montreal's climate, so a first method to assess a model calibration is to represent the overall energy use of a building versus the ambient temperature. Hourly or daily values produce a scatter plot that can generally be fitted by a broken line: a horizontal section representing the baseload (average value of non-heating electricity use in the building), and a sloped section representing the heating-related energy use. Figure 3.2 helps us understand these notions by presenting the comparison of the daily average energy power, function of the outdoor temperature (Tout), between the model and the measured data from the utility. The heat loss coefficients are represented by the slopes of the left part of the broken lines, and the baseline power (usually ALE power) are represented by the flat part of the scatter plot, with an average of 1.05 kW/day for the measured data for the residential building "House2".

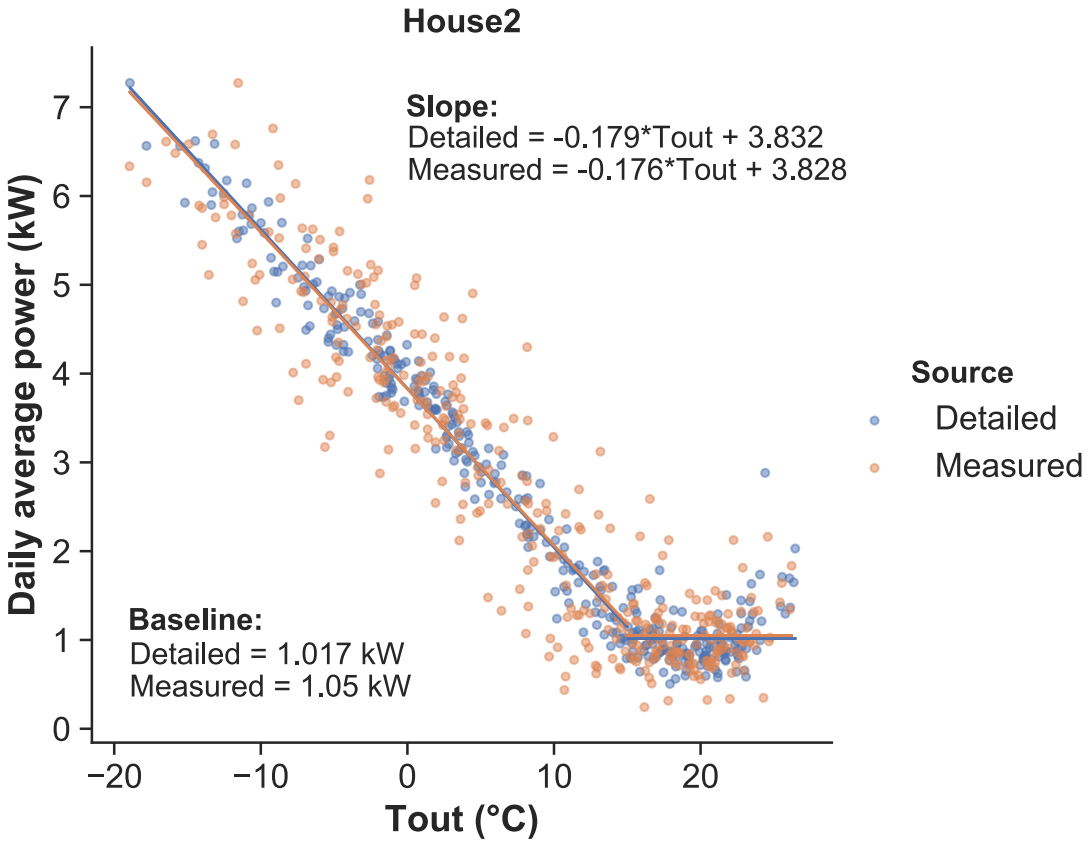

Figure 3.2 – Comparison of energy consumption, function of the outdoor temperature, between the model and the measured data to determine heat loss coefficient and baseline consumption

To check the calibration results, we used the prevalent statistical coefficients suggested by the ASHRAE Guideline 14 known as the normalized mean bias error (NMBE) and the coefficient of variation of the root mean square error (CVRMSE). They are determined as followed:

$$NMBE = \frac{\sum_{i=0}^{n}(y_i - \hat{y}_i)}{(n-p) * \bar{y}} * 100 \quad (2)$$

$$CVRMSE = 100 * \left(\left[\frac{\sum_{i=0}^{n}(y_i - \hat{y}_i)^2}{(n-p)} \right]^{1/2} / \bar{y} \right) \quad (3)$$

Where y_i is the measured datum, $\hat{y}_i$ the simulation predicted datum, $\bar{y}$ the mean value, and n the number of data points. For Eq. 2 p=0, while for Eq. 3 p=1 (ASHRAE, 2014).

The following table (Table 3.1) lists the acceptable range as stated by the guideline to ensure good model calibration (ASHRAE, 2014).

Table 3.1 − ASHRAE-14 ratios ranges to verify building calibration

	Hourly	**Monthly**
NMBE	10 %	5 %
CVRMSE	30 %	15 %

3.2.5.2 Calibration results

After calibrating different single-family apartments (3 terrace houses) and one office building, we obtain accurate slope and baseline as shown in Figure 3.2 for each case (3.5 % difference max). Furthermore, Table 3.2 present the maximum values of the hourly and monthly NMBE and CVRMSE obtained for residential and commercial sectors.

Table 3.2 − ASHRAE-14 ratio results for building calibration

	Residential		**Commercial**	
	Hourly	Monthly	Hourly	Monthly
NMBE	1.87 %	1.87 %	3.61 %	3.61 %
CVRMSE	59.4 %	9.06 %	30.3 %	6.52 %

We notice for the residential buildings that the calibration shows some limitations. All NMBE values are within the guideline recommendations, as well as monthly CVRMSE values. But the hourly CVRMSE is over the limit, hinting that the good monthly fit may result from canceling

errors. (e.g. overestimating the U-value of windows but compensating the extra thermal losses by a reduced infiltration). Table 3.3 summarizes the parameters used in each model.

*Table 3.3 − UMI parameters for different archetype versions. *Infiltration rates: first line for detailed archetypes, second line for adjusted archetypes*

Archetype parameters		Residential buildings						Commercial building		
		UMI Default	UMI Code (IECC)	UMI Statistics (EnerGuide)	Detailed Calibrated House1	Detailed Calibrated House2	Detailed Calibrated House3	UMI Default	UMI Code (NECB)	Detailed Calibrated
Geometric parameters										
WWR	-	Determined for each house depending on their geometries. House1: 30 %, House2: 20 %, House3: 10 %						40 %		40 %
Dimensions	-	Real geometry/shoeboxer			Real geometry / multizone model			Real geometry/shoeboxer		Not geometric/model by functional zone
Non-geometric parameters										
U value (W/m^2-K)	Walls	0.35	0.32	0.50	0.22	1.02	0.43	0.48	0.49	0.33
	Floor	1.41	0.18	0.90	0.22	1.08	0.44	1.41	0.29	0.29
	Roof	0.30	0.16	0.29	0.23	1.49	0.49	0.31	0.18	0.21
Window	U value (W/m^2-K)	3.17	1.82	2.66	2.82	2.82	2.82	3.166	2.2	3.18
	SHGC (-)	0.76	0.40	0.62	0.64	0.64	0.64	0.757	0.6	0.42
	Tvis (-)	0.80	0.88	0.64	0.65	0.65	0.65	0.797	0.21	0.6
Occupancy density (p/m^2)	-	0.0250	0.0134	0.0188	0.0212	0.0217	0.0198	0.055	0.05005	0.05
ALE power density (W/m^2)	Equipment	4.00	6.53	6.74	15.72	37.00	22.50	8	7.5	7.53
	Lighting	7.00	1.70	2.84	-	-	-	12	11	11.3
Heating	Setpoint (°C)	20	22.22	20.1	20.1	20.1	20.1	20	22	22
	COP (-)	1	1	1	1	1	1	0.9	0.8	1
	Limit capacity (W/m^2)	-	-	-	-	-	-	-	60.88	-
Cooling	Setpoint (°C)	24	23.88	-	-	27	-	24	24	23
	COP (-)	3	3	-	-	3	-	3	4.8675	3.52
	Limit capacity (W/m^2)	-	-	-	-	-	-	-	60.78	-
	On/Off	On	On	Off	Off	On	Off	On	On	On
Infiltration (ACH)	(1/h)	0.350	0.303	0.391	0.20* 0.25*	0.82* 0.30*	0.70* 0.13*	0.35	0.57	0.45
Ventilation	m^3/s-m^2	-	-	-	-	-	-	0.0003	0.0003	0.004634
	m^3/s-p	-	-	-	-	-	-	0.0025	0.0025	0.0093
DHW	Supply temp (°C)	55	49	50	56.5	56.5	56.5	55	60	50
	Consumption (L/day-m^2)	1.44	0.14	1.16	0.66	1.32	0.73	0.72	0.025	0.11

3.3 Results

The results presented below were obtained from the scaled prototype buildings and the successively refined UMI models and are compared to the detailed (and calibrated) simulation results and the total measured energy consumption.

3.3.1 Annual Energy Consumption

The results in this section (see bar plots, Figure 3.3) present the yearly energy consumption per end-use (except for the measured data for which only the total is known). For the 3 residential buildings, measured values show a large variation in energy intensity, from 90 kWh m^{-2} y^{-1} to 240 kWh m^{-2} y^{-1}. Populating UMI archetypes with code or statistical values can deliver a reasonable approximation (House 3 for code, House 2 for statistics) but can also lead to very large differences. The largest difference is observable for House 2 with a total EUI ranging from 144 kWh/m^2-year to 320 kWh/m^2-year. Archetype differences related to the geometry (for each buildings), such as WWR, external vs. adjacent walls/ceilings, envelope-t-floor area ratio, etc. exist but are minor, so that the UMI archetypes give similar results for the 3 houses when using the same parameters (compare e.g. the UMI code results for the 3 houses). Populating UMI archetypes with code or statistical values can deliver a reasonable approximation (House 3 for code, House 2 for statistics) but also lead to very large differences (House 1 for code and statistics).

The scaled prototype buildings deliver a good approximation of the total energy consumption for House 2 and House 3 but a large overestimation for House 1. These results are different from the UMI results using the same parameters (UMI Code, which also uses the IECC 2012 code).

It is also interesting to note that applying the “best guess” thermal parameters (i.e. calibrated values from the detailed models) to the UMI archetypes can in fact lead to larger errors (see Houses 2 and 3). As discussed above, canceling errors are probably at play in all models, but in different ways. But it is surprising that the differences between the detailed model and the UMI archetype using the same parameters can go from a slight underestimation (House 1) to a very large overestimation (House 3) of the heating load.

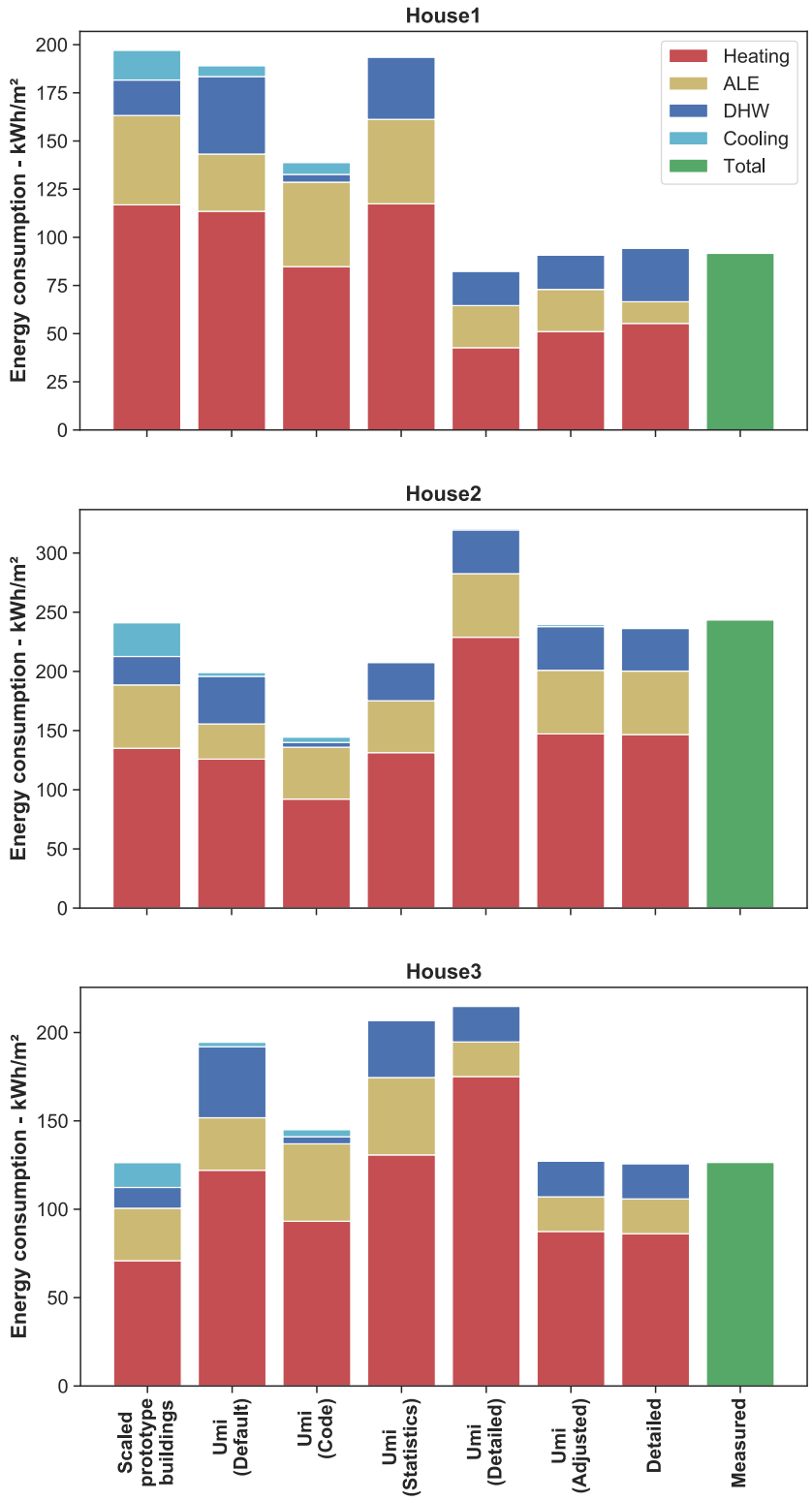

Figure 3.3 − Total end-use energy consumption per square meter area for residential buildings (Top: House 1, Middle: House 2, Bottom: House 3)

For the medium office building (Figure 3.4), the most striking difference between UMI archetypes and the detailed model is the absence of fans and pumps. The UMI approach ignores HVAC systems and applies fixed COPs *a posteriori*, so degrading the COP could probably lead to a better approximation of the total energy, but the heat / cold / electricity ratio would still be poorly estimated, which is a disadvantage for district energy studies. The impact of fan power on the heating and cooling load is also missed. Because of these aspects, no attempt was made to adjust infiltration in the UMI model to match the total energy use, so there is no "UMI (Adjusted)" model for the office building. The comparison between the scaled prototype building (first bar) and the detailed model (second to last bar) shows that the SIMEB model assumes a much larger energy use for pumps and fans.

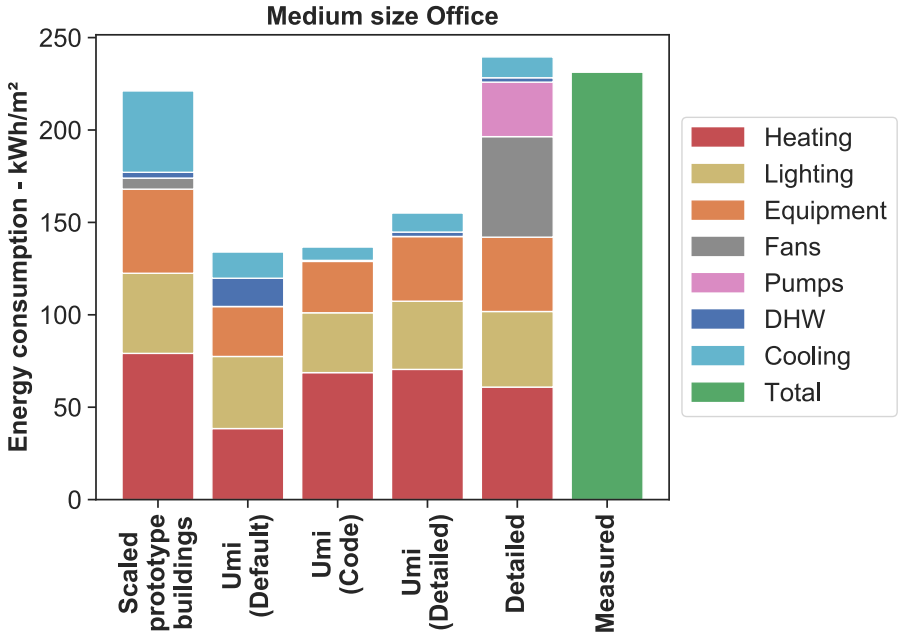

Figure 3.4 – Total end-use energy consumption per square meter area for a medium size building office

Yearly results show large variations between each archetype developed for the residential and commercial buildings between the different buildings and when comparing the archetypes for the same building (e.g. House 2, Figure 3.3 middle), especially for UMI variants. One of the reasons for the variability in UMI is that the software does not take into account ground heat transfer or adiabatic surfaces between buildings for row houses (in this study, residential buildings are all row houses). UMI then considers that those surfaces are directly in contact with the outside

environment, which has thermal characteristics (temperature, solar radiation, etc.) with higher variability than an adiabatic surface for example.

3.3.2 Daily Energy Use

Figure 3.5 shows the daily average energy use for different residential models (House 3), for a selected winter week. The UMI and US-DOE archetypes all show a strong variation between the week days, with a slow decrease during the week. This variation is not apparent in the measured energy use nor in the detailed model. Using adjusted values improves the goodness-of-fit but does not remove this – apparently incorrect – trend.

Figure 3.6 shows the daily average energy use for the office building during a winter week (Feb 2 and 3 are Saturday and Sunday). Schedules and the missing fans/pumps category (see above) cause large differences between the UMI archetypes and the detailed model.

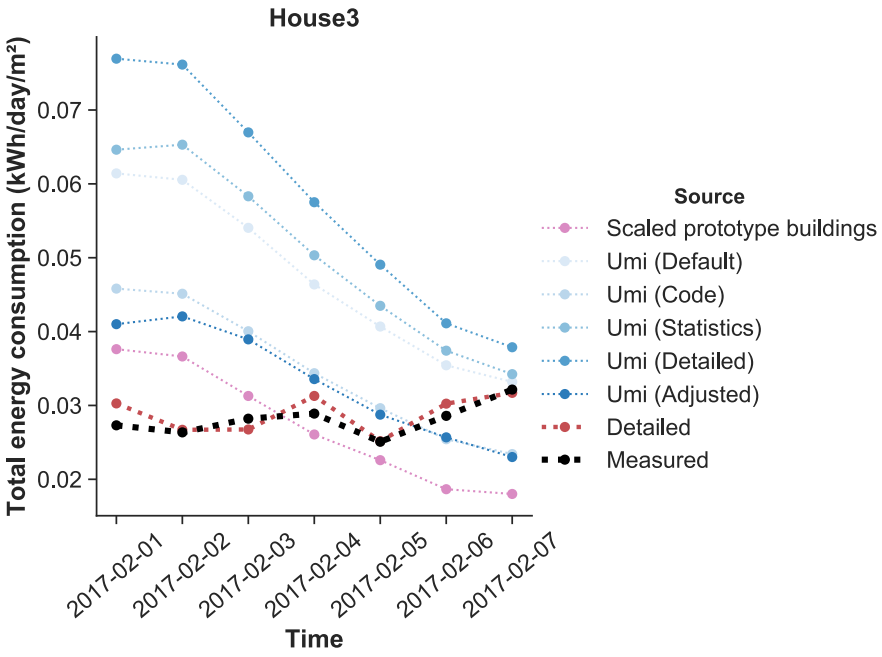

Figure 3.5 – Average daily energy consumption of a residential building for a winter week

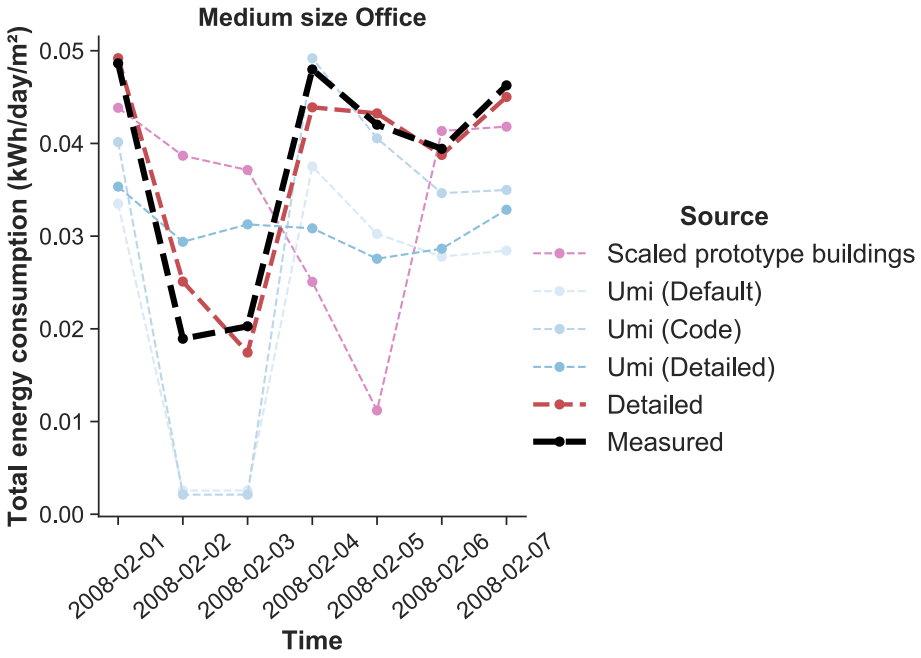

Figure 3.6 – Average daily energy consumption of a commercial building for a winter week

3.3.3 Hourly Energy Use

Figure 3.7 shows the hourly energy use for a winter day (February 2nd 2017) in House 3. The graph shows that UMI archetypes seem to underestimate the dynamic variations of heating load over the day.

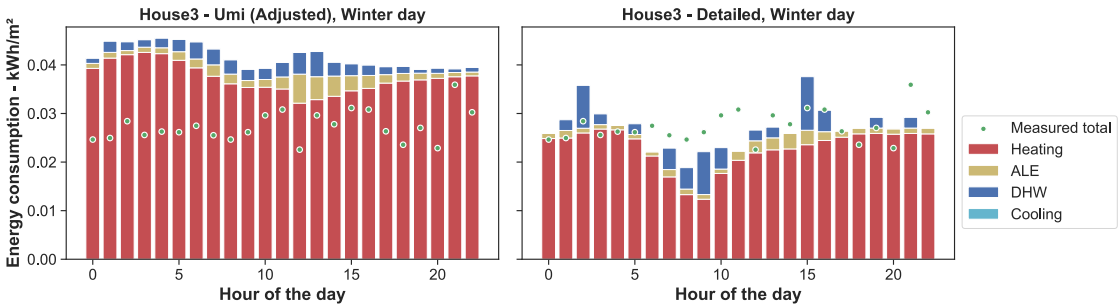

Figure 3.7 – Hourly energy consumption of a residential building for a winter day

Figure 3.8 shows a winter weekday for the office building. Even though schedules were adapted in the UMI archetypes, the dynamic profile seems largely off, partly because of the missing fans/pumps energy use, but also partly because of an apparent difference of the heating load during occupied hours (increasing in the detailed model, decreasing in the UMI archetype).

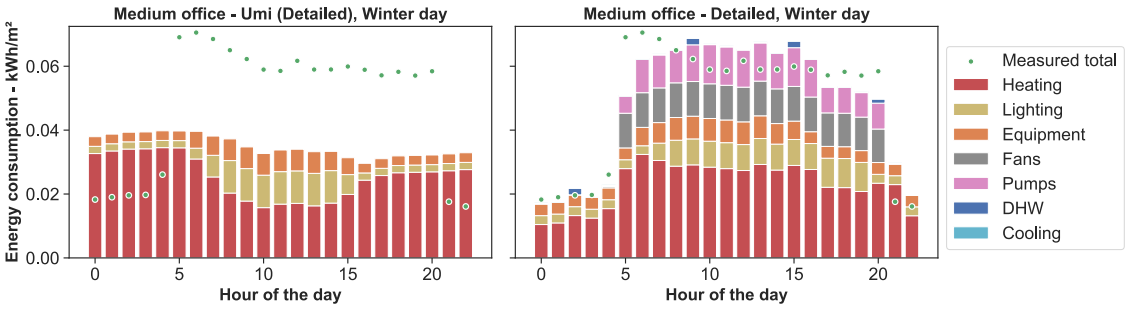

Figure 3.8 – Hourly energy consumption of a commercial building for a winter day

3.3.4 Load duration curves

In the context of this thesis, urban energy models are used to assess district energy scenarios. The heat load duration curve, which presents the number of hours that a given load is exceeded, is a useful representation of the dynamic district load to perform optimization studies (Letellier-Duchesne et al., 2018) Figure 3.9 presents load duration curves of the heat loads (space heating and DHW) for the residential buildings (the 3 houses were aggregated in these curves). The UMI Default, Statistics, and Detailed variants largely overestimate the annual heating energy, so the load duration curve is always above the one for the Detailed model. But adjusting the UMI parameters to match the yearly load seems to lead to a duration curve that underestimates the early part of the duration curve (higher loads) and overestimates the duration of lower loads. This confirms that adjusting the yearly energy use does not guarantee a better estimation of the dynamic energy use, which is important for energy flexibility and district systems studies. The scaled US-DOE Prototype building (blue curve) follows the same trend as the UMI "adjusted" variant.

Figure 3.10 shows the same load duration curve (space heating + DHW) for the office building. In this case the annual heat load is not very far from the results of the Detailed model (see Figure 3.4), but the load duration curve shows very large deviations, once more showing that a reasonable annual heating load estimate does not guarantee that the dynamic profile will be correctly estimated. A striking difference is also apparent in the peak hourly load, which ranges from 73 W/m² (Detailed) to 220 W/m² (UMI Default). In order to get a reasonable approximation of the hourly peak load at the neighborhood level, diversity would need to be addressed in all cases (including for the Detailed model) to study the impact of thermal parameters on dynamic results. But there is no easy way to do this in the current UMI user interface, which focuses on obtaining

annual and monthly energy performance indicators. However, one could introduce diversity using two methods, the first manually and the second parametrically. In the first method, users produce template variations by enforcing different parameter ranges. The second method involves the use of the parametrical development plugin, Grasshopper, another Rhinoceros's plugin. The measured data only provides the total energy use, not the share of heating and DHW, so load duration curves were plotted for the total energy use.

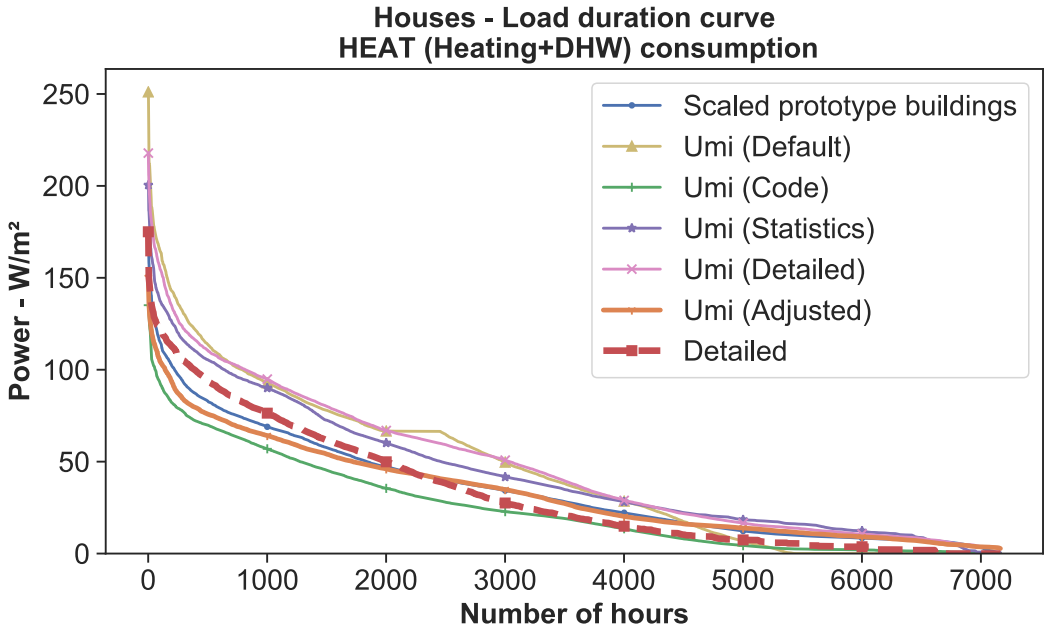

Figure 3.9 – HEAT (Heating+DHW) load duration curve for the 3 residential buildings (combined)

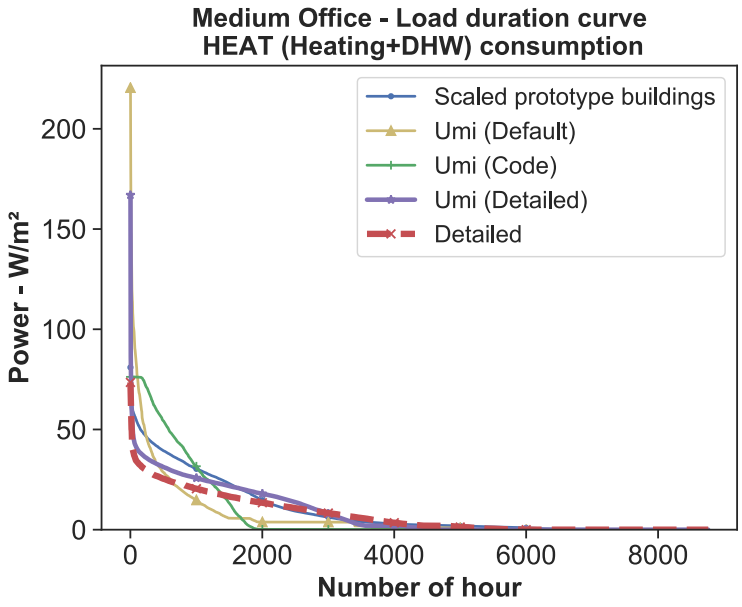

Figure 3.10 – HEAT (Heating+DHW) load duration curve for a commercial building

3.4 Conclusion

Archetypes used in Urban Building Energy Modelling (UBEM) approaches do not intend to represent individual buildings accurately, but they should provide a reasonable estimate of aggregated energy performance indicators. Their parameters must be adapted to represent the local context, and different data sources are typically used for that purpose: building codes, statistical data, and measured energy use. The hourly energy use profiles of different archetype parametrizations were obtained for selected residential and commercial buildings in UMI, a state-of-the-art UBEM environment. These results were compared to scaled prototype buildings modeled in EnergyPlus and detailed simulation models developed in other simulation tools (TRNSYS and SIMEB using the DOE-2 engine), as well as to hourly measured data.

The results show that archetypes using more refined estimates of thermal and building usage parameters do not necessarily deliver better results for the selected buildings, hinting that canceling errors may be at play (both in the urban-level and in the detailed models). This can be problematic when studying building retrofit options (e.g. insulation), because physical parameters might be poorly calibrated. One practical conclusion is that parameters obtained from calibrated detailed models cannot be directly transferred to archetypes.

UMI archetypes used in this work were shown to deliver reasonable annual energy use results, in line with the tool focus, with two caveats. UMI archetypes seem to react differently from detailed models to changes in boundary conditions (external vs. adjacent walls, and contact with the ground). The simplified modelling approach, which focuses on envelope and solar aspects and adopts fixed COP values to represent HVAC systems, leads to the absence of some energy end-uses, such as fans and pumps, which can be significant in commercial buildings.

The scaled US-DOE prototype buildings require little effort to define and simulate the models, and show good results (in fact better than most UMI variants) except for House 1.

Hourly profiles were assessed by comparing representative days and load duration curves, which are relevant for district energy studies. The hourly results show large differences between the urban-level archetypes and detailed models, indicating that there may be a need to improve the modelling approach if the aim of urban-level analyses evolves from assessing annual indices to assessing energy flexibility and dynamic grid interaction at the neighborhood or city level. Further work should aim at generalizing the results of this study, based on a very small number of buildings, and further investigating differences between detailed and urban-level models.

CHAPTER 4 CASE STUDY: ASSESSING HEAT-SHARING NETWORK OPPORTUNITIES IN A MONTREAL NEIGHBORHOOD

4.1 Context

This chapter presents the case study that will be used in the next two chapters discussing the Urban Energy Model and the district energy system model. It is largely inspired by a real study commissioned by the Ville-Marie borough in Montréal (Écohabitation, 2019). The author participated in the project team where he was responsible for modelling the buildings and district energy scenarios.

The considered neighborhood is currently undergoing significant redevelopment, with over 1.2 million square meters of floor area to be built over the coming years. The borough wanted to assess the potential of heat-sharing networks to reduce the carbon footprint of the newly developed buildings and to avoid rejecting heat in the ambient air while improving resilience. The study included a variant where a large data centre would be located on the site, and all results presented in this thesis assume the presence of that data centre. One objective of the study was to assess the impact of all scenarios on the peak electrical demand at the neighborhood level.

4.2 Building stock

The study in question is on the construction of a new neighborhood (the *Faubourgs* neighborhood in *Ville-Marie* district, Montreal). A top view of the neighborhood is presented in Figure 4.1, with the different blocks representing 3 sites (*Radio-Canada*, *Molson*, *Portes Sainte-Marie*) with 126 buildings spread over 20 blocks. The block numbers in the Figure refer to their site, so there are 3 “number 1” blocks, etc.

Figure 4.1 – Modelled sites and blocks

Figure 4.2 shows a 3D view of the modelled buildings. Blue represents residential units, red represents commercial activities, and yellow represents offices. This 3D model was obtained from the Ville-Marie borough as a Sketchup model and was imported into Rhino.

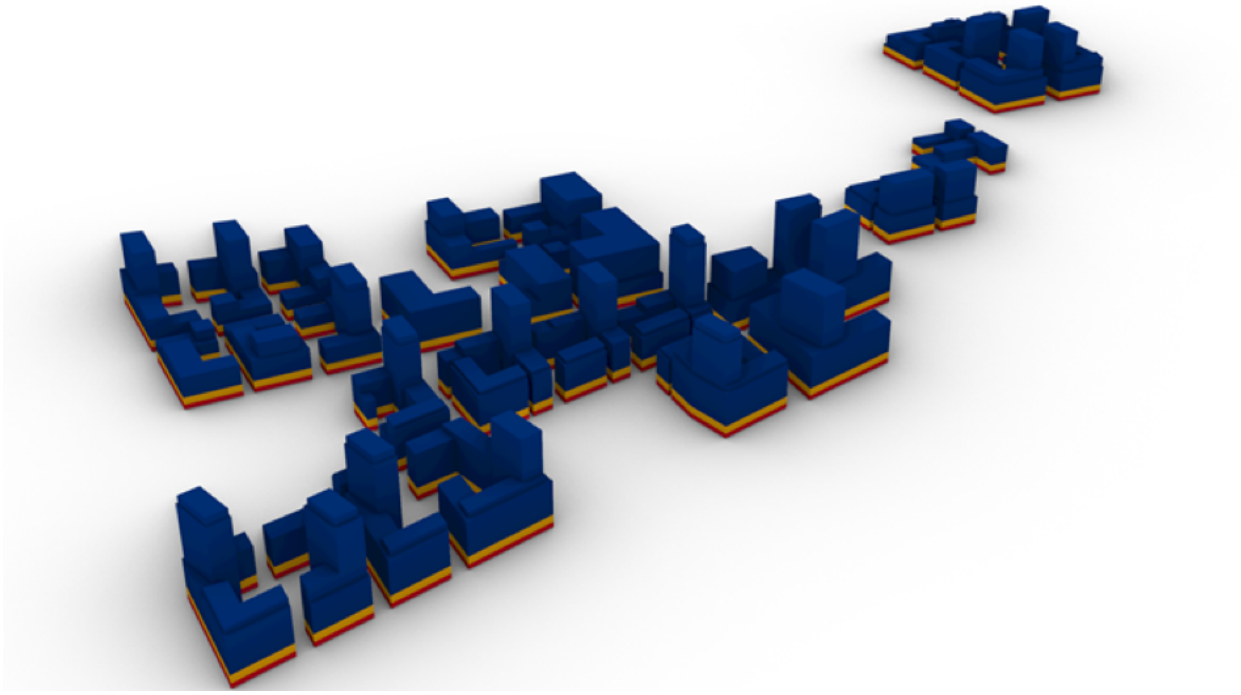

Figure 4.2 – 3D view of modelled buildings

Figure 4.3 shows the breakdown of building's usage based on the targets defined by the Ville-Marie borough (75 % residential and 25 % commercial/office). Each building has a 4 m high commercial floor (the ground floor), 2 floors of 3 m high offices (floors 1 and 2), and a variable number of 3 m high residential floors (floor 3 to the top). The height of each building was assumed to be the maximum permissible height according to current urban planning regulations. The total surface floor area covers 1.2 million square meters.

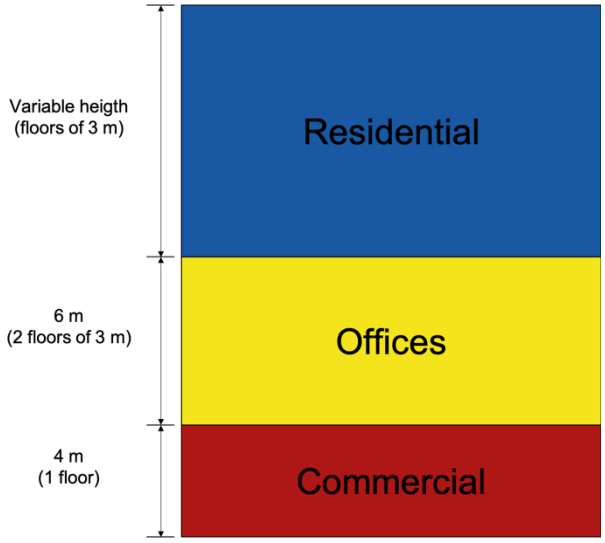

Figure 4.3 − Breakdown of building's usage

4.3 Data centre

Attracting data centres to the Province of Québec is one of the key measures in Hydro-Québec's 2016-2020 strategic plan (Hydro-Québec, 2016), with a target of 2.3 million square meters of floor area. Locating some of these data centres in Montréal is also an objective, as the city was voted as the best place to set up a data centre in 2019 (Hydro-Québec, 2019a).

The assumptions on the data centre included in the study are the following: the data centre has a constant electrical power demand of 12 MW for computer equipment and all accessories, not including the air conditioning system, it has its own cooling equipment (depending on the presence of an energy sharing network or not in the neighborhood), and its heating demand is neglected.

CHAPTER 5 URBAN BUILDING ENERGY MODEL

This chapter presents and compares the results of two urban building energy modelling approaches, a context-free method based on predefined archetypes scaled by floor area and a context-dependent method using UMI.

5.1 Model assumptions

As mentioned in Chapter 4, the data centre is assumed to have a constant cooling load equal to 12 MW. The building is not modelled, this constant cooling load is simply added to the results of other buildings.

The buildings shown in Figure 4.3 are modelled by archetypes derived from the Commercial Prototype Buildings (US DOE - BTO, 2018) and adapted for the Canadian context by Natural Resources Canada (CanmetENERGY). The performance level of the archetypes modified by CanmetENERGY meets the 2011 National Energy Code for Buildings (NECB 2011) with small modifications to take into account the Québec regulations (see below). These open-source archetypes represent a convenient solution and a reasonable estimation of the characteristics to be expected in new build. One could argue that some – if not most – developers will adopt a more stringent performance level, e.g. for LEED certification, but it is well known that the vast majority of existing buildings do not meet their design target, a problem known as the "performance gap". A recent study of 18 LEED-certified Canadian buildings found this performance gap to be in the range of 30 %, with individual buildings reaching up to 60 % (Samuelson et al., 2015). Using a less stringent building code represents a simple way to cope with this problem. In their current version, the prototype buildings do not include mixed-used buildings, so the commercial, office, and residential parts of each buildings was modelled using separate archetypes:

- Commercial floor: Retail Standalone
- Offices: Large Office
- Residential: Midrise Apartment

Some additional assumptions were made by the project team based on their experience and recently completed projects:

- The Window-to-Wall Ratio was set at 40 % for each building orientation (North, East, South, West).
- The thermal loss coefficient (U-value) of the glazing is set at 1.53 W/m²-K, according to the EnergyStar standards (2019).
- The thermal resistance values of the exterior walls and roof are chosen respectively at 3.4 m²-K/W and 5.46 m²-K/W, according to the "Règlement sur l'économie de l'énergie dans les nouveaux bâtiments" of Quebec (Légis Québec, 2019).
- Infiltration rate is calculated by a model taking into account wind speed, and the Leakage Rate at 75 Pa (LR_{75}) is set at 2.2 L/s-m^2, which represents new buildings with a good level of performance. Infiltration only affects the external zones.

5.2 UBEM creation

As mentioned previously, 2 types of UBEMs were developed for this case study. A context-dependent UBEM (geometry, shading, radiation, etc.) created in UMI and a context-free UBEM created using scaled archetypes in EnergyPlus.

5.2.1 Context-dependent UBEM (UMI)

Modelling a neighborhood in UMI requires 2 main steps:

- draw the geometry in Rhino
- create (and apply) the templates gathering the thermal parameters of each archetype used (in our case, 3 different archetypes) to represent the modelled buildings.

The geometrical information obtained from the Ville-Marie borough as a Sketchup model was imported in Rhino and building use types were assigned according to the assumptions described above (see Figure 4.3).

The UMI templates were created from a tool developed by Letellier-Duchesne (2019) that allows simulationist to translate an EnergyPlus input file (IDF) to a json file, that is used as an input file in UMI for thermal parameters (i.e. UMI template).

After applying the selected archetypes (templates) to the buildings (delimited geometry) we ran the simulation in UMI, with a typical weather file representing the Montreal climate (Morris, 2016).

5.2.2 Context-free UBEM (Scaled archetypes)

Modelling an UBEM with the context-free approach is easier than developing a context-dependent UBEM (e.g. in UMI) since each part of the buildings is individually modelled, regardless of its context, by an archetype representing the type of use. Therefore, in this case study, only 3 different archetypes where simulated in EnergyPlus (*Retail Standalone*, *Large Office* and *MidRise Apartment* from CanmetENERGY).

Then, hourly loads for space heating (abbreviated as "heating"), domestic hot water (DHW), air conditioning (abbreviated as "cooling"), and power consumption for appliances/lighting/equipment (ALE) are extracted from the simulation results with EnergyPlus, and converted into unit values per m² of floor area. These values are then multiplied by the floor area of each part (retail, office, residential) of the represented buildings in the building stock.

5.3 Results

5.3.1 Comparing UBEM approaches

The results of the modelled buildings energy use are presented for the two methods in this section and compared with each other.

Table 5.1 shows the annual and peak loads per end-use for the two different models. It should be noted that the particular version of UMI available at the time of writing seems to have a bug related to DHW load, which is largely underestimated. Earlier versions did not display this problem, so for this work the results from the “raw” archetypes (identical to the context-free results) were assumed.

Annual loads for heating and cooling are very different for the two approaches, with UMI producing a much smaller heating load and a higher cooling load. Peak values show a similar trend, although less exacerbated. ALE loads are higher in UMI, which can be attributed to the zone aggregation process and contributes to the difference in heating and cooling loads. But this difference in internal gains alone cannot explain the difference in heating and cooling loads, and

taking the building context into account would result in lower solar gains in most cases, so at least part of the difference is attributable to the different zoning approaches (detailed multizone archetypes in the context-free model, shoeboxes in the context-aware model). It should also be noted that the automated tool developed to convert complex EnergyPlus models to UMI archetype templates is still in development and must be further validated.

Table 5.1 − Comparison of end-use loads for the simulation of a context-dependent (UMI) and a context-free (Scaled archetypes) models of the same neighborhood

	Loads	DHW	ALE	Cooling	Heating
Scaled Archetypes	**Annual (kWh/m^2)**	18.6	37.4	14.7	43.3
	Peak (W/m^2)	6.5	8.6	21.4	24.0
UMI	**Annual (kWh/m^2)**	18.6*	47.3	20.4	23.7
	Peak (W/m^2)	6.5*	11.9	26.2	23.8

**Values not modelled in UMI, see text*

Figure 5.1 presents daily heat demands (heating, DHW and cooling, top of the figure) for the 2 different models presented in this section. As discussed above, peak loads are of the same magnitude but the cooling load is more spread out over the year in UMI. The figure also presents the hourly heat loads for winter (middle) and summer (bottom) weeks: the coldest week of the year (week of January 9th) and a very hot and sunny week (week of August 28th). Winter week results show a larger baseline for space heating load for the context-free UBEM, around 10 Wh/m^2 compare to 5 Wh/m^2 for the context-dependent UBEM. Moreover, it shows that there is no morning peak for space heating for the context-free UBEM, showing another suspicious result from UMI. The summer week results (bottom graphs) agree with the results from Table 5.1. It can be noted that the context-free UBEM has a slight space heating load during the summer week. After investigation, we found out this load was coming from the *Retail Standalone* archetype.

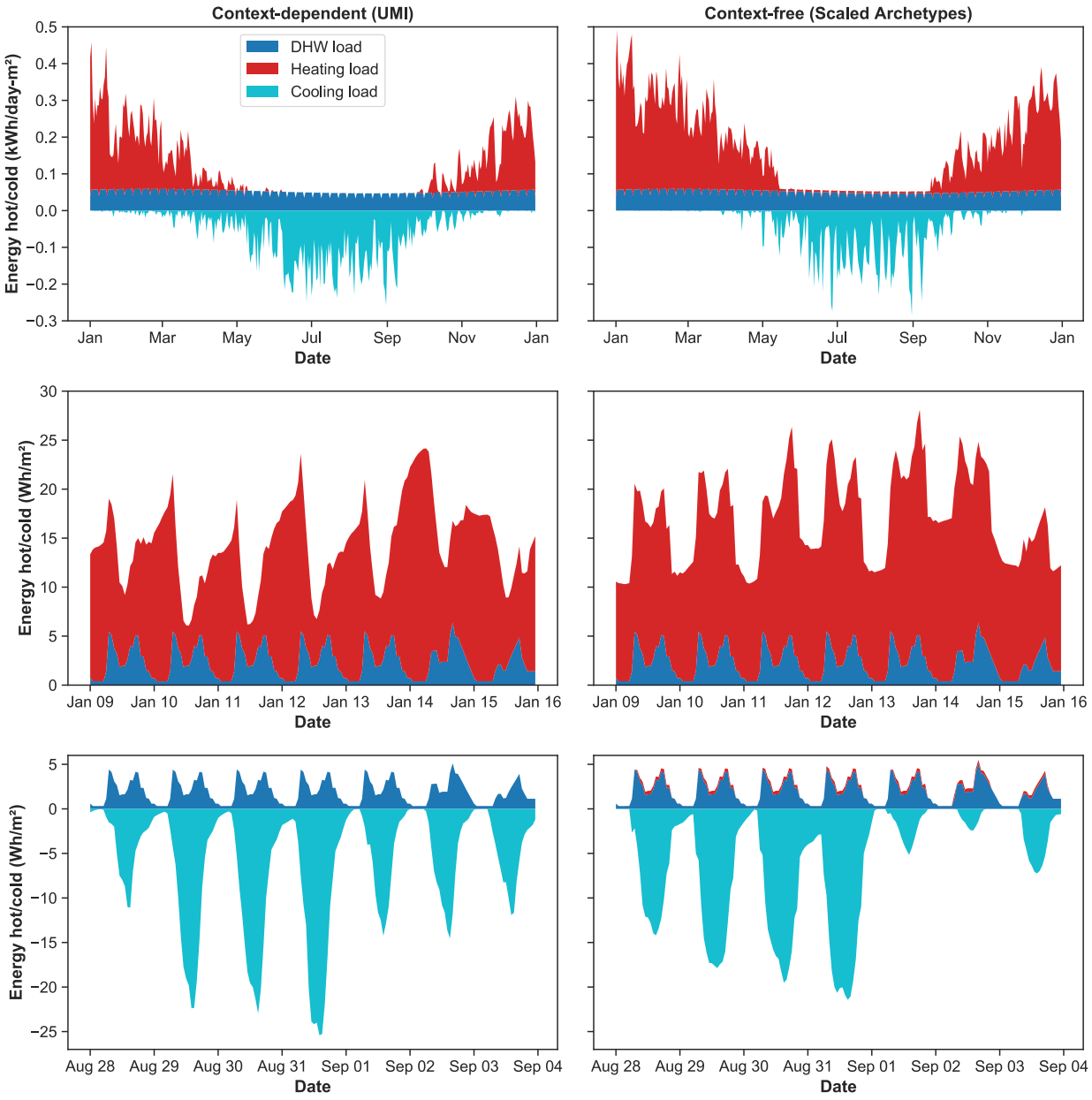

Figure 5.1 – Daily profile for a typical year (top), and hourly profiles for a winter week (middle) and a summer week (bottom) of heat loads (heating, DHW and cooling) for a context-dependent (left) and a context-free (right) models of the same building stock

In the absence of more detailed models (and measured data, since the buildings have not been built), there is no truth standard to decide which modelling approach should be considered as the most realistic. A quick comparison with a SIMEB model of one of the buildings showed good agreement with the context-free results, and the results of Chapter 3 also showed that the prototype buildings were closer to measured data, and – as mentioned above – doubts remain on the robustness of the automatic EnergyPlus to UMI conversion tool. It was therefore decided to keep the results from the context-free model for the rest of the work. To take into account diversity in the building stock, energy profiles of each building were randomly shifted by more or less one hour by steps of 15 minutes (hourly simulation results were first upsampled to a time step of 15 minutes, then profiles were shifted and finally results were resampled at a 1-hour time step).

5.3.2 Energy use at the neighborhood level: defining the Business As Usual Case

The results above showed the heating, cooling and DHW loads calculated for the buildings. In a Business As Usual (BAU) case, those loads would be met by individual systems in each building. Simple annual efficiencies were defined by the project team using engineering judgement and experience with similar recent projects.

The energy performance of this scenario represents the baseline to which the district energy options will be compared.

5.3.2.1 Heating, Ventilation and Air-Conditioning system efficiencies

Air conditioning loads are assumed to be met by chillers with a seasonal average Coefficient of Performance (COP) (including all accessories) of 2.5. The electrical power is therefore obtained by dividing the cooling load by 2.5.

Domestic hot water is provided by a gas system with an overall efficiency of 80 %, representing a typical collective system installed in new condo buildings in Montreal.

Space heating: it is assumed that 30 % of the total building floor area is heated entirely by electricity with 100 % efficiency (electric baseboards). The remaining building area is heated by a hybrid electric/gas system: electrical resistances (100 % efficiency) provide up to 30 % of peak demand, and a natural gas system (90 % efficiency) provides the remainder of demand. This assumption

corresponds to the traditional sizing in large Montréal buildings in order to limit power demand costs.

5.3.2.2 Data centre cooling system

The data centre has a constant electrical power demand of 12 MW for computer equipment and all accessories, with the exception of the air conditioning system. In the reference case (BAU), the data centre is air-conditioned by a cooling system with a COP of 4, which requires a power of 3 MW to satisfy the air conditioning demand of 12 MW, and therefore releases 15 MW of heat into the ambient air.

5.3.2.3 Calculation of GHG emissions

Emissions are quantified by an equivalent amount of CO_2 (tonnes of $CO_{2,eq}$) calculated from electricity and gas consumption on site and the emissions due to refrigerant leaks over the lifetime of heat pumps/chiller equipment (see appendix A for calculation methodology). The emission factors used are those recommended by *Transition Énergétique Québec* (2019):

- Emissions associated with the combustion of natural gas: 179.4 g of $CO_{2,eq}$ per kWh of gas consumed by gas-fired boilers and water heaters.
- Emissions associated with electricity consumption: 2 g of $CO_{2,eq}$ per kWh of electricity consumed on site.

5.3.3 Simulation results

5.3.3.1 Overview of consumption, peak demand and GHG emissions

Table 5.2 provides a summary of the main performance indicators for the BAU scenario. The winter peak corresponds to the time of the maximum heat demand (heating + DHW) of the reference case (BAU) during the period from October to April (inclusive), and the summer peak corresponds to the time of the maximum cooling demand of the reference case (BAU) during the period from May to September (inclusive).

Table 5.2 − Consumption, peak demand, and emission for the Business as Usual scenario

	Consumption (GWh)	Summer peak (MW)	Winter peak (MW)	GHG (t_{eqCO_2})
Gas	32.6	2.9	19.9	5857
Electricity	234.5	33.1	39.9	469
Total	267.1	-	-	7588

5.3.3.2 Annual consumption and peak demand

Figure 5.2 shows a diagram of the reference case (BAU) scenario and presents its results for annual consumption and peaks in electricity (heating and air conditioning) and gas (heating and DHW). Emissions in CO_2 equivalent (black cloud in the diagrams) and thermal emissions into the atmosphere (white cloud) are also presented.

Note on the figure interpretation

Heat pumps and air conditioners are represented by the following icon : 

For the annual balance shown in Figure 5.2 (top), the cooling loads of the building stock (without the data centre) are 18.1 GWh. This amount of heat is extracted from the building by air conditioners (the blue arrow represents an air-conditioning requirement). The air conditioners consume 7.3 GWh of electricity (orange arrow) and release 25.4 GWh of heat into the ambient air (brown arrow). Heating loads (red arrows) are partly met by electric baseboard heaters (49.7 GWh of heat corresponding to 49.7 GWh of electricity) and partly by gas boilers (26.5 GWh of heat corresponding to 32.6 GWh of gas). The symbols on the left side of the figure represent total electricity consumption (234.5 GWh), total gas consumption (32.6 GWh), GHG emissions (6325 t_{eqCO_2}) and heat emissions to ambient air (156.8 GWh), respectively.

The winter and summer peaks shown in Figure 5.2 (middle and bottom) follow the same principle.

As expected with the Montreal climate, the annual heating demand (space heating + DHW) of buildings are higher than those for cooling with a load of 76.2 GWh/year (49.7+26.5, Figure 5.2 below) compared to 18.1 GWh/year. However, with the presence of a data centre, the cooling demand largely increases to 123.1 GWh/year. The heating and cooling peaks of buildings are of the same order of magnitude (33.8 MW for heating (16.6+17.2, Figure 5.2 below) and 38.2 MW

for cooling). The presence of a data centre results in simultaneous heating and cooling demands all year round.

The heat rejection to ambient air is about 156.8 GWh annually, i.e. approximately 784 kWh/m² of roof area per year. By way of comparison, the solar radiation absorbed per m² of flat roof area is about 700 kWh/m² in Montreal (assuming an albedo of 0.5). The next chapter will show that with district energy systems this heat can be partly re-used and partly rejected to the sewer or to a river, reducing the impacts on the urban heat island effect.

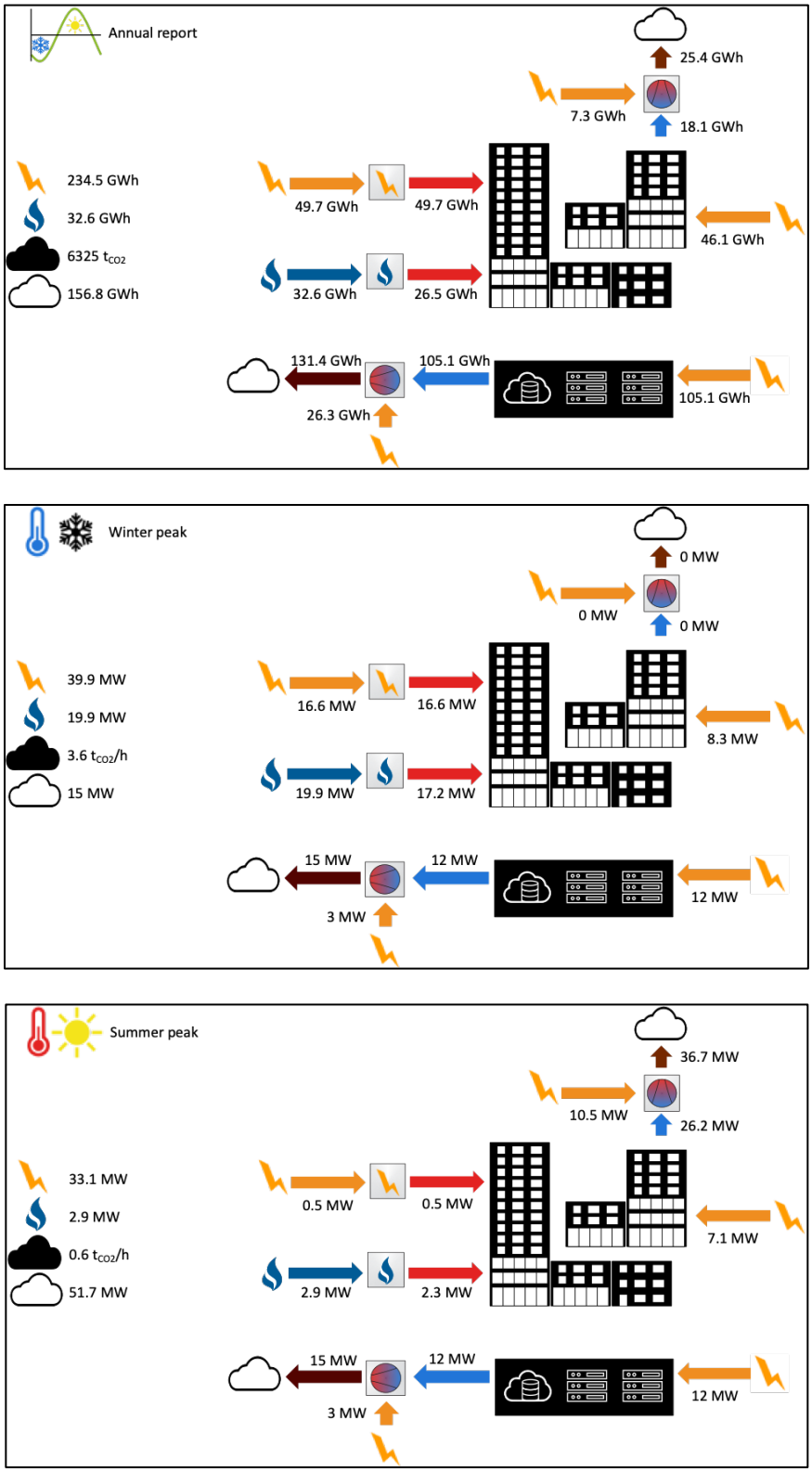

Figure 5.2 – Business as Usual: annual consumption (top), winter peak (middle), summer peak (bottom)

5.3.3.3 Dynamic demand profiles

This section presents the heating (heating and DHW) and cooling loads for the studied neighborhood, and the energy source (gas or electricity) consumption to meet those. Heating demands are shown as positive values in Figure 5.3, while cooling loads are shown as negative values.

For the BAU, there is a year-round gas consumption for the DHW load, and gas also contributes to peak space heating, although electricity consumption dominates in the winter. The data centre in the neighborhood increases the cooling demands (see Figure 5.3). This results in a constant cooling requirement throughout the year of 12 MW. This phenomenon can be seen during winter periods (e.g. January to March) when a constant cooling base of 288 MWh/day is observed. The annual consumption is then dominated by the cooling load, which account for 62 % (equivalent to 123.2 GWh/year) of the heat loads (heating and cooling combined).

The peak demand for heating and cooling is of the same order of magnitude with 33.8 MW of maximum power demand for heating (heating + DHW) and 38.2 MW for cooling.

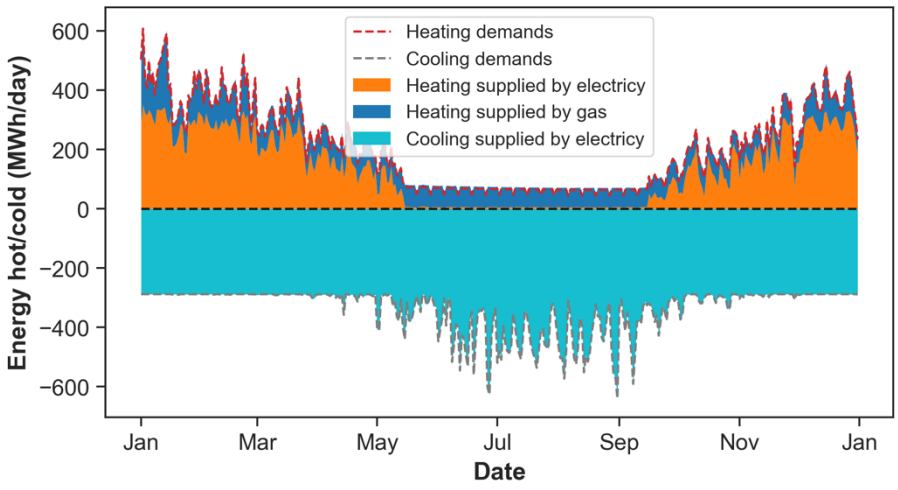

Figure 5.3 – BAU: Heat demands by energy source

Figure 5.4 presents the hourly electrical power capacities of the neighborhood for winter and summer weeks: the coldest week of the year (week of January 9th) and a very hot and sunny week (week of August 28th).

The stacked areas represent the different contributions to building electricity consumption: heating (excluding domestic hot water only satisfied by gas), cooling, and ALE (Appliances, Lighting and Equipment). The demand for the data centre (DC) is also shown.

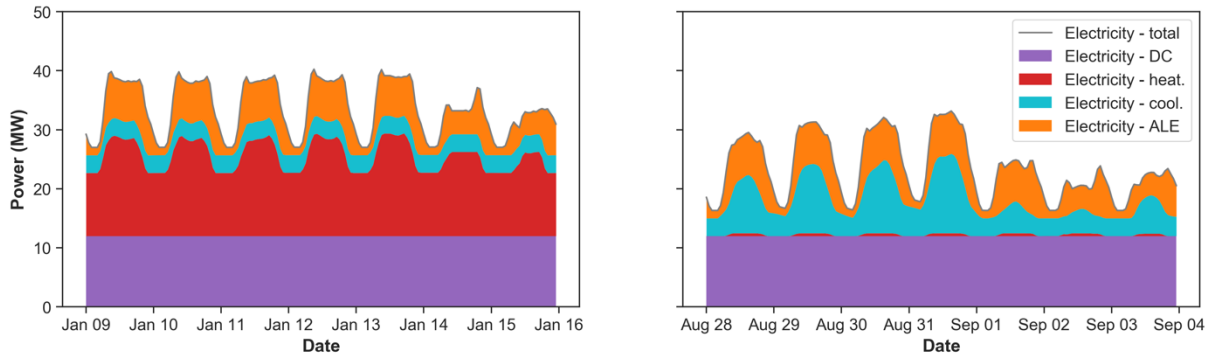

Figure 5.4 – BAU: Electrical power demand profile during winter (left) and summer (right) peak weeks

During the winter week (Figure 5.4, left), the electrical demand for space heating dominates, mainly due to cold outside temperatures. This high consumption, compared to the cooling load, is also due to the fact that the heating system is less efficient (efficiency of 1) compared to the cooling system (COP of 2.5).

During summer week (Figure 5.4, right) the electrical power used for air-conditioning is larger than the heating and ALE electric consumption due to the high outside temperatures and the heat gains from solar radiation during this week.

The electrical consumption from the ALE is similar for the 2 weeks, with only 2 % difference for the total ALE electric consumption over the week.

5.4 Conclusion

Using NRCan archetypes following the NECB-2011, 2 UBEMs were created: one context-dependent (in UMI) and one context-free (scaled archetypes) of a Montrealer neighborhood.

The context-dependent model consist of creating the geometry of the UBEM thanks to a CAD software (here Rhino) and then apply thermal parameters to the geometry depending on the building usages and run the simulation with UMI in our case. This approach allows to take into account the interactions between the buildings (geometry, shading, radiation, etc.)

The context-free model results in the independent modelling of each required archetype, and then aggregates the results of each one according to the floor area it represents in the building stock. With this method, the model does not take into account any interaction between the simulated buildings.

When looking at the total end-use peaks, the 2 models offer similar results, with a maximum difference of 5 %, except for the domestic hot water load where UMI seems to underestimate it. However, when observing the total end-use loads and hourly results over a typical year, large differences are observable between the 2 UBEMs, in particular with shifted cooling and heating loads for the UBEM realized with UMI.

The context-free UBEM developed with EnergyPlus was chosen to study the energy dynamics (load and consumption) of the neighborhood due to its more realistic results. The results showed that the energy consumption of the buildings with the presence of a data centre was dominated in cooling, while peak loads are of the same order of magnitude for cooling and heating (38 MW and 34 MW respectively). The resulting peak electricity demand is 33 MW in summer and 40 MW in winter, due to the use of direct electric heating to meet a share of the heating load.

CHAPTER 6 ENERGY SHARING NETWORK MODEL

The results of the context-free UBEM selected in the previous chapter will be used to study the feasibility of the implementation of an energy sharing network in the neighborhood presented in Chapter 4. First, a simple pseudo steady-state model of 2 different networks (4th and 5th generations) will be presented and will provide an opportunity to discuss the usefulness of an energy sharing network by comparing the result of those models with the reference case (Business As Usual, BAU) exposed earlier (see section 5.3.2). The results of the simple model will be compared with a more complex model for the 4th generation energy sharing network.

6.1 Early planning: pseudo steady-state models of energy sharing networks

This section presents the assumptions made in developing the pseudo steady-state models of the 4th and 5th generation heating/cooling networks (abbreviated as 4G and 5G respectively) based on the neighborhood's energy needs (see section 5.3.3). The models were implemented as Python scripts. They represent a level of detail in line with pre-feasibility studies such as the one commissioned by the borough of Ville-Marie which is described in Chapter 4.

Note: In the following, the term “Heat Pump” (HP) is used to denote one or several machine(s) performing a given function (for example transferring heat from a cold loop to a hot loop). In reality, large systems would probably include banks of heat pumps, so the term “central heat pump” represents a group of machines performing a given function.

6.1.1 Modelling assumptions

6.1.1.1 4th generation network: heating and cooling networks with recovery

The first scenario of energy sharing networks, which we will denote by the term "4th generation network" (4G), corresponds to the implementation of 2 centralised networks: a moderate temperature district heating network (with a supply temperature of 70 °C) which directly satisfies the space heating and domestic hot water needs of buildings, and a chilled water network (at a supply temperature of 6 °C) which directly satisfies the air conditioning loads of buildings.

The networks satisfy 100 % of the heating (heating + DHW) and cooling (air conditioning) loads of the buildings, without requiring any additional equipment. Heat losses are assumed to represent

5 % of the annual heat demand (heating + DHW) for the heating network, and heat gains representing 3 % of the annual cooling demand for the cooling network.

In the case of simultaneous needs on both networks, the first source of supply for the hot network is a heat pump (HP) for recovery from the cooling network (which therefore makes it possible to satisfy both the heat demand from the heating network and the cooling demand from the cooling network). This heat pump has a COP of 3 in heating. So, when it supplies 3 units of heat to the hot loop, it extracts 2 units of heat from the cold loop (and consumes one unit of electricity that is converted into heat in the hot loop).

The remaining heating or cooling load is met by a heat pump that uses the sewer system as a heat source or sink. This HP has a COP of 2.5 in heating mode (injection of heat into the hot loop from the renewable source) and 4 for cooling (rejection of heat to the renewable source from the cold loop).

The heat pumps are sized to meet 100 % of the cooling load, and their cooling and heating capacities are assumed to be equal. Given the presence of a data centre, the peak cooling load is higher than the peak heating load, so that no auxiliary heating is required. In existing systems, heat pumps are often sized to meet a given fraction of the peak heating load, with auxiliary systems (e.g. gas boilers) providing peaking capacity. The assumption of a heat pump-only system here is in line with the Ville-Marie mandate, which requested to assess potential decarbonized systems, and also results from the presence of a data centre.

6.1.1.2 5th generation network: mixed water loop

The second energy sharing network scenario, which we will denote by the term "5th generation network" (5G), corresponds to the implementation of a water loop maintained close to ambient temperatures, between 15 °C and 35 °C. The temperature of the water loop is not directly usable for heating, DHW or air conditioning, so individual buildings are equipped with heat pumps (denoted as “decentralized heat pumps”) which draw heat from or reject heat to the district water loop.

For this network, it is assumed that heat losses or gains are negligible.

It is assumed that the decentralized heat pumps satisfy 100 % of the heating and DHW needs of buildings (with a COP of 3), and 100 % of the cooling demand (with a COP of 4). Again, existing systems may in fact include auxiliary peaking boilers for heating and DHW, but the assumption of a heat pump-only system is in line with the Ville-Marie request and matches the design implemented in existing 4G and 5G networks where decarbonization is the main priority.

The mixed loop inherently allows heat to be shared between buildings, but it is not necessarily balanced. If the amount of heat rejected by buildings exceeds the amount of heat extracted, the mixed water loop is maintained at its maximum operating temperature (35 °C) by a central HP that reject their heat in a renewable source (sewer system), with a COP of 6. Otherwise (heat rejections lower than the amount of heat extracted from the loop), the mixed loop is maintained at its minimum temperature (15 °C) by a central HP that extract their heat from a renewable source, with a COP of 6.

As for the 4G network, HPs are designed to meet 100 % of the cooling load of the network, and it is assumed that their heating capacity is equal to their cooling capacity. With the loads resulting from our case study including a data centre, this results in a heat pump-only system that does not require auxiliary peaking boilers.

6.1.1.3 Data centre cooling system

As mentioned in section 5.3.2.2, the studied neighborhood is modelled with the buildings described earlier (see section 4.2) and also with a high power data centre with a constant electrical power demand of 12 MW.

In the case of a 4th generation network, the data centre is cooled directly by the cold-water loop at 6 °C, and therefore rejects a constant thermal power of 12 MW into this loop. For the 5th generation network, the data centre is air-conditioned by a cooling system with a COP of 6, so this system requires 2 MW of power to satisfy the 12 MW air conditioning demand, and it rejects 14 MW into the mixed water loop.

6.1.2 Simulation results

This section presents the results for the pseudo steady-state model of the 4G and 5G networks, and compares them with the simulation results of studied neighborhood (BAU scenario) presented in section 5.3.3.

6.1.2.1 Overview of consumption, peak demand and GHG emissions

Table 6.1 provides a summary of the main performance indicators for the different scenarios. The winter peak corresponds to the time of the maximum heat load (heating + DHW) of the reference case (BAU) during the period from October to April (inclusive), and the summer peak corresponds to the time of the maximum cooling demand of the reference case (BAU) during the period from May to September (inclusive). Greenhouse gas (GHG) emissions include the impact of refrigerants used in heat pumps, as described in section 6.1.3 below.

Table 6.1 − Consumption, peak demand, and emission for the different scenarios

	Gas - total			Electricity - total			Total	
	Consumption (GWh)	**Summer peak (MW)**	**Winter peak (MW)**	**Consumption (GWh)**	**Summer peak (MW)**	**Winter peak (MW)**	**Consumption (GWh)**	**GHG ($t_{eq_{CO_2}}$)**
BAU[1]	32.6	2.9	19.9	234.5	33.1	39.9	267.1	7588
4G	0	0	0	196.4	29.3	33.2	196.4	950
5G	0	0	0	214.7	36.1	34.9	214.7	1524

An interesting conclusion is that the 4th generation network leads to a greater reduction in peak demand on the electricity grid. Both types of networks are beneficial in the presence of a data centre, allowing significant energy savings, a very significant reduction in CO_2 emissions (reduced by a factor of 5), and a reduction in electrical peaks. Compared to the BAU, switching to a 4th or 5th generation network reduces CO_2 emissions by more than 80 % while reducing the peak power

[1] Results from section 5.3.3 (Table 5.2)

demand from 40 MW to 33 MW (4G) or 36 MW (5G) and the electric consumption by at least 8.5 %.

6.1.2.2 Annual consumption and peak demand

Figure 6.1 (p. 62) and Figure 6.2 (p. 63) show more details on the annual results and the values during the winter and the summer peak and can be compared to Figure 5.2 (p. 52).

6.1.2.2.1 4th generation network (4G)

In the case of a 4th generation network, total energy consumption is significantly lower than the reference case with a total of 196.4 GWh of electricity and 0 GWh of gas (see Figure 6.1), compared to 234.5 GWh and 32.6 GWh for the BAU (see Figure 5.2). These differences are explained first of all by the use of a heat pump (with a COP of 2.5) to meet the total hot loop's demands, while the base case uses an electric heating by Joule effect (e.g. electric baseboards) with a COP of 1. In addition, heat recovery between the 2 loops reduces the energy demand to meet heating needs, since they are satisfied by a HP with a COP of 3 in the case of recovery.

Compared to BAU, the peak cooling load for the 4G network source is reduced by heat recovery between the hot and cold loops, although it is slightly increased by heat gains through the pipes. The cooling peak is 37.1 MW (compared to 38.2 MW for the BAU). Even if heat losses are considered in the case of the 4G system, the heating peak decreases as there is heat recovery during the heat peak period. The peak heating demand is 35.4 MW (compared to 33.8 MW in the reference case), which is provided with the electric system (heat pumps) while for the BAU, the total peak demand (33.8 MW) is supplied with both electric and gas systems.

6.1.2.2.2 5th generation network (5G)

For the scenario with the 5th generation network, as for the 4G network, total energy consumption is significantly lower than the reference case with a total of 214.7 GWh of electricity and 0 GWh of gas (see Figure 6.2), compared to 234.5 GWh and 32.6 GWh for the BAU. These differences are explained first of all by the use of a heat pump (with a COP of 6) to meet cooling and heating needs, while the base case uses an electric heating by Joule effect (e. g. electric baseboards) with a

COP of 1. In addition, heat recovery in the mixed water loop reduces the primary energy demand to meet heating and cooling needs.

Heat recovery is more efficient in the 5G network than in the 4G network because the heat is immediately shared in the district loop, whereas in the 4G a heat pump is required to transfer heat from the cold loop to the hot loop. The net heat demand on the loop is also lower, since decentralised heat pumps remove only 22.5 MW from the loop during the winter peak to give 33.8 MW to the buildings (the difference coming from the electricity consumed by decentralised heat pumps). The peak demand on the network is therefore reduced.

The peak cooling requirement met by the electric system (heat pumps) is reduced by heat recovery within the mixed water loop, but is increased by the consumption of decentralized heat pumps. This results in an cooling peak of 44.8 MW (see Figure 6.2), which is higher than the BAU and 4G cases. The loop peak heating load decreases as there is heat recovery during the heat peak period. The peak heat load is therefore 8.5 MW (compared to 33.8 MW in the reference case).

One advantage of the 4G over the 5G is that it only uses one “level” of heat pumps, while the 5G network uses two “levels”. It should be noted that the assumptions selected for COP and the need for a centralized heat pump depend on the temperature level of the renewable source. In some cases, direct rejection or extraction to/from the renewable source can be possible. In this case, we assumed that the sewer system would be too cold in winter for direct rejection, and the results neglect the fact that installed heat pumps could be bypassed whenever the operating temperatures allow it. This should be kept in mind when comparing the 4G and 5G results.

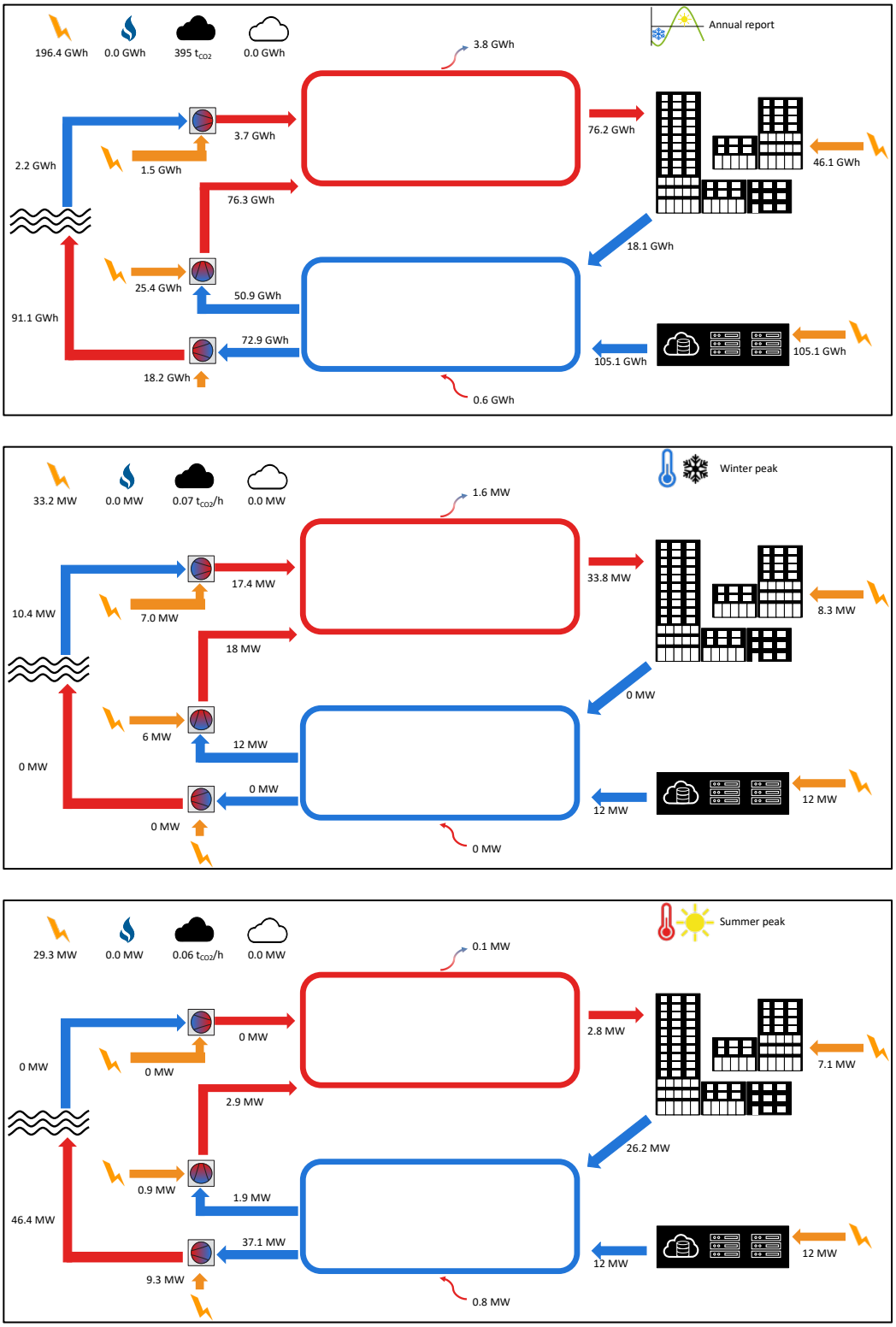

Figure 6.1 – 4G network (pseudo-steady state): annual consumption (top), winter peak (middle), summer peak (bottom)

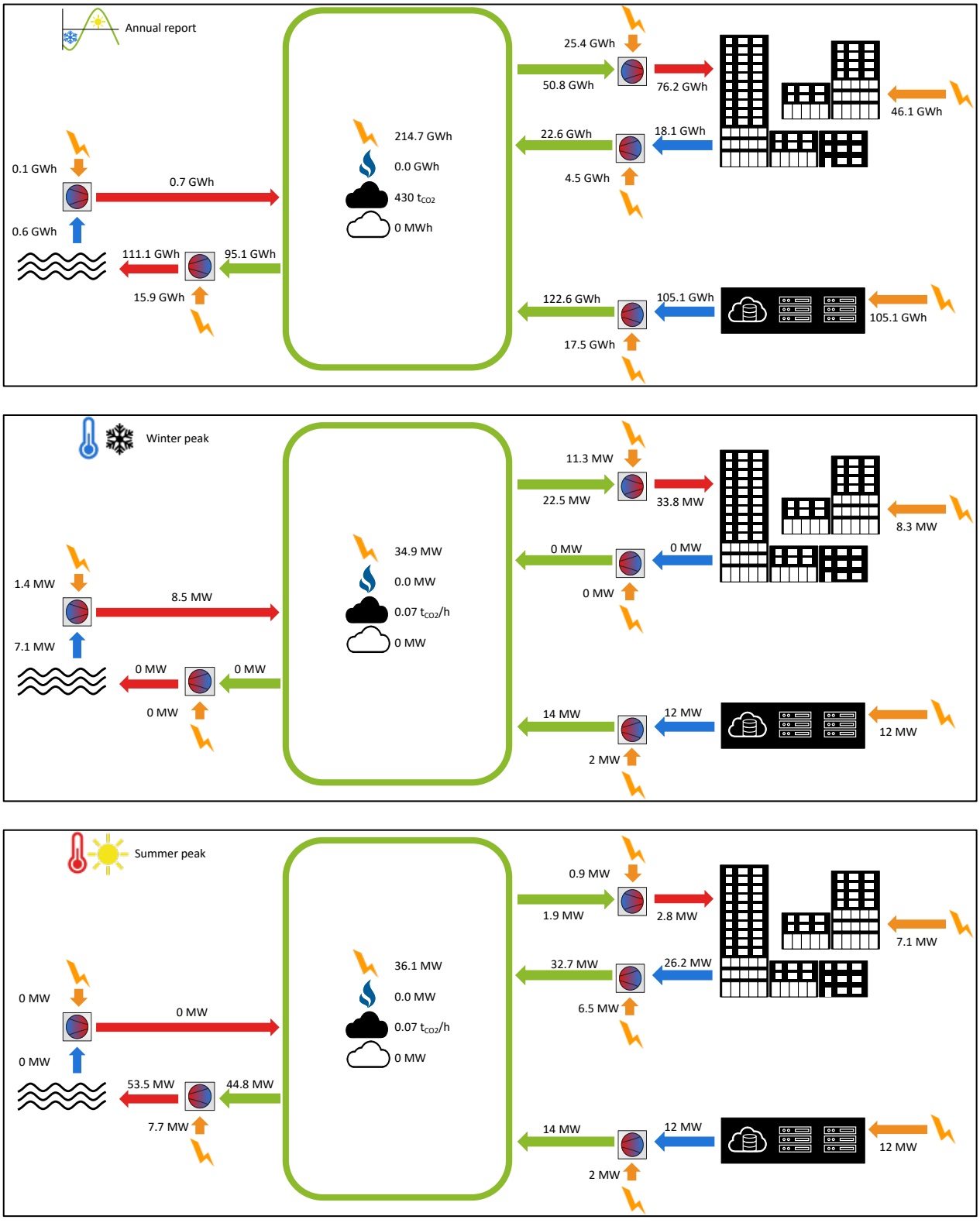

Figure 6.2 – 5G network: annual consumption (top), winter peak (middle), summer peak (bottom)

6.1.2.3 Annual energy use profiles

This section presents the heating (heating and DHW) and cooling loads for the different energy sharing network scenarios, and the energy sources (gas or electricity) to meet those. Heating loads are shown as positive values in the graphs, while cooling demands are shown as negative values.

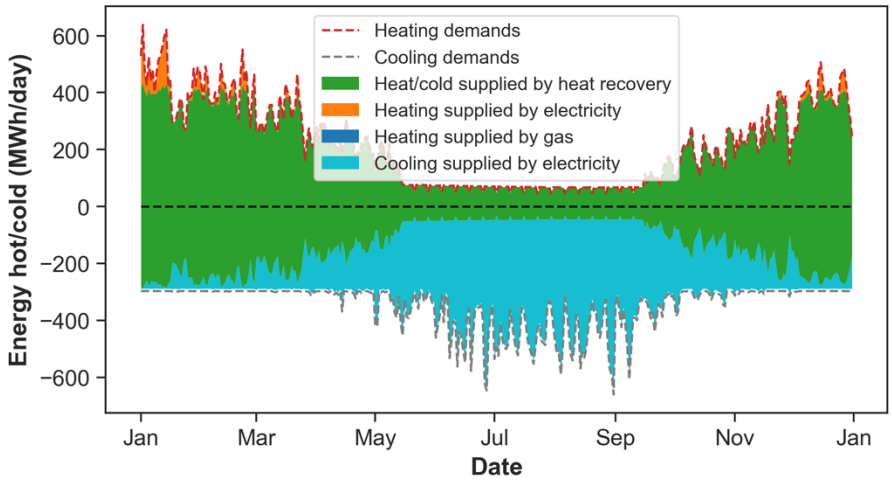

Figure 6.3 – 4G (pseudo steady-state): Heat demands by energy source

Compared to the BAU (see Figure 5.3), the cooling load, for the 4th generation network, provided by the heat pumps is reduced thanks to the heat recovery between the hot and cold loops (in green on Figure 6.3) and slightly increased by the heat losses in the pipes. They are 72.9 GWh (compared to 126.5 GWh for the BAU). The contribution of this recovery is 3/2 times higher for the hot network than for the cold network due to the COP of the heat pump, as explained above.

Heating peak and consumption supplied by gas or electric sources are drastically reduced as there is heat recovery throughout the year thanks to the presence of the data centre. The heating peak is slightly higher than the BAU case because of the heat losses (see assumptions) in the pipes. The heat demand met by gas is 0 GWh, the heat demand met by electricity (HP) is 3.7 GWh, and the heat demand met by recovery is 76.3 GWh. For a total heating demand of 80 GWh (compared to 76.2 GWh in the reference case).

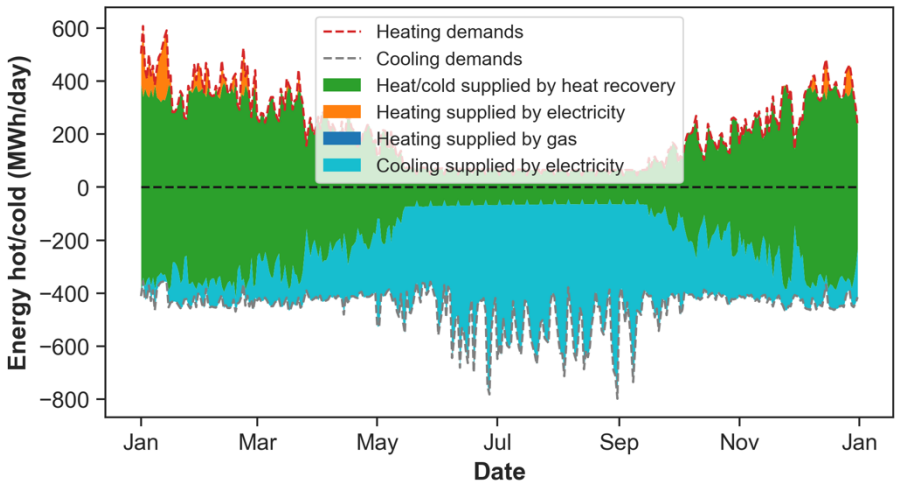

Figure 6.4 – 5G: Heat demands by energy source

For the 5th generation network, recovery is achieved within the water loop and $Q_{heat_{recovery}} = Q_{cool_{recovery}} = 72$ GWh/year. The cooling demand met by heat pumps is reduced due to heat recovery but is increased due to the use of decentralised heat pumps. This results in a total electricity consumption for cooling of 37.9 GWh, which is higher than the BAU and 4G cases.

The heating loads supplied by gas or electric sources are also reduced compared to the BAU since there is heat recovery throughout the year thanks to the presence of the data centre. The heat demand met by gas is zero, the heating demand met by electricity (heat pump) is 0.7 GWh, and the heating demand met by recovery is 72 GWh.

6.1.2.4 Typical profiles of electrical power demand on the grid

This section presents the hourly power demand of the 4G and 5G scenarios for winter and summer weeks: the coldest week of the year (week of January 9th) and a very hot and sunny week (week of August 28th), and can be compared to Figure 5.4 (p. 54).

The stacked areas represent the different contributions to building and network electricity consumption: heat pumps (centralized (4G and 5G) and decentralized (5G)) and ALE (Appliances, Lighting and Equipment). The consumption for the data centre (DC) is also included.

Figure 6.5 shows the hourly power demand profile for the 4th generation network scenario during the winter (left) and summer (right) peak weeks.

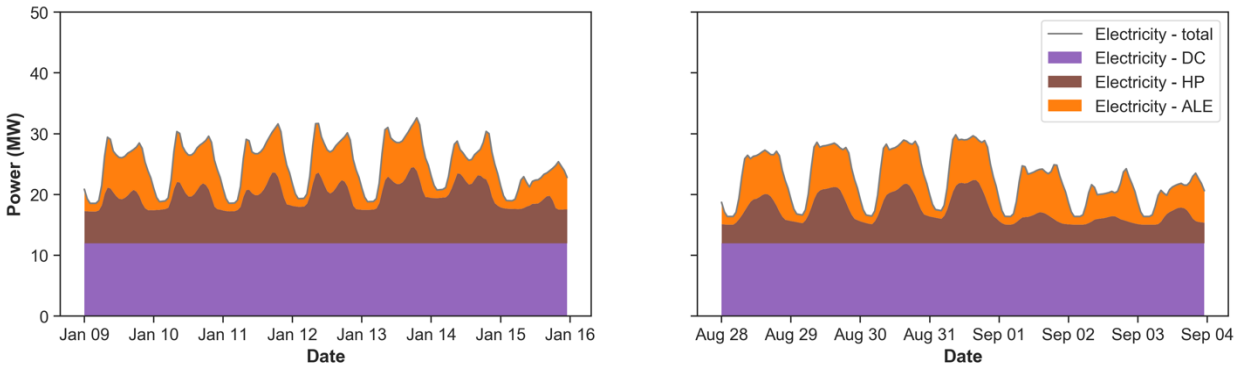

Figure 6.5 – 4G (pseudo steady-state): Power demand profile during winter (left) and summer (right) peak weeks

Figure 6.6 shows the hourly power demand profile for the 5th generation network scenario during the winter (left) and summer (right) peak weeks.

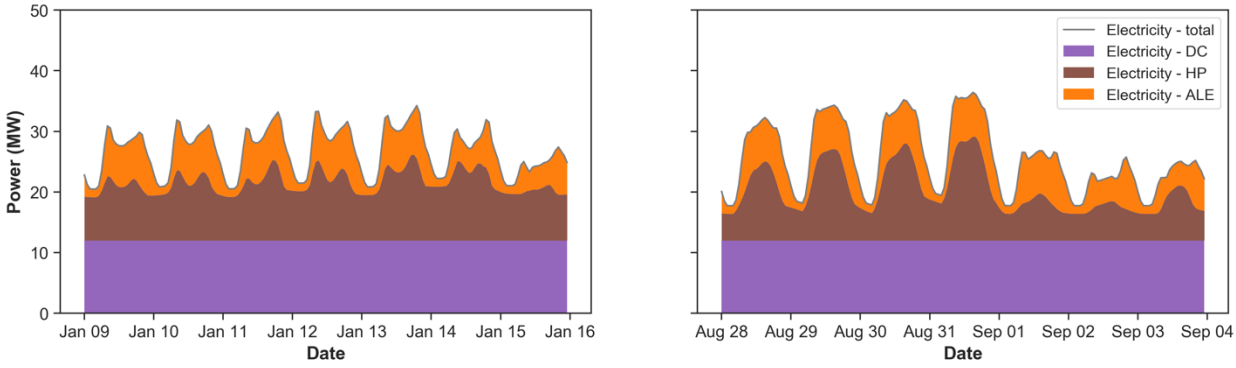

Figure 6.6 – 5G: Power demand profile during winter (left) and summer (right) peak weeks

The winter electricity peak is higher for the reference case (see Figure 5.4) than the scenarios with energy sharing networks. This is partly explained by the fact that heating is provided by more efficient equipment in the case of the energy sharing networks (heat pumps) than in the reference scenario (baseboard heaters). Heat recovery, in the case of heat networks, amplifies this aspect, especially when there is a data centre, allowing recovery even during periods (winter) when the buildings do not require air conditioning. Both types of networks (4G and 5G) have very similar electric peaks and demand profiles.

The trend changes for the summer week, with the highest peak demand being reached in the case of the 5G network, slightly above the BAU, itself slightly above 4G. Even though the equipment used for cooling is more efficient in district energy systems, the 5G network requires decentralized

heat pumps in each building as well as central heat pumps (given the selected assumptions), significantly increasing the electricity consumption for this scenario.

6.1.3 GHG emissions

Table 6.2 presents the TEWI (Total Equivalent Warming Impact) index (tons of CO_2 equivalent) for each scenario, which characterizes the overall impact of a facility on global warming during its operational life. This index includes GHG emissions from electricity and gas consumption and those generated by fugitive refrigerant emissions from chillers and HPs (see appendix A for methodology and calculations).

We assume that all chillers or heat pumps use refrigerants with a very high global warming potential (GWP) (1300 for HFC-134a and 1924 for HFC-410a). An economically and technically interesting alternative is to use ammonia (NH_3) as refrigerant in heat pumps and chillers. This refrigerant is toxic, so it is generally limited to relatively large systems for which the required safety measures (monitoring, containment) are economically justifiable. For example, many arenas in Canada are equipped with ammonia cooling systems. This refrigerant is also applicable for district heating/cooling applications that require relatively high temperatures, as demonstrated by the Malmö system in Sweden that uses sewer heat to supply a heating network (Accelerate Europe, 2018). Table 6.2 therefore presents two alternatives for the 4G and 5G network scenarios, in which central heat pumps use the refrigerant R-134a and ammonia (NH3). The heat pumps and chillers installed in the individual buildings (including the data centre) always use R-410a and R-134a.

Table 6.2 − GHG emissions for the BAU, 4G and 5G scenarios

	Electric/gas consumption $[t_{eqCO_2}]$	**Refrigerants** $[t_{eqCO_2}]$	**Refrigerants (NH_3)†** $[t_{eqCO_2}]$	**Total** $[t_{eqCO_2}]$	**Total (NH_3)†** $[t_{eqCO_2}]$
BAU	6326	1262	1262	7588	7588
4G	392	558	129	950	521
5G	429	1095	613	1524	1042

† These results assume that 4G and 5G central heat pumps use ammonia as a refrigerant.

It is interesting to note that with conventional refrigerants (Figure 6.7, left), in the case of the 4G network, GHG emissions from refrigerants are approximately equal to those from primary energy consumption (electricity and gas). In the case of the 5G network, these emissions are more than double the emissions from electricity and gas consumption. Fugitive emissions from the 5G network are higher than those from the 4G network because of the decentralized heat pumps present in the 5G system, almost doubling the installed capacity of the heat pumps. Refrigerant fugitive emissions are still the highest for the BAU case, since it involves the installation of many decentralized air conditioners that have a higher specific refrigerant charge and a shorter service life than the large centralized units used in the case of energy sharing networks.

These conclusions are reinforced when ammonia is used as a refrigerant (Figure 6.7, right) in central heat pumps in 4G and 5G systems.

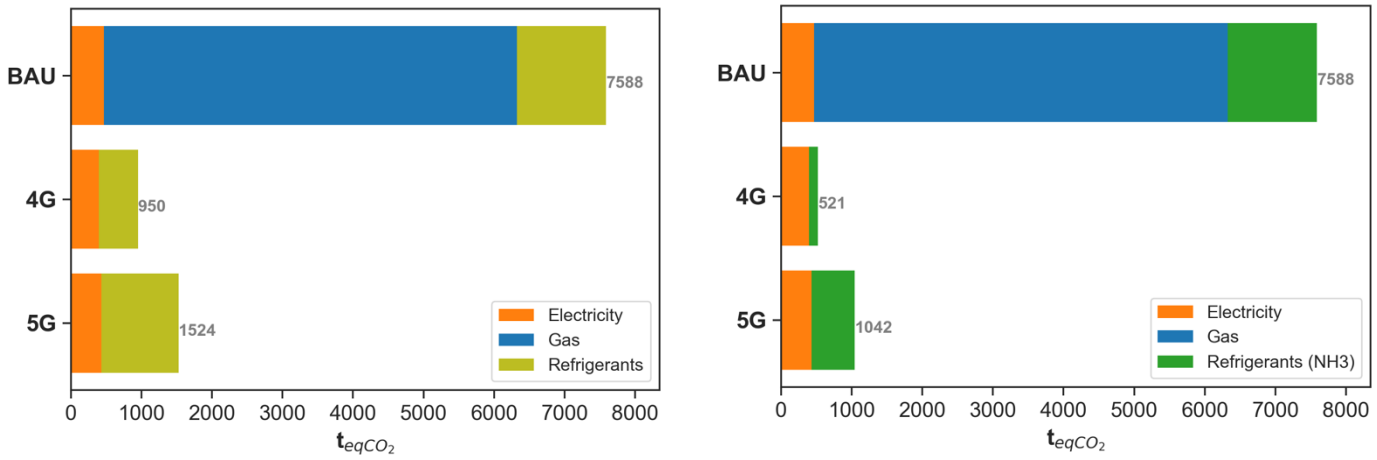

Figure 6.7 – Site-wide GHG emissions with common refrigerants (left) and ammonia as refrigerant (right)

6.2 Detailed model of a 4th generation energy sharing network

The objective of this section is to present a dynamic model of the 4th generation district energy system described above and compare its results to those of the simple pseudo steady-state model.

6.2.1 Methodology

The dynamic model of the 4th generation network is implemented in TRNSYS. Building loads from the UBEM model (see section 5.2.2) are read in a text file and imposed through a component known

as Type 682. The 2 loops (one hot and one cold) are modelled with buried pipes, defined with Type 952, and variable-speed pumps (Type 110). The characteristics of the pipes (diameters, conductivity of materials, etc.) come from catalog data (Logstor, 2020). The loads are met by heat pumps which can transfer heat between the two loops and/or use the sewer system as a source or sink. A heat exchanger modelled with Type 91 (constant effectiveness of 90 %) transfers heat between the sewer system and the heat pumps. Figure 6.8 presents the layout and different elements of the TRNSYS model.

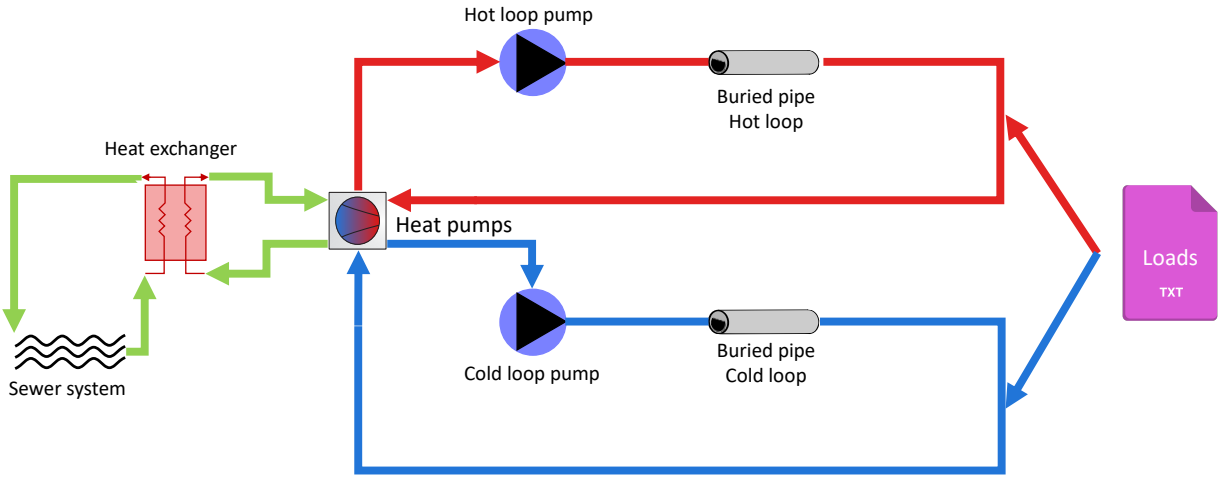

Figure 6.8 – 4th generation network dynamic model in TRNSYS

The sewer system temperature is modelled using a sine curve fitted from data provided by the Ville-Marie borough for the main interceptor (largest sewer pipes) in the neighborhood, as shown in Figure 6.9.

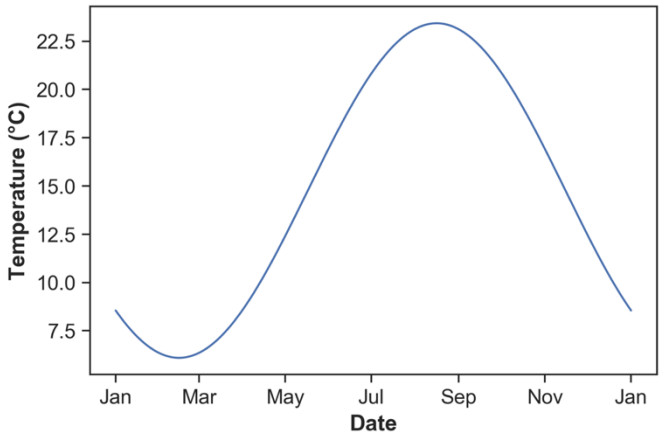

Figure 6.9 – Sewer temperature for a typical year

The heat pumps are modeled by a component that was developed to represent a bank of water-to-water heat pumps capable of operating in three modes: heat recovery, heating from source, cooling to source. Priority is given to the recovery mode (transfer from the cold loop to the hot loop), and one of the two other modes is activated to provide the additional heating or cooling required.

The heat pump rated performance and operating limits were selected to represent typical large heat pumps installed in district energy systems (David, Mathiesen, Averfalk, Werner, & Lund, 2017; Hoffman, 2018). The heat pump has a coefficient of performance of 2.5 for entering water temperatures of 7 °C (evaporator side) and 50 °C (condenser side) and a hot water supply temperature of 70 °C. The heat pump model relies on a performance map that was obtained by adapting data from a commercially available high-temperature water-to-water heat pump (Daikin Applied, 2011), which had to be slightly extrapolated to allow operation in the conditions reported in (David et al., 2017; Hoffman, 2018). The rated cooling capacity is 40 MW, which matches the maximum cooling load in the case study.

The component models a bank of identical machines and assumes that their capacity can be varied to match the loads. No degradation was assumed for part-load performance because of the ability to stage machines operating in parallel, but the model can read a part-load factor correction if desired.

6.2.2 Results

Figure 6.10 shows the hourly COP values for both models. The overall COP is defined here to include heat recovery, as the ratio between the total load met by the heat pump (heating + cooling) and its electrical consumption. The pseudo steady-state model assumes constant COP values for each operation mode, but the relative weight of these modes varies throughout the year, leading to values between 3.5 and 4.9. The detailed TRNSYS model calculates the COP at each time step depending on the operating conditions, leading to a wider variation (3.7 and 6.4) and to a higher annual COP (5.2 vs. 4.4). The fixed COP values adopted in the pseudo steady-state model could have been adapted to cancel this difference, but the work presented in 6.1 used values that were estimated by the project team before the detailed model was completed, to reflect the pre-feasibility study context.

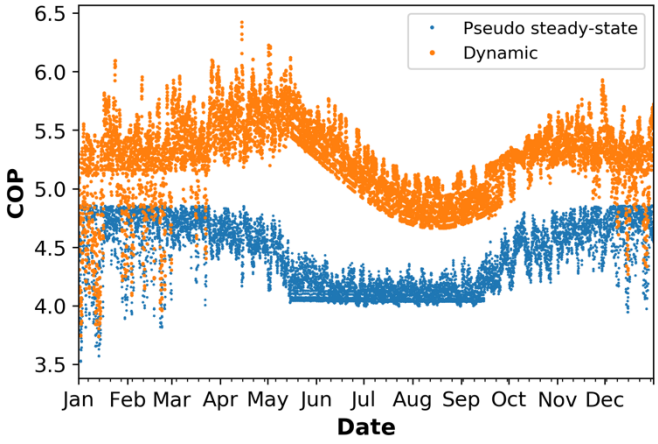

Figure 6.10 – Overall COP evolution for the pseudo steady-state and dynamic models

Figure 6.11 presents the diagram of the 4G network scenario and present its results for annual consumption and peaks in electricity (heating and air conditioning) and gas (heating and DHW) for the dynamic model. Emissions in CO_2 equivalent (black cloud in the diagrams) and thermal emissions into the atmosphere (white cloud) are also presented. When comparing to Figure 6.1 we observe that the thermal losses (total or during peaks) are higher in the pseudo steady-state model than the dynamic one. This results from using a more conservative approach for the pseudo steady-state model. Moreover, the electrical consumption and power peaks for the HPs are lower for the dynamic model because the overall COP is higher for this model. However, the distribution of energy/peak demands satisfied by the heat pumps is very similar for both models.

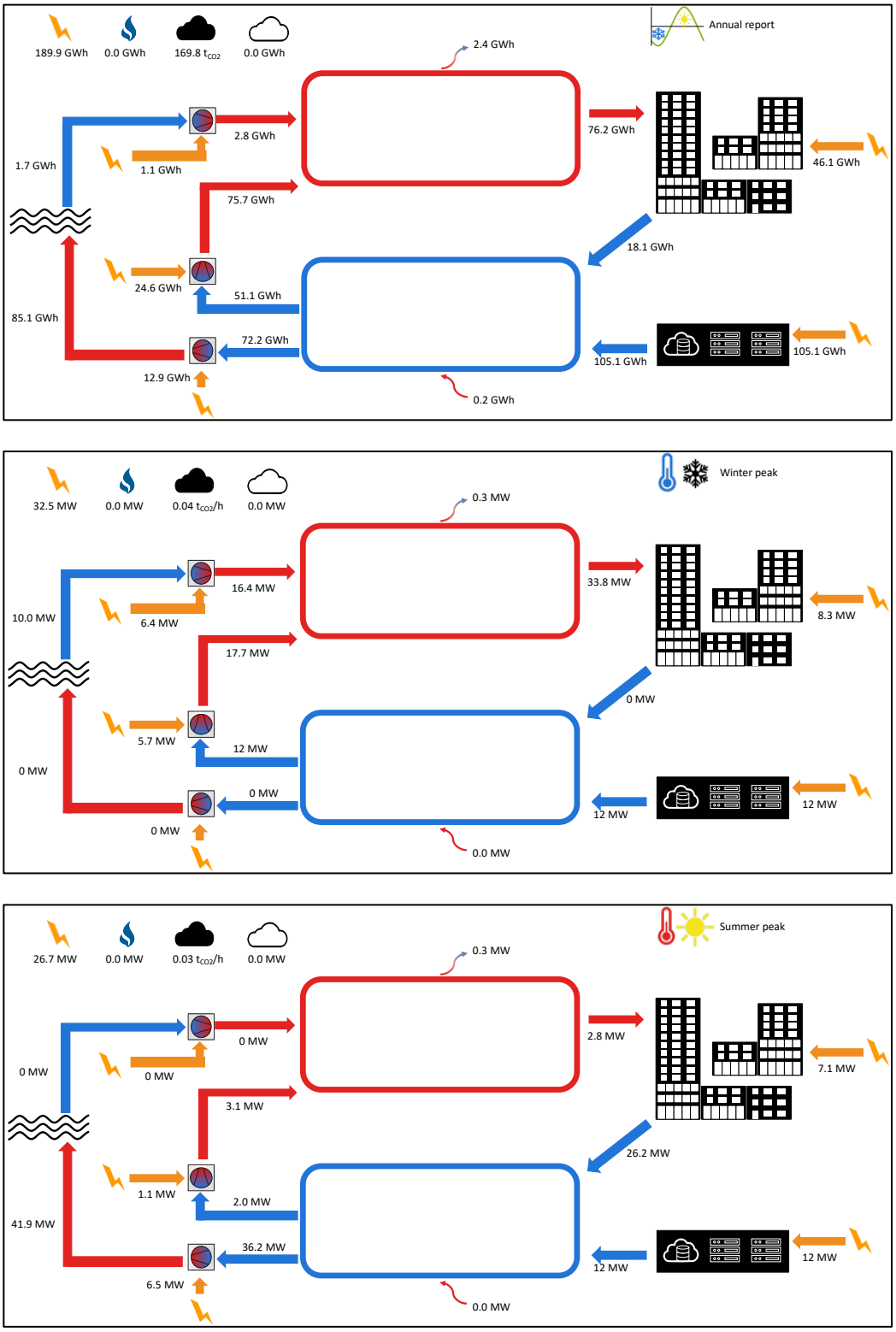

Figure 6.11 – 4G (dynamic): annual consumption (top), winter peak (middle), summer peak (bottom)

Figure 6.12 presents the heating (heating and DHW) and cooling loads for the different 4G network dynamic model, and the energy sources (heat recovery or electricity (heat pumps in both cases)) to meet those. Heating loads are shown as positive values in the graphs, while cooling loads are shown as negative values.

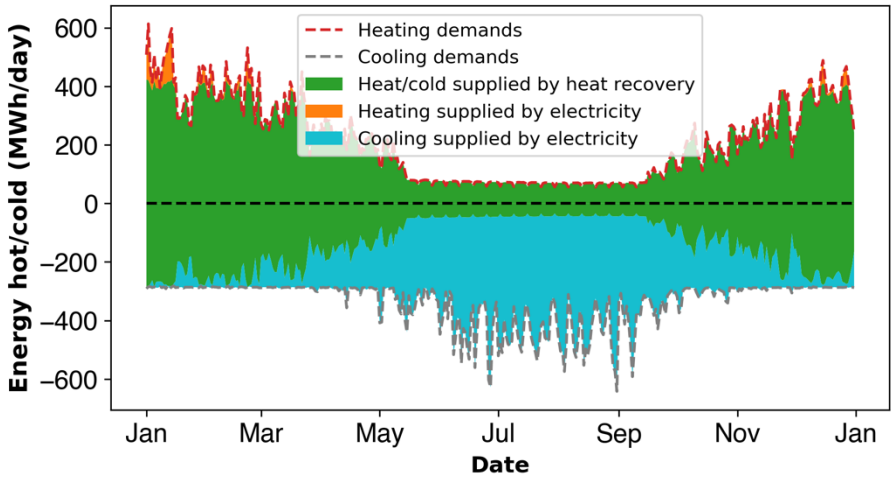

Figure 6.12 – 4G (dynamic): Heat demands by energy source

When comparing to Figure 6.3 (4G pseudo steady-state model), the source allocation for each heat demand is approximately the same. For the dynamic model, 75.7 GWh/year of heating loads are met by recovery and 72.1 GWh/year of the cooling loads met by electricity (HP rejecting heat to the sewer system), against 76.3 GWh/year and 72.9 GWh/year for heating and cooling loads respectively for the pseudo steady-state model.

Figure 6.13 shows the hourly power demand profile for the dynamic model of the 4th generation network for winter and summer weeks: the coldest week of the year (week of January 9th) and a very hot and sunny week (week of August 28th), and can be compared to Figure 6.5 (p. 66).

The stacked areas represent the different contributions to building and network electricity consumption: heat pumps, pumps and ALE (Appliances, Lighting and Equipment). The consumption for the data centre (DC) is also included.

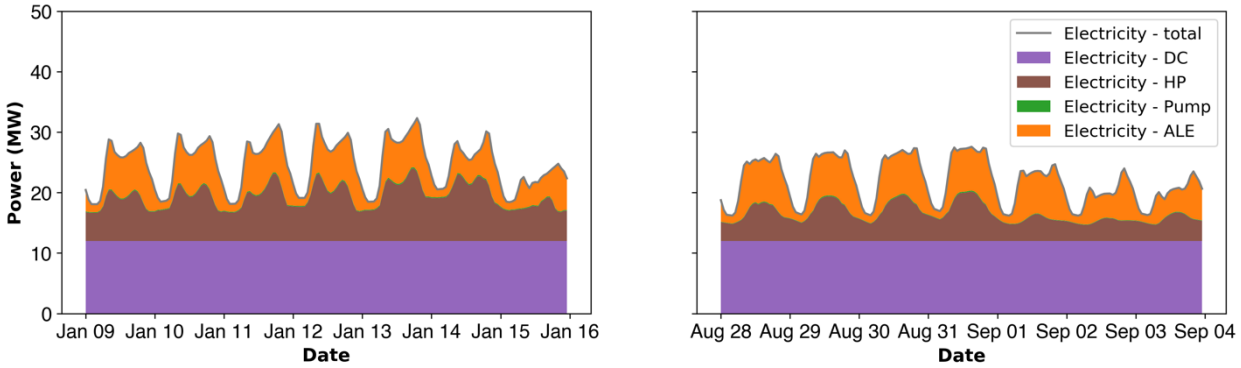

Figure 6.13 – 4G (dynamic): Power demand profile during winter (left) and summer (right) peak weeks

The winter electricity peak is slightly smaller for the dynamic model than the pseudo steady-state one (see Figure 6.5) with 1.4 % difference. Even if the electricity consumption for water pumping (in green on Figure 6.13) is taken into account for the detailed model, and not for the pseudo steady-state one, this energy consumption is negligible. The difference for winter electricity peak is explained by the fact that the heat pumps in the dynamic model consume in average 6.4 % less electricity. The difference is very small because during this period, the hourly COP of both models are almost equal (see Figure 6.10).

This trend is increasing for the summer week, with a total electricity consumption 3.3 % higher for the pseudo steady-state model. This difference is explained by the fact that the heat pumps of the dynamic model consume in average 15.9 % less electricity than the heat pumps in the pseudo steady-state model. Figure 6.10 shows that at this period of the year, the COP of the dynamic model is higher than the COP of the pseudo steady-state model.

6.3 Discussion and conclusions

Different district energy scenarios (4^{th} and 5^{th} generations) were compared to a Business As Usual (BAU) scenario for the case study neighborhood which includes a large data centre. Both types of district energy networks allow to recover heat from the data centre and other buildings efficiently and avoid rejecting heat into the ambient air. With the selected sizing assumptions, they lead to significant GHG emission reductions, even when accounting for emissions related to refrigerants. The 4^{th} generation network presents a slightly better energy performance because of the presence of two levels of heat pumps in the 5^{th} generation network, but a more detailed design could alter

these differences by allowing operation without central heat pumps. Refrigerant-related emissions of the 5th generation network are also higher, especially if it is assumed that large central heat pumps can use an alternative refrigerant such as ammonia.

By recovering the heat rejected by the data centre, both types of networks allow to effectively decarbonize the built environment without increasing significantly the peak demand on the electric grid. The winter peak demand is slightly lower for the 4th generation network, again due to the requirement to operate decentralized and central heat pumps in the 5th generation network.

Both types of networks avoid rejecting close to 160 GWh into the ambient air, rejecting instead 90 GWh and 110 GWh into the sewer system respectively for 4th and 5th generation networks.

A comparison between a simple pseudo steady-state model and a more detailed dynamic model in TRNSYS was performed for the 4th generation network. The simple model uses constant performance parameters (e.g. constant annual COP for heat pumps) that were estimated by the project team and have not been tuned after the detailed model was completed. The dynamic model shows a lower electricity consumption than the pseudo steady-state model (on average 14 % lower over the year for heat pumps consumption), due to a higher COP of the system for the dynamic model. When looking at electricity consumption for winter and summer peak weeks, it shows that during winter electric consumptions are really similar between both models (1.4 % difference), while for summer season there is larger differences mainly due to a better COP of the heat pumps for the dynamic model during this season. The very good agreement is a testimony to the engineering skills of the project team involved in the case study for the Ville-Marie borough. A detailed model would still be useful to compare different heat pumps or control strategies, especially if thermal storage or different heat sources/sinks such as geothermal wells were investigated, as these technologies are difficult to account for in the pseudo-steady state model.

CHAPTER 7 CONCLUSIONS AND RECOMMENDATIONS

This work allowed us to study different modelling/simulation approaches to investigate the potential of heat-sharing energy networks in urban environments. Our work addressed the calibration of building archetypes for specific individual buildings, Urban Building Energy Modelling (UBEM), and the modelling of heat-sharing networks themselves.

As a first step, we compared different urban-level models of 4 selected buildings (residential and commercial) with measured data, expanding the work presented in a conference paper (Leroy et al., 2019). Successive refinements of the archetypal characterizations were implemented in UMI and the hourly energy consumption at the building level was compared with the measured data, prototype building models developed by the US-DOE and ran in EnergyPlus, and also with detailed and calibrated models. Results show that archetypes using more refined estimates of thermal and building usage parameters do not necessarily deliver better results for the selected buildings, hinting that canceling errors may be at play. Results also show that parameters obtained from calibrated detailed models cannot be directly transferred to archetypes. Further work should aim at generalizing the results of this study by selecting more buildings with different types of usage to be able to use a greater diversity of archetypes. Improving the calibration process and automatizing it also seems an interesting research avenue.

Two UBEM approaches were then compared on a case study originating in a study commissioned by the Ville-Marie borough in Montréal. Future buildings totaling 1.2 million square meters were modelled using a context-free approach (prototype buildings modelled in EnergyPlus) and a context-dependent approach using UMI. When looking at the total end-use loads and peaks, the 2 models offer similar results, with maximum differences in the order of 25 %, except for a large underestimation of the domestic hot water load which can be attributed to a version-specific bug in UMI. However, when observing the hourly results over a typical year, large differences are observable between the 2 models. UBEM is still a very young field, which has originally focused on annual performance analysis, so further work is required to validate the dynamic response of simple urban-level models such as those used in UMI. A data centre was included in the neighborhood, and the UBEM results were used as a baseline (Business as usual case) to assess different energy network scenarios: a 4th generation network (hot and cold loop with heat recovery) and a 5th generation network (one “ambient” temperature loop).

The modelling of the different scenarios showed that the implementation of an energy sharing network in this neighborhood would reduce the energy consumption (gas or electricity) thanks to the use of more efficient centralised equipment and heat recovery between heating and cooling needs, for both 4th generation and 5th generation networks. These networks would make it possible to reduce the neighborhood's greenhouse gases emissions by avoiding the use of gas for heating peaks and domestic hot water, even taking into account emissions related to refrigerants. In addition, the implementation of an energy sharing network eliminates thermal rejection into the ambient air, reducing the urban heat island effect by dumping excess heat into the sewer system.

A comparison between a simple pseudo steady-state model and a more detailed dynamic model in TRNSYS was performed for the 4th generation network. The dynamic model shows a lower electricity consumption than the pseudo steady-state model. It would therefore be interesting to carry out a dynamic model for the 5G network and compare the results with the dynamic 4G model to analyse whether the same conclusions can be drawn as for the pseudo steady-state models. The TRNSYS component developed to model the central heat pumps and their different operation modes should be tested in different configurations and validated against existing components in specific configurations.

Finally, if measured data of the studied neighborhood (presently in construction) is available in the future, it would be interesting to compare it with the results from the developed UBEMs and energy sharing networks.

REFERENCES

7-Technologies A/S. (2012). Termis Simulation Modes. Retrieved March 4, 2020, from http:///7t.dk/products/termis/Product-Information/termis-simulation-modes.aspx

Accelerate Europe. (2018). Sweden gets the ammonia treatment. *Accelerate Europe – Advancing HVAC&R Naturally, Autumn 2018, Pp. 18-20*. Bruxelles, BEL: Schecco Europe.

Allegrini, J., Orehounig, K., Mavromatidis, G., Ruesch, F., Dorer, V., & Evins, R. (2015). A review of modelling approaches and tools for the simulation of district-scale energy systems. *Renewable and Sustainable Energy Reviews*, *52*, 1391–1404. https://doi.org/10.1016/j.rser.2015.07.123

ASHRAE. (2013). *Climatic Data for Building Design Standards (Standard 169-2013)*. Atlanta, GA, USA: American Society of Heating, Refrigerating and Air-conditioning Engineers.

ASHRAE. (2014). *Guideline 14 - Measurement of Energy, Demand, and Water Savings* (Vol. 14). Atlanta, GA, USA: American Society of Heating, Refrigerating and Air-conditioning Engineers.

Averfalk, H., & Werner, S. (2018). Novel low temperature heat distribution technology. *Energy*, *145*, 526–539. https://doi.org/10.1016/j.energy.2017.12.157

Buffa, S., Cozzini, M., Antoni, M. D., Baratieri, M., & Fedrizzi, R. (2019). 5th generation district heating and cooling systems : A review of existing cases in Europe. *Renewable and Sustainable Energy Reviews*, *104*(June 2018), 504–522. https://doi.org/10.1016/j.rser.2018.12.059

CanmetENERGY. (2019). Building Technology Assessment Platform (BTAP). Ottawa, ON, CAN: Natural Resources Canada.

Cerezo, C., Sokol, J., Reinhart, C., & Al-Mumin, A. (2015). Three methods for characterizing building archetypes in urban energy simulation. A case study in Kuwait City. *14th Conference of International Building Performance Simulation Association*, 2873–2880.

Cerezo Davila, C., Reinhart, C. F., & Bemis, J. L. (2016). Modeling Boston: A workflow for the efficient generation and maintenance of urban building energy models from existing geospatial datasets. *Energy*, *117*, 237–250. https://doi.org/10.1016/j.energy.2016.10.057

Daikin Applied. (2011). *Templifier Heat Recovery Water Heaters*. *Catalog 614-2*. Minneapolis, MN, USA: Daikin Applied Americas.

Dassault Systemes. (2020). Dymola – Dynamic Modeling Laboratory. Retrieved March 4, 2020, from https://www.3ds.com/products-services/catia/products/dymola

David, A., Mathiesen, B. V., Averfalk, H., Werner, S., & Lund, H. (2017). Heat Roadmap Europe: Large-scale electric heat pumps in district heating systems. *Energies*, *10*(4). https://doi.org/10.3390/en10040578

Deru, M., Field, K., Studer, D., Benne, K., Griffith, B., Torcellini, P., … Crawley, D. (2011). U.S. Department of Energy Commercial Reference Building Models of the National Building Stock. *NREL*. Golden, CO, USA: National Renewable Energy Laboratory.

Écohabitation. (2019). *Étude d'opportunité pour le développement d'un réseau thermique (« District energy sharing ») dans le secteur des Faubourgs, arrondissement Ville-Marie, Ville de Montréal.* Montréal, QC, CAN: Écohabitation.

Edwards, S., Beausoleil-Morrison, I., & Laperrière, A. (2015). Representative hot water draw profiles at high temporal resolution for simulating the performance of solar thermal systems. *Solar Energy*, *111*, 43–52. https://doi.org/10.1016/j.solener.2014.10.026

Energy Soft. (2020). EnergyPro. Retrieved March 3, 2020, from http://www.energysoft.com/

Energy Star. (2019). Residential Windows, Doors & Skylights. Retrieved December 10, 2019, from https://www.energystar.gov/products/building_products/residential_windows_doors_and_skylights/key_product_criteria

EQUA. (2014). IDA Indoor Climate and Energy. Solna, S: EQUA Simulation Technology Group.

Filogamo, L., Peri, G., Rizzo, G., & Giaccone, A. (2014). On the classification of large residential buildings stocks by sample typologies for energy planning purposes. *Applied Energy*, *135*, 825–835. https://doi.org/10.1016/j.apenergy.2014.04.002

Filonenko, K., Howard, D., Buck, J., & Veje, C. (2019). Comparison of two simulation tools for district heating applications. In *9th International Conference & Workshop REMOO2019* (pp. 1–10).

Hawk-Eye. (n.d.). Windows as seen through HOT2000 modeling software for R-2000 and EnerGuide Rating Services. *Construction Reference Guide #3*, pp. 5–7.

Heiple, S., & Sailor, D. J. (2008). Using building energy simulation and geospatial modeling techniques to determine high resolution building sector energy consumption profiles. *Energy and Buildings*, *40*(8), 1426–1436. https://doi.org/10.1016/j.enbuild.2008.01.005

Hoffman, K. (2018). *Large scale heat pumps for high efficiency district heating projects*. *Ior*. UK: SIRACH.

Huang, J., Akbari, H., Rainer, L., & Ritschard, R. (1991). 481 Prototypical Commercial Buildings for 20 Urban Market Areas. Berkeley, CA, USA: Lawrence Berkeley Laboratory.

Hydro-Québec. (2016). Hydro-Québec is poised to attract data centres. Retrieved March 4, 2020, from http://news.hydroquebec.com/en/press-releases/1045/hydro-quebec-is-poised-to-attract-data-centres/

Hydro-Québec. (2019a). Montréal the Best Place in the World to Set up a Data Center. Retrieved March 4, 2020, from http://news.hydroquebec.com/en/press-releases/1503/montreal-the-best-place-in-the-world-to-set-up-a-data-center/

Hydro-Québec. (2019b). Simulation énergétique des bâtiments. Retrieved January 27, 2019, from https://www.simeb.ca/

IBPSA Project 1. (2019). BIM/GIS and Modelica Framework for building and community energy system design and operation. Retrieved March 4, 2020, from https://ibpsa.github.io/project1/index.html

IPCC. (2006). Chapter 7: Emissions of Fluorinated Substitutes for Ozone Depleting Substances. In *2006 IPCC Guidelines for National Greenhouse Gas Inventories - Volume 3, Industrial Processes and Product Use*. Geneva, CHE: International Panel on Climate Change.

IPCC. (2013). Chapter 8: Anthropogenic and Natural Radiative Forcing. In *Climate Change 2013: The Physical Science Basis. Contribution of Working Group I to the Fifth Assessment Report of the Intergovernmental Panel on Climate Change*. Geneva, CHE: International Panel on Climate Change.

IPCC. (2019). Chapter 7: Emissions of Fluorinated Substitutes for Ozone Depleting Substances. In

2019 Refinement to the 2006 IPCC Guidelines for National Greenhouse Gas Inventories - Volume 3, Industrial Processes and Product Use. Geneva, CHE: International Panel on Climate Change.

Johnson, G., & Beausoleil-Morrison, I. (2017). Electrical-end-use data from 23 houses sampled each minute for simulating micro-generation systems. *Applied Thermal Engineering*, *114*, 1449–1456. https://doi.org/10.1016/j.applthermaleng.2016.07.133

Klein, S. A., Beckman, W. A., Mitchell, J. W., Duffie, J. A., Duffie, N. A., Freeman, T. L., … Duffy, M. J. (2018). TRNSYS 18 – A TRaNsient SYstem Simulation Program, User Manual. Version 18.0. Madison, WI: University of Wisconsin-Madison.

Kohler, N., & Hassler, U. (2002). The building stock as a research object. *Building Research and Information*, *30*(4), 226–236. https://doi.org/10.1080/09613210110102238

LBNL. (2013). *THERM 6.3 / WINDOW 6.3 NFRC Simulation Manual*. Berkeley, CA, USA: Lawrence Berkeley National Laboratory.

LBNL. (2020). Modelica Buildings Library – Open source library for building energy and control systems. Berkeley, CA, USA: Lawrence Berkeley National Laboratory.

Légis Québec. (2019). *Règlement sur l'économie de l'énergie dans les nouveaux bâtiments*. (Éditeur officiel du Québec, Ed.).

Leroy, L., Letellier-Duchesne, S., & Kummert, M. (2019). Using Model Calibration to Improve Urban Modeling. In *Building Simulation 2019* (pp. 3531–3539). IPBSA.

Letellier-Duchesne, S. (2019). *Planning an integrated design of urban heat-sharing networks*. (Doctoral dissertation) Polytechnique Montréal.

Letellier-Duchesne, S., Nagpal, S., Kummert, M., & Reinhart, C. (2018). Balancing demand and supply: Linking neighborhood-level building load calculations with detailed district energy network analysis models. *Energy*, *150*, 913–925. https://doi.org/10.1016/j.energy.2018.02.138

Li, W., Tian, Z., Lu, Y., & Fu, F. (2018). Stepwise calibration for residential building thermal performance model using hourly heat consumption data. *Energy and Buildings*, *181*, 10–25. https://doi.org/10.1016/j.enbuild.2018.10.001

Logstor. (2020). *Product Catalogue District Energy*. Løgstør, DK. https://doi.org/10.4324/9781315771519-10

Lund, H., Werner, S., Wiltshire, R., Svendsen, S., Eric, J., Hvelplund, F., & Vad, B. (2014). 4th Generation District Heating (4GDH) Integrating smart thermal grids into future sustainable energy systems. *Energy*, *68*, 1–11. https://doi.org/10.1016/j.energy.2014.02.089

Mata, É., Sasic Kalagasidis, A., & Johnsson, F. (2014). Building-stock aggregation through archetype buildings: France, Germany, Spain and the UK. *Building and Environment*, *81*, 270–282. https://doi.org/10.1016/j.buildenv.2014.06.013

MIT Sustainable Design Lab. (2017). umidocs. Retrieved April 9, 2020, from https://umidocs.readthedocs.io/en/latest/index.html

Morris, R. (2016). *Final Report – Updating CWEEDS Weather Files*. Toronto, ON, CAN: Environment and Climate Change Canada.

National Research Council Canada. (1999). Specifications for Calculation Procedures for Demonstrating Compliance to the Model National Energy Code for Buildings Using Whole Building Performance. *Performance Compliance for Buildings*. https://doi.org/https://doi.org/10.4224/20378714 NRC

Natural Resources Canada. (2018). EnerGuide for houses. Retrieved September 21, 2018, from https://www.nrcan.gc.ca/energy/efficiency/homes/16654

Natural Resources Canada. (2019). Tools for industry professionals (HOT2000). Retrieved January 31, 2019, from https://www.nrcan.gc.ca/energy/efficiency/homes/20596

NRC-IRC. (2011). National Energy Code for Buildings 2011. Ottawa, ON, CAN: National Research Council of Canada, Institute for Research in Construction.

Poggi, F., Macchi-Tejeda, H., Leducq, D., & Bontemps, A. (2008). Refrigerant charge in refrigerating systems and strategies of charge reduction. *International Journal of Refrigeration*, *31*(3), 353–370. https://doi.org/10.1016/j.ijrefrig.2007.05.014

Reinhart, C. (2019). Urban Modeling Interface. Retrieved January 27, 2019, from http://urbanmodellinginterface.ning.com/

Reinhart, C. F., & Cerezo Davila, C. (2015). Urban building energy modeling - A review of a

nascent field. *Building and Environment*, *97*, 196–202. https://doi.org/10.1016/j.buildenv.2015.12.001

Robert McNeel & Associates. (2019). Rhinoceros. Retrieved January 27, 2019, from https://www.rhino3d.com/#

Samuelson, H. W., Ghorayshi, A., & Reinhart, C. F. (2015). Analysis of a simplified calibration procedure for 18 design-phase building energy models. *Journal of Building Performance Simulation*, *9*(1), 17–29. https://doi.org/10.1080/19401493.2014.988752

Seskus, T. (2019). Why Canada needs better information about all the energy it produces. Retrieved March 4, 2019, from https://www.cbc.ca/news/business/canada-energy-data-1.5027115

Sokol, J., Cerezo Davila, C., & Reinhart, C. (2017). Validation of a Bayesian-based method for defining residential archetypes in urban building energy models. *Energy and Buildings*, *134*, 11–24. https://doi.org/10.1016/j.enbuild.2016.10.050

TEQ. (2019). Facteurs d'émission et de conversion. QC, Canada: Transition Énergétique Québec.

Theodoridou, I., Papadopoulos, A. M., & Hegger, M. (2011). A typological classification of the Greek residential building stock. *Energy and Buildings*, *43*(10), 2779–2787. https://doi.org/10.1016/j.enbuild.2011.06.036

UNEP. (2015). *District Energy in Cities - Unlocking the Potential of Energy Efficiency and Renewable Energy*. Nairobi, KEN: United Nations Environment Programme.

US DOE. (2012). Residential Prototype Building Models. *US Department of Energy*. Washington, DC, USA: United States Department of Energy.

US DOE. (2018). House Simulation Protocols report. Washington, DC, USA: United States Department of Energy.

US DOE. (2019a). Building Energy Code Program. Washington, DC, USA: United States Department of Energy.

US DOE. (2019b). Combined Heat and Power Basics. Washington, DC, USA: United States Department of Energy.

US DOE - BTO. (2018). Commercial Prototype Building Models. Washington, DC, USA: United States Department of Energy, Building Technologies Office.

US DOE - BTO. (2019). EnergyPlus. Washington, DC, USA: United States Department of Energy, Building Technologies Office.

Vela Solaris. (2020). Polysun. Retrieved March 3, 2020, from https://www.velasolaris.com/?lang=en

Wetter, M. (2016). *GenOpt - Generic Optimization Program - User Manual, version 3.1.1*. Berkeley, CA, USA: Lawrence Berkeley National Laboratory.

APPENDIX A GHG EMISSIONS RELATED TO REFRIGERANTS

The methodology used to account for GHG emissions associated with refrigerants used in heat pumps, chillers and air conditioners is the one recommended by the Intergovernmental Panel on Climate Change (IPCC), as formulated in the 2006 guidelines (IPCC, 2006) with the 2019 refinements (IPCC, 2019). The method chosen is the one known as the Tier 2a - Emission-factor approach.

1. Refrigerant emissions over the lifetime

The total emissions (in kg of refrigerant) E_{tot} are the result of 4 contributions:

$$E_{tot} = E_{container} + E_{charge} + E_{lifetime} + E_{endOfLife} \quad (4)$$

$E_{container}$ represents the refrigerant emissions [kg] related to leakage during transfer between bulk containers (40 tonnes and over) to smaller capacity containers. These emissions are neglected here.

E_{charge} represents the refrigerant emissions [kg] during refrigerant charging in new equipment during manufacturing:

$$E_{charge} = M_0 \cdot k \quad (5)$$

Where M_0 is the initial mass (charge) of refrigerant [kg] in the machine. k is the rate of refrigerant leakage during assembly and filling. This rate is between 0.1 % and 3 % in general, and between 0.2 % and 1 % for residential and commercial air conditioning/heat pump systems or chillers (IPCC, 2019 - Table7.9). The lower value (0.2 %) was selected here, assuming that the systems would be factory assembled. The initial refrigerant charge depends on the application (see below).

$E_{lifetime}$ represents the refrigerant emissions [kg] over the lifetime of the equipment:

$$E_{lifetime} = \sum_{n=1}^{d} M_n \cdot x \quad (6)$$

Where M_n is the mass of refrigerant [kg] in the systems at the year n, and d is the service life of the equipment [years]. The leakage rate per year, x, is expressed in %/year. Leakage rate and service life depend of the application type of the system (see below). The refrigerant mass M_n gradually decreases over the service life due to leakage, and may increase if the equipment is recharged during maintenance or repair.

$E_{endOfLife}$ represents the refrigerant emissions [kg] at the end of the life of the equipment:

$$E_{endOfLife} = M_0 \cdot p \cdot (1 - \eta) \tag{7}$$

Where p [%] is the fraction of the initial mass of refrigerant that is present in the end-of-life equipment (so $M_0 \cdot p$ represents the mass of refrigerant in the system at the end of its life). η [%] is the fraction of the refrigerant that is recovered at the end-of-life, ranging from 0 % (in countries where refrigerant control is lax or non-existent) to 95 % for (large) chillers.

The equation for refrigerant emissions [kg] over lifetime can therefore be written as follows:

$$E_{tot} = M_0 \cdot k + \sum_{n=1}^{d} M_n \cdot x + M_0 \cdot p \cdot (1 - \eta) \tag{8}$$

2. Equivalent annual CO_2 emissions

The equivalent emission factor for refrigerants is known as the Global Warming Potential (GWP), expressed in kg of CO_2 equivalent per kg of refrigerant. The refrigerant most commonly found in practice in residential air-conditioning systems is R-410a (HFC-410a), while central chillers and high-temperature heat pumps for heating systems most often use R-134a (HFC-134a). The values used for GWP are the 100-year equivalent values recommended by the IPCC (IPCC, 2013).

$GWP_{HFC\text{-}134a,100\text{-}year} = 1300$ [$kg_{CO2,eq}$/kg]

$GWP_{HFC\text{-}410a,100\text{-}year} = 1924$ [$kg_{CO2,eq}$/kg] (note: HFC-410a is a 50 % / 50 % mix of HFC-32 and HFC-125)

The equivalent emissions in tonnes of CO_2 per year are therefore calculated as following (1000 is a conversion factor between tonnes and kg):

$$E_{GES,eq}\left[t_{CO_2}/y\right] = \frac{E_{tot}}{d} \cdot \frac{GWP}{1000} \quad (9)$$

Where E_{tot} is the total amount of refrigerant emitted [kg] over the service life (d years).

3. Mass (charge) of refrigerant in mechanical systems

The mass of refrigerant depends on the size of the machine, so it is convenient to express it in terms of the rated output of the heat pump or air conditioner:

$$M_0 = m \cdot P_{rated} \quad (10)$$

Where P_{rated} is the nominal power of the machine [kW], and m is the specific refrigerant charge per power unit [kg/kW].

It should be noted that m is not constant: larger centralized machines often use proportionally less refrigerant than smaller residential systems, and will therefore have a smaller m value. Some distributed systems (such as VRF systems, for Variable Refrigerant Flow) also have longer pipe lengths that require a higher refrigerant charge.

Representative refrigerant charge values are shown in Table 3. The residential examples are taken from the KeepRite series DLC4 A/H and Mitsubishi M series catalogues (and represent an average where there are slight differences). For standard chillers/heat pumps, the examples are from the Carrier (XW30 Series) and York (YVWA Series) catalogues. For high-temperature chillers / heat pumps, the data is taken from Daikin catalogue (TGZ series, Daikin Applied (2011)). A Multistack catalogue shows significantly lower values (approx. 0.1 kg/kW) which could not be verified and were therefore not used.

Table 1 − Refrigerant charge rate for some equipment

Equipment type	Refrigerant	m [kg/kW]
Residential air conditioner 2.5 kW (0.75 ton)	HFC-410A	0.45
Residential air conditioner 3.5 kW (1 ton)	HFC-410A	0.30
Residential air conditioner 7 kW (2 ton)	HFC-410A	0.25
Residential air conditioner 10.5 kW (3 ton)	HFC-410A	0.20
Chiller / heat pump 250 kW	HFC-134a	0.30
Chiller / heat pump 500 kW	HFC-134a	0.25
Chiller / heat pump 1000 kW	HFC-134a	0.20
Chiller / heat pump 1500 kW	HFC-134a	0.15
High-temperature chiller / heat pump 100 kW	HFC-134a	0.20
High-temperature chiller / heat pump 250 kW	HFC-134a	0.18
High-temperature chiller / heat pump 500 kW	HFC-134a	0.15

The following assumptions were selected:

For residential systems (BAU scenario), a specific load m of 0.3 kg/kW has been selected, representing an average mini-split air conditioning unit of 0.75 to 3 ton (2.5 to 10.5 kW).

For the 4G network, a specific load m of 0.15 kg/kW was chosen for the central heat pumps (those connected to the renewable source and those recovering between the cold and hot loops). It should be noted that the parallel installation of identical machines does not change the specific load.

For the 5G network, a specific load of 0.15 kg/kW was chosen for central heat pumps connected to the renewable source, and a specific load of 0.2 kg/kW was chosen for heat pumps distributed in buildings. This assumption takes into account the fact that the substations are likely to be installed per building and not per block, with a representative capacity of 800 kW per building.

For the chillers in the data centre, a specific load of 0.15 kg/kW has been chosen.

The values selected are close to those presented by Poggi et al. (2008) for split residential equipment (from 0.24 kg/kW to 1 kg/kW) and water-to-water chillers or heat pumps (0.2 kg/kW), which is the hypothesis adopted here. Large-capacity machines with evaporators/condensers where the refrigerant and the air are directly in contact can have much higher specific loads, of the order of several kg/kW.

4. Refrigerant emission rate (choice of values of k, d, x, p, and η)

As mentioned above, the emission rate k at initial filling is set at 0.2 %.

The annual leakage rate x depends on the application. The recent update of the IPCC guidelines (IPCC, 2019) gives representative values of 2 % to 15 % for chillers and 1 % to 10 % for residential and commercial systems (including heat pumps). Tables 7A.1 to 7A.3 (IPCC, 2019) present results from studies in California, Japan and Germany, which give a fairly wide range of values that do not show a clear trend with respect to equipment size. A uniform rate of 6.7 % was applied in all cases - this rate is within the likely range and this exact value was chosen because it results in a remaining refrigerant quantity of 50 % of the initial mass after 10 years.

The service life of d equipment was set at 10 years for residential systems and 20 years for centralized systems.

The annual refrigerant mass is calculated from the initial mass and the initial leakage rate. It is assumed that systems are recharged if they reach a charge rate of less than 50 %. With the leakage rate selected, this situation occurs exactly at the end of the service life for residential systems and half of the service life for centralized systems. For the latter, there will be one refill over the lifetime. The same initial emission rate k is applied to this fill as when the equipment was installed.

With the assumptions used for annual leakage and maintenance fill, all systems end their service life with 50 % of the refrigerant present (the rate p is 50 %). The recovery rate η is estimated at 50 % for residential systems and 80 % for central systems (large building scale or heating system scale).

5. Equipment rated power

The rated power for the different machines is the one obtained by the simulations. For example, in the BAU case, the total capacity of residential air conditioners is assumed to be 26.2 MW (Figure 5.2). In reality, the installed capacity would probably be higher than the simulation results, because the sizing procedures take into account more stringent conditions and safety factors, but this is not taken into account here.

6. Calculations for the 3 scenarios and the data centre

a. Business as usual (BAU)

- Total capacity of residential air conditioners: $P_{rated} = 26.2 \text{ MW} = 26200 \text{ kW}$
- Specific refrigerant charge: $m = 0.3 \text{ kg/kW}$
- Initial mass of refrigerant: $M_0 = 26200 \cdot 0.3 = 7860 \text{ kg}$, rate of refrigerant leakage: $k = 0.2\ \%$
- Therefore $E_{charge} = M_0 \cdot k = 7860 \cdot 0.002 = 15.7 \text{ kg}$
- Leakage rate per year: : $x = 6.7\ \%$, lifetime: $d = 10$ ans
- Thus $E_{lifetime} = \sum_{n=1}^{d} M_{n-1} \cdot x$ with $M_{n-1} = M_0 \cdot (1-x)^{n-1}$
- $E_{lifetime} = M_0 \cdot \sum_{n=1}^{d} x\,(1-x)^{n-1} = M_0 \cdot (1-(1-x)^d) = 7860 \cdot (1-(1-0.067)^{10}) = 3930 \text{ kg}$
  (we observe that we lost half of the initial mass in 10 years, thus half of the initial mass remains in the system at the end of the 10-year service life)
- Mass of refrigerant in the system at the endlife: $M_o \cdot p = 7860 \cdot 0.5 = 3930 \text{ kg}$
- Recovered fraction: $\eta = 50\ \%$ (residential system)
- $E_{endOfLife} = M_0 \cdot p \cdot (1-\eta) = 7860 \cdot 0.5 \cdot (1-0.5) = 1965 \text{ kg}$
- Therefore $E_{tot} = E_{charge} + E_{lifetime} + E_{endOfLife} = 15.7 + 3930 + 1965 = 5911 \text{ kg}$
- We assume residential systems use R-410a with $GWP_{HFC\text{-}410a,100\text{-}year} = 1924$ [$kg_{CO2,eq}$/kg]

- Finally $E_{GES,eq}\left[t_{eqCO_2}/y\right] = \frac{E_{tot}}{d} \cdot \frac{GWP}{1000} = 5911 \cdot 1924/(10 \cdot 1000) = 1137\ t_{eqCO_2}$/year

b. 4th generation network (4G)

- Total capacity of centralized heat pumps: $P_{rated} = 37.1 + 2.9 = 40$ MW $= 40000$ kW
    - Note: we used the heating output of the heat pumps (red arrows, Figure 6.1, middle and bottom)
- Specific refrigerant charge: $m = 0.15$ kg/kW
- Initial mass of refrigerant: $M_0 = 6000$ kg, rate of refrigerant leakage: $k = 0.2$ %
- We assume that the system is filled after 10 years, when it has reached a 50 % fill rate, therefore $E_{charge} = \left(M_0 + \frac{M_0}{2}\right) \cdot k = \left(6000 + \frac{6000}{2}\right) \cdot 0.002 = 18$ kg
- Leakage rate per year: : $x = 6.7$ %, lifetime: $d = 20$ years (and so we do get a 50 % fill rate after 10 years, just before filling at the end of the year 10)
- We can use the same equation as for the BAU case if we split the lifetime into 2 periods of 10 years, since we refill the system at the end of the year 10
  $E_{lifetime} = 2 \cdot M_0 \cdot (1 - (1 - x)^{10}) = 2 \cdot 6000 \cdot (1 - (1 - 0.067)^{10}) = 6000$ kg
  (we observe that half of the initial mass has been lost twice in a row, and therefore over 20 years the leaks represent 100 % of the initial mass)
- Mass of refrigerant in the system at the end life: $M_o \cdot p = 6000 \cdot 0.5 = 3000$ kg
- Recovered fraction: $\eta = 80$ % (centralized system)
- $E_{endOfLife} = M_0 \cdot p \cdot (1 - \eta) = 6000 \cdot 0.5 \cdot (1 - 0.8) = 600$ kg
- Therefore $E_{tot} = E_{charge} + E_{lifetime} + E_{endOfLife} = 18 + 6000 + 600 = 6618$ kg
- We assume centralized systems use R-134a with $GWP_{HFC\text{-}134a,100\text{-}year} =$ 1300 [$kg_{CO2,eq}$/kg]
- Finally $E_{GES,eq}\left[t_{eqCO_2}/y\right] = \frac{E_{tot}}{d} \cdot \frac{GWP}{1000} = 6618 \cdot 1300/(20 \cdot 1000) = 430\ t_{eqCO_2}$/year

c. 5th generation network (5G)

There are two different categories of heat pumps: central heat pumps (which extract heat from or reject heat to the sewer system or river) and decentralized heat pumps installed in each buildings.

- Total capacity of centralized heat pumps: $P_{rated} = 44.8\ \text{MW} = 44800\ \text{kW}$, $m = 0.15\ \text{kg/kW}$
- Total capacity of decentralized heat pumps: $P_{rated} = 33.8\ \text{MW} = 33800\ \text{kW}$, $m = 0.20\ \text{kg/kW}$
    - Note: we used the heating output of the heat pumps (red arrows, Figure 6.2, middle and bottom)
- Initial mass of refrigerant: $M_0 = 44800 \cdot 0.15 + 33800 \cdot 0.20 = 13480\ \text{kg}$, rate of refrigerant leakage: $k = 0.2\ \%$
- We assume that the system is filled after 10 years, when it has reached a 50 % fill rate, therefore $E_{charge} = \left(M_0 + \frac{M_0}{2}\right) \cdot k = \left(13480 + \frac{13480}{2}\right) \cdot 0.002 = 40.4\ \text{kg}$
- Leakage rate per year: : $x = 6.7\ \%$, lifetime: $d = 20$ years (and so we do get a 50 % fill rate after 10 years, just before filling at the end of the year 10)
- We can use the same equation as for the BAU case if we split the lifetime into 2 periods of 10 years, since we refill the system at the end of the year 10
  $E_{lifetime} = 2 \cdot M_0 \cdot (1 - (1 - x)^{10}) = 2 \cdot 13480 \cdot (1 - (1 - 0.067)^{10}) = 13480\ \text{kg}$
  (we observe that half of the initial mass has been lost twice in a row, and therefore over 20 years the leaks represent 100 % of the initial mass)
- Mass of refrigerant in the system at the end life: $M_o \cdot p = 13480 \cdot 0.5 = 6740\ \text{kg}$
- Recovered fraction: $\eta = 80\ \%$ (centralized and decentralized HPs)
- $E_{endOfLife} = M_0 \cdot p \cdot (1 - \eta) = 13480 \cdot 0.5 \cdot (1 - 0.8) = 1348\ \text{kg}$
- Therefore $E_{tot} = E_{charge} + E_{lifetime} + E_{endOfLife} = 40.4 + 13480 + 1348 = 14868\ \text{kg}$

- We assume centralized systems use R-134a with $GWP_{HFC\text{-}134a,100\text{-}year} = 1300$ [$kg_{CO2,eq}$/kg]
- Finally $E_{GES,eq}\left[t_{eqCO_2}/y\right] = \frac{E_{tot}}{d} \cdot \frac{GWP}{1000} = 14868 \cdot 1300/(20 \cdot 1000) = 966\ t_{eqCO_2}$/year

d. Data centre

In the BAU and 5G scenarios, the data centre has its own cooling system that releases its heat to the ambient air (BAU) or to the network (5G). In the 4G scenario, the data centre is connected to a cold water network and therefore does not require chillers (Figure 6.1). However, it is likely that chillers will still be installed to ensure the operation of the data centre in the event of a major problem on cold loop of the network. The results therefore include the same cooling system (12 MW, R-134a) in all scenarios.

Calculations for the data centre cooling system:

- Total cooler capacity: $P_{rated} = 12$ MW $= 12000$ kW, specific refrigerant charge: $m = 0.15$ kg/kW
- Initial mass of refrigerant: $M_0 = 1800$ kg, rate of refrigerant leakage: $k = 0.2$ %
- We assume that the system is filled after 10 years, when it has reached a 50 % fill rate, therefore $E_{charge} = \left(M_0 + \frac{M_0}{2}\right) \cdot k = \left(1800 + \frac{1800}{2}\right) \cdot 0.002 = 5.4$ kg
- Leakage rate per year: : $x = 6.7$ %, lifetime: $d = 20$ years (and so we do get a 50 % fill rate after 10 years, just before filling at the end of the year 10)
- We can use the same equation as for the BAU case if we split the lifetime into 2 periods of 10 years, since we refill the system at the end of the year 10
  $E_{lifetime} = 2 \cdot M_0 \cdot (1 - (1 - x)^{10}) = 2 \cdot 1800 \cdot (1 - (1 - 0.067)^{10}) = 1800$ kg
  (we observe that half of the initial mass has been lost twice in a row, and therefore over 20 years the leaks represent 100 % of the initial mass)
- Mass of refrigerant in the system at the end life: $M_o \cdot p = 1800 \cdot 0.5 = 900$ kg
- Recovered fraction: $\eta = 80$ % (centralized system)
- $E_{endOfLife} = M_0 \cdot p \cdot (1 - \eta) = 1800 \cdot 0.5 \cdot (1 - 0.8) = 180$ kg

- Therefore $E_{tot} = E_{charge} + E_{lifetime} + E_{endOfLife} = 5.4 + 1800 + 180 = 1985.4$ kg
- We assume centralized systems use R-134a with $GWP_{HFC\text{-}134a,100\text{-}year} = 1300$ [$kg_{CO2,eq}$/kg]

Finally $E_{GES,eq}\left[t_{eqCO_2}/y\right] = \frac{E_{tot}}{d} \cdot \frac{GWP}{1000} = 1985.4 \cdot 1300/(20 \cdot 1000) = 129\ t_{eqCO_2}$/year